INVESTIGATION OF THE PATHOMECHANISM AND POTENTIAL THERAPEUTIC TARGETS IN RADIATION-INDUCED HEART DISEASE IN A RAT MODEL

Ph.D. Thesis

Mónika Gabriella Kovács MD

Supervisor: Márta Sárközy MD Ph.D.

Department of Biochemistry

Doctoral School of Multidisciplinary Medical Sciences

Albert Szent-Györgyi Medical School

University of Szeged

Szeged

2022

Table of contents

List of publications

The publications served as the basis of the Ph.D. thesis (IF: 10.771):

I. **Mónika Gabriella Kovács**, Zsuzsanna Z. A. Kovács, Zoltán Varga, Gergő Szűcs, Marah Freiwan, Katalin Farkas, Bence Kővári, Gábor Cserni, András Kriston, Ferenc Kovács, Péter Horváth, Imre Földesi, Tamás Csont, Zsuzsanna Kahán, Márta Sárközy. Investigation of the Antihypertrophic and Antifibrotic Effects of Losartan in a Rat Model of Radiation-Induced Heart Disease. *Int. J. Mol. Sci.* 2021, *22*(23), 12963; https://doi.org/10.3390/ijms222312963 (**IF**: 5.923, **D1**)

II. Márta Sárközy, Renáta Gáspár, Ágnes Zvara, Laura Kiscsatári, Zoltán Varga, Bence Kővári, **Mónika Gabriella Kovács**, Gergő Szűcs, Gabriella Fábián, Gábor Cserni, László G. Puskás, Thomas Thum, Zsuzsanna Kahán, Tamás Csont, Sándor Bátkai. Selective heart irradiation induces cardiac overexpression of the pro-hypertrophic miR-212. Front Oncol. 2019 Jul 16;9:598. doi: 10.3389/fonc.2019.00598. eCollection 2019 (**IF**: 4.848, **Q1**)

Other publications published during the Ph.D. scholarship:

III. Márta Sárközy, Zsuzsanna Kovács, **Mónika Gabriella Kovács**, Renáta Gáspár, Gergő Szűcs, László Dux. Mechanisms and Modulation of Oxidative/Nitrative Stress in Type 4 Cardio-Renal Syndrome and Renal Sarcopenia (**IF**: 3.201, **Q2**)

IV. Márta Sárközy, Ágnes Zvara, Renáta Gáspár, Andrea Siska, Bence Kővári, Gergő Szűcs, Fanni Márványkövi, **Mónika Gabriella Kovács**, László Bodai, Nóra Zsindely, Márton Pipicz, Kamilla Gömöri, Krisztina Kiss, Péter Bencsik, Gábor Cserni, László G. Puskás, Imre Földesi, Thomas Thum, Zsuzsanna Kahán, Sándor Bátkai, Tamás Csont. Chronic kidney disease induces cardiac overexpression of the pro-hypertrophic microRNA-212 (**IF**: 3.998, **D1**)

V. Márta Sárközy, Zoltán Varga, Renáta Gáspár, Gergő Szűcs, **Mónika G Kovács**, Zsuzsanna Z A Kovács, László Dux, Zsuzsanna Kahán, Tamás Csont. Pathomechanisms and therapeutic opportunities in radiation-induced heart disease: from bench to bedside.

Clin Res Cardiol. 2021 Apr;110(4):507-531. doi: 10.1007/s00392-021-01809-y. Epub 2021 Feb 16 (**IF**: 5.46, **D1**)

VI. Zsuzsanna Kovács, Gergő Szűcs, Marah Freiwan, **Mónika G Kovács**, Fanni M Márványkövi, Hoa Dinh, Andrea Siska, Katalin Farkas, Ferenc Kovács, András Kriston, Péter Horváth, Bence Kővári, Bálint Gábor Cserni, Gábor Cserni, Imre Földesi, Tamás Csont, Márta Sárközy. Comparison of the antiremodeling effects of losartan and mirabegron in a rat model of uremic cardiomyopathy. Sci Rep. 2021 Sep 1;11(1):17495. doi: 10.1038/s41598-021-96815-5 (**IF**: 4.379, **D1**)

Cumulative impact factor of other papers published during the Ph.D. scholarship: 17.038

Total IF: 27.809

List of abbreviations

ACE: angiotensin-converting enzyme
Agt: angiotensinogen
AKT: protein kinase B
AngI: angiotensin I
AngII: angiotensin II
ARB: angiotensin II receptor blocker
AT1R: angiotensin II type 1 receptor
AT2R: angiotensin II type 2 receptor
AWTd: diastolic anterior wall thickness
AWTs: systolic anterior wall thickness
Cma: chymase
CO: cardiac output
Col1a1: collagen type I alpha 1 chain
Ctgf: connective tissue growth factor
DD: diastolic dysfunction
EF: ejection fraction
ERK1: extracellular signal-regulated kinase 1
ERK2: extracellular signal-regulated kinase 2
E-velocity: early ventricular filling velocity
e'-velocity: diastolic septal mitral annulus velocity
FOXO3: forkhead box O3
FS: fractional shortening
Gapdh: glyceraldehyde-3-phosphate dehydrogenase
GDF-15: growth differentiation factor 15
HE: hematoxylin-eosin
HF: heart failure
HFpEF: heart failure with preserved ejection fraction
HFrEF: heart failure with reduced ejection fraction
Hgprt: hypoxanthine-guanine phosphoribosyl transferase 1
HR: heart rate
IL1: interleukin-1
IL6: interlekin-6
IWTd: diastolic inferior wall thickness
IWTs: systolic inferior wall thickness
LVEDD: left ventricular end-diastolic diameter
LVEDV: left ventricular end-diastolic volume
LVESD: left ventricular end-systolic diameter
LVESV: left ventricular end-systolic volume
LVH: left ventricular hypertrophy
Mmp2: matrix metalloproteinase 2
Myh6: α -myosin heavy chain
Myh7: β -myosin heavy chain
NFAT: nuclear factor of activated T cells
PSFG: picrosirius red/fast green
Ppia: peptidyl-prolyl isomerase A
PWTd: diastolic posterior wall thickness
PWTs: systolic posterior wall thickness
RAAS: renin-angiotensin-aldosterone system
RIHD: radiation-induced heart disease
RpIp2: ribosomal protein lateral stalk subunit P2
RT: radiotherapy
SMAD2/3: mothers against decapentaplegic homolog 2/3
STAT3: signal transducer and activator of transcription 3
SV: stroke volume
SWTd: diastolic septal wall thickness
SWTs: systolic septal wall thickness
TAC: transverse aortic constriction
TGFβ: transforming growth factor-β
TGFβRII: transforming growth factor-β receptor II
Tnfa: tumor necrosis factor α

Summary

Radiation-induced heart disease (RIHD) is a potential late side-effect of thoracic radiotherapy resulting in left ventricular hypertrophy (LVH) and fibrosis due to a complex pathomechanism leading to heart failure (HF). MicroRNA-212 (miR-212) is a crucial regulator of pathologic LVH via forkhead box O3 (FOXO3)-mediated pathways in pressure-overload-induced HF. Angiotensin-II receptor blockers (ARBs), including losartan, are frequently used to control HF of various etiologies. Preclinical evidence is lacking on the anti-remodeling effects of ARBs in RIHD, while the results of clinical studies are controversial. We aimed to i) set up a rat model in the acute, early chronic, and late chronic phases of RIHD, ii) investigate whether miR-212 and iii) its selected target FOXO3 play a role in the development of RIHD, iv) and test the effects of losartan in our rat model of RIHD. In our studies, RIHD was induced by selective heart irradiation (50 Gy) in male Sprague-Dawley rats. In our model setup study, 1, 3, and 19 weeks after selective heart irradiation, transthoracic echocardiography was performed to monitor cardiac morphology and function. At the endpoints, qRT-PCR was performed to measure the gene expression changes of miR-212 and *Foxo3* in all follow-up time points. Cardiac expression of FOXO3 and phospho-FOXO3 (pFOXO3) were investigated at the protein level by Western blot at week 19. In RIHD, diastolic dysfunction (DD) was present at every time point. Mild hypertrophy developed at week 3, and a marked LVH with interstitial fibrosis developed at week 19 in the irradiated hearts. In our RIHD model, cardiac miR-212 was overexpressed at weeks 3 and 19, and *Foxo3* was repressed at the mRNA level only at week 19. In contrast, the total FOXO3 protein level failed to decrease in response to heart irradiation at week 19. In conclusion, miR-212 seems to play a role in the development of LVH via FOXO3-independent mechanisms in RIHD. In our treatment study, male Sprague-Dawley rats were studied in three groups: 1) control, 2) radiotherapy (RT) only, 3) RT treated with losartan (per os 10 mg/kg/day), and were followed for 1, 3, or 15 weeks. 15 weeks postirradiation, losartan alleviated the echocardiographic and histological signs of LVH and fibrosis and reduced the LV overexpression of chymase (*Cma*), connective tissue growth factor (*Ctgf*), and transforming growth factor-beta (*Tgfb*) measured by qRT-PCR; likewise, the level of the SMAD2/3 protein determined by Western blot decreased. In both RT groups, the pro-survival phospho-AKT/AKT and the phospho-ERK1,2/ERK1,2 ratios were increased at week 15. The antiremodeling effects of losartan seem to be associated with the repression of *Cma* and several elements of the TGF-β/SMAD signaling pathway in our RIHD model.

1. Introduction

Cardiovascular diseases and cancer are the leading causes of morbidity and mortality worldwide [1,2]. The most common cancerous diseases are breast and lung cancers in women and men, respectively [1]. Cancer therapy has undergone significant improvement, which led to increased long-term survival rates among cancer patients. About 50% of cancer patients receive RT, which also has an important role in the treatment of malignancies superposed on the chest wall, such as breast cancer and thoracic malignancies, including lung, and esophageal cancers, Hodgkin's lymphoma, and thymoma [3,4]. While high-energy ionizing radiation (i.e., RT) successfully kills tumor cells, it could have harmful effects on the surrounding healthy tissues [5]. Depending on the RT technique and dose used in thoracic and breast malignancies, the heart can be at risk of being exposed to ionizing radiation resulting in radiogenic sequelae in a dose-dependent manner [6,7].

The syndrome of unwanted cardiovascular side effects of thoracic RT is termed radiation-induced heart disease (RIHD), which is a critical concern in current oncology and cardiology practice [8-10]. RIHD is a progressive multifactorial disease that covers a broad spectrum of cardiac pathology [8-10]. Its clinical manifestation includes acute and chronic pericarditis, conduction system abnormalities, ischemic heart disease, cardiomyopathy, heart failure with preserved ejection fraction (HFpEF) or reduced ejection fraction (HFrEF), and valvular heart disease [8-10]. RT simultaneously causes damage to the cardiac macrovasculature (i.e., coronary arteries) and microvasculature, as well as the myocardium (i.e., diffuse injury), leading to the complex pathomechanism of RIHD [11,12]. However, the precise molecular mechanisms in the progression of RIHD from acute to chronic heart diseases are not clearly understood yet. Evidence suggests that RT-induced direct nitro-oxidative damage of macromolecules, including DNA, proteins, and lipids, initiates the development of RIHD. At this acute phase of RIHD, the elevated nitro-oxidative stress causes injury to the endothelial and other cells, eventually leading to various forms of cell death and acute inflammation [9,12,13]. In the early chronic phase of RIHD, the sublethally damaged surviving cardiomyocytes develop hypertrophy accompanied by endothelial cell proliferation as a compensatory mechanism [9,12,13]. If these compensatory mechanisms are exhausted, chronic inflammatory processes, fibrosis, and endothelial senescence play the primary role in the progression of RIHD [9,12,13]. Several pathomechanisms, including nitro-oxidative stress, cell death,

and inflammatory processes, overlap in the acute and chronic phases of RIHD [9]. The injury of the capillaries or coronary arteries disturbs circulation and leads to hypoxia which aggravates tissue damage [9]. These mechanisms seem to activate and potentiate each other leading to a vicious cycle in the progression of RIHD [9]. Unfortunately, therapeutic options for RIHD are currently insufficient. Therefore, understanding the exact molecular mechanisms in the progression of RIHD is essential for developing preventive and therapeutic strategies together with testing drugs that do not interfere with the anti-cancer effects of RT.

Endogenous microRNAs (miRs, 22 bp) are non-coding RNA species that are post-transcriptional regulators targeting specific mRNAs, resulting in an increase of mRNA degradation via complementary binding and the suppression of protein synthesis, thus influencing cellular function, including cell death and antioxidative mechanisms, inflammatory processes, cardiac hypertrophy, and fibrosis [14]. MiRNAs have been described as "master switches" in cardiovascular biology, and the dysregulation of specific miRs are key pathological factors in many cardiovascular diseases [15-18]. The miR-212/132 cluster is considered to be a central regulator in the development of pressure-overload-induced LVH and HF via the repression of the antihypertrophic transcription factor FOXO3 in mice with transverse aortic constriction (TAC) [19]. Moreover, the overexpression of miR-212, separate from miR-132, was reported to play a role in the development of LVH and HF via fetal gene reprogramming in human hearts [20]. Furthermore, the prohypertrophic potential of miR-212 was also confirmed in primary neonatal rat cardiomyocytes [21]. So far, there is no literature data available on cardiac miR-212 and its targets in the development of RIHD.

Chronic activation of the renin-angiotensin-aldosterone system (RAAS) plays a pivotal role in cardiovascular pathophysiology, including hypertension, cardiac hypertrophy, and HF via different systemic and tissue-specific mechanisms such as elevated nitro-oxidative and endoplasmic reticulum stress, inflammation, apoptosis, and fibrosis via transforming growth factor-β (TGF-β) signaling, and the transactivation of various intracellular protein kinases such as extracellular signal-regulated kinases (ERKs) and protein kinase B (AKT) [22,23]. There is some preclinical evidence that irradiation could upregulate angiotensin II (AngII) expression in the rat heart [24] and lungs [25] in a dose-dependent manner [26]. Interestingly, preclinical studies evaluating the cardiac effects of the widely used selective AngII type 1 receptor (AT1R) blockers in RIHD are lacking in the literature. Only two

clinical studies investigated the effects of angiotensin II receptor blockers (ARBs) in cancer patients treated with thoracic RT, and their results were controversial [27,28].

2. Aims of the thesis

The aims of the present thesis were the following:

i) set up a rat model with diastolic dysfunction in the acute phase, mild LVH in the early chronic phase, and severe LVH and HFpEF in the late chronic phase of RIHD,

ii) investigation of the potential role of miR-212 and

iii) its selected target FOXO3 in the development of radiation-induced cardiac pathologies, particularly hypertrophy and fibrosis, and

iv) test the effects of the ARB losartan (widely used in standard HF therapy) on the development of radiation-induced cardiac remodeling in the acute, early chronic, and late chronic phases of RIHD in our rat model (Figure 1).

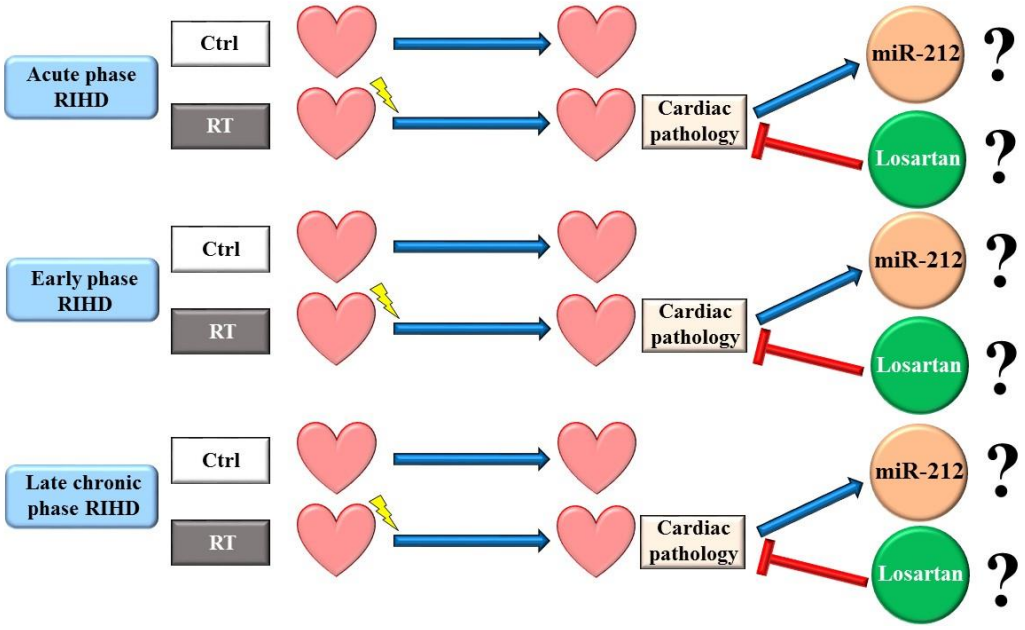

Figure 1 After radiotherapy, several cardiac pathologies can occur in the heart. Possible changes in miR-212 levels and the potential effects of losartan on the development of radiation-induced heart disease were investigated. Ctrl, control; miR-212, microRNA-212, RIHD, radiation-induced heart disease, RT, radiotherapy.

3. Materials and methods

This thesis is based on two different studies. The first one is the model setup study aiming to set up a rat model of RIHD in the acute, early chronic, and late chronic phases and investigate the role of miR-212 and its selected target FOXO3 in the development of LVH and fibrosis RIHD. The second study aimed at testing the effects of the ARB losartan on the development of cardiac remodeling in our previously set up rat model in the acute, early chronic, and late chronic phases of RIHD. The latter will be mentioned as the treatment study in this thesis.

3.1. Ethics approval

The studies were conducted according to the recommendations of the National Institutes of Health Guide for the Care and Use of Laboratory Animals (NIH Publication No. 85-23, Revised 1996) and guidelines of the Declaration of Helsinki. All institutional and national guidelines for the care and use of laboratory animals were followed. The studies were approved by the University of Szeged and the regional Animal Research Ethics Committee of Csongrád County (Csongrád county, Hungary; project licenses: XV.1181/2013 for the model setup study and XV./800/2019 for the treatment study).

3.2. Animals

Male Sprague-Dawley rats (6–8 weeks old) were used in the experiments. The animals were housed in pairs in individually ventilated cages (Sealsafe IVC system, Italy) in a temperature-controlled room with a 12 h:12 h light/dark cycle. After 1 week of acclimatization in a temperature-controlled room (22 ± 2◦C; relative humidity 55 ± 10%), the animals were randomly assigned to different groups. In the case of the model setup study, the standard rat chow was supplemented with 5% fat (Innovo Kft., Gödöllő, Hungary) [29]. In the case of the treatment study, standard rat chow was used [30]. Rat chow and tap water were supplied *ad libitum* in both studies.

3.3. Experimental setup

3.3.1. Setup of the rat model of RIHD

A total of 48 male Sprague-Dawley rats (200-220 g, 6-7 weeks old) were divided into three control and three irradiated groups in separate experiments (n=8 in each group) (Figure 2). A total of 24 animals received selective heart irradiation to induce RIHD, and a total of 24 animals served as controls. In the irradiated groups, animals received a single

dose of 50 Gy delivered to the whole heart to induce RIHD. Groups were followed up for 1, 3, and 19 weeks, respectively. Cardiac morphology and function were assessed by transthoracic echocardiography in all time points. The development of LVH and fibrosis in chronic RIHD was verified by the measurement of myocardial fiber diameters as well as picrosirius red and fast green staining for collagen at week 19. Total RNA was isolated from the hearts, and the myocardial expression of miR-212 and its direct target forkhead box O3 (FOXO3) was measured by qRT-PCR at every time point. Moreover, cardiac expression of FOXO3 and pFOXO3 were measured by Western blot technique at week 19.

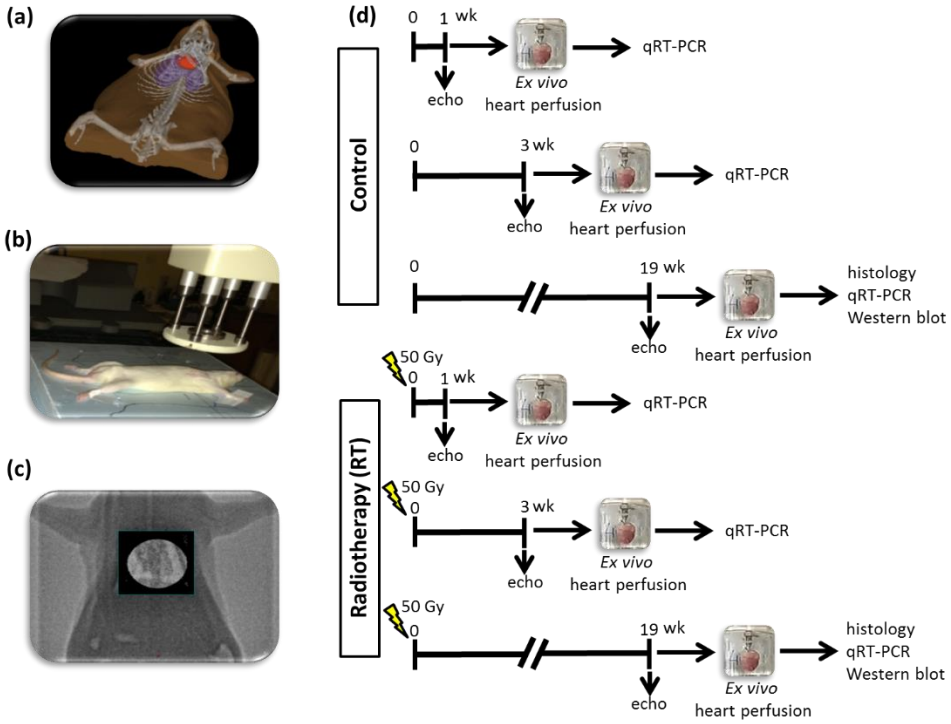

Figure 2 Experimental protocol figure. (a) 3D visualization of the rat heart based on CT scans, (b) positioning of the rat for delivering the radiation dose with a Primus linear accelerator under sodium pentobarbital anesthesia, (c) appropriate position of the animal proven by portal imaging, (d) experimental protocol.

3.3.2. Investigation of the cardiac effects of losartan in our rat model of RIHD

A total of 63 male Sprague-Dawley rats (220–300 g, 6–8 weeks old) were used in three separate experiments. A total of 21 animals served as controls, and a total of 42 animals received a single dose of 50 Gy delivered to the whole heart to induce RIHD as described previously [29,31]. Rats were divided into three groups (n = 6–9 in each group, Figure 3) and treated via oral gavage daily for 1, 3, and 15 weeks, respectively, as follows: (i) control group treated with tap water (per os 2 mL/kg/day, n = 7), (ii) RT only group treated with tap water (per os 2 mL/kg/day, n = 6–7), and (iii) RT plus losartan group

treated with losartan (per os 10 mg/kg/day dissolved in tap water in 2 mL/kg end volume, Arbartan 50 mg film-coated tablets, Teva Pharmaceutical Industries Ltd., Debrecen, Hungary, n = 7–9). Cardiac morphology and function were assessed by transthoracic echocardiography at the end-point of each experiment (Figure 3). At the end of the different follow-up times, rats were anesthetized with sodium pentobarbital (Euthasol, ip. 40 mg/kg Produlab Pharma b.v., Raamsdonksveer, The Netherlands). Then blood was collected from the abdominal aorta to measure routine laboratory parameters (Figure 3). After the blood sampling, hearts, lungs, and tibias were isolated, and the blood was washed out from the heart in calcium-free Krebs-Henseleit solution. Then left and right ventricles were separated and LV samples were prepared for histology and biochemical measurements. The development of LVH and fibrosis in the irradiated groups were verified by the measurement of cardiomyocyte cross-sectional areas on hematoxylin-eosin (HE)-stained slides and picrosirius red and fast green-stained (PSFG) slides (Figure 3). Total RNA was isolated from the left ventricles, and the expression of hypertrophy and fibrosis (i.e., *Myh6, Myh7, Ctgf, Tgfb*, *Col1a1*, and *Mmp2*), RAAS-associated (i.e., *Cma* and *Agt*), and inflammatory (i.e., *Il1*, *Il6*, and *Tnf*) markers were measured at the transcript level by qRT-PCR in every time point (Figure 3). Moreover, LV protein levels of angiotensin II receptor type 1 (AT1R), angiotensin II receptor type 2 (AT2R), transforming growth factor-beta receptor type 2 (TGF-βRII), mothers against decapentaplegic homolog 2/3 (SMAD2/3), total and phosphorylated signal transducer and activator of transcription 3 (STAT3 and pSTAT3), total and phosphorylated protein kinase B (AKT and pAKT), total and phosphorylated extracellular signal-regulated kinase 1 and 2 (ERK1, ERK2, pERK1, and pERK2), were measured by using Western blot technique at weeks 1, 3, and 15.

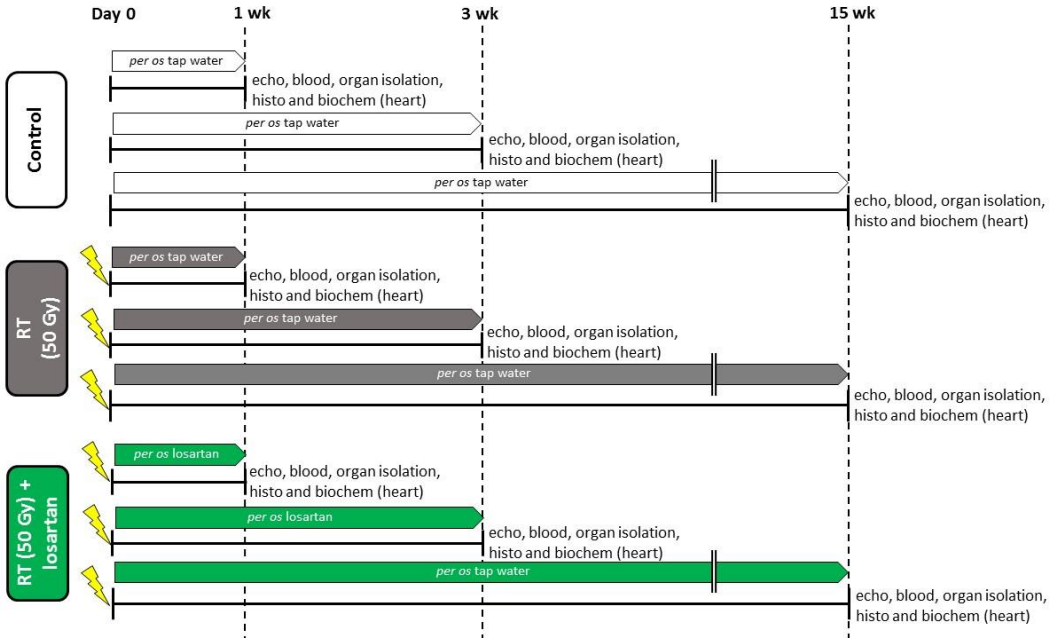

Figure 3 Experimental setup. Rats (n = 63) were divided into three groups (n = 6–9) and treated via oral gavage daily for 1, 3, or 15 weeks, respectively, as follows: (i) control group treated with tap water, (ii) radiotherapy (RT) only group treated with tap water, and (iii) RT plus losartan group treated with losartan (per os 10 mg/kg/day) dissolved in tap water. Cardiac morphology and function were assessed by transthoracic echocardiography (echo) at the end-points of each experiment under anesthesia. Then, blood was collected from the abdominal aorta to measure routine laboratory parameters, and hearts, lungs, and tibias were isolated. Left and right ventricles were separated, and LV samples were prepared for histology (histo) and biochemical measurements (biochem). The development of LVH and fibrosis in the irradiated groups was investigated by the measurement of cardiomyocyte cross-sectional areas on HE-stained slides and picrosirius red and fast green-stained slides. The expression of selected genes related to LVH and fibrosis, HF, RAAS, and inflammation were measured at the transcript level by qRT-PCR. Left ventricular levels of selected proteins related to the RAAS, cardiac hypertrophy, and fibrosis pathways were measured by Western blot.

3.4. Heart irradiation

Heart irradiation with a single dose of 50 Gy in the RT groups of both studies was carried out as described previously [29]. Before the irradiation, rats were anesthetized with sodium pentobarbital (Euthasol, ip. 40 mg/kg, Produlab Pharma b.v., Raamsdonksveer, The Netherlands), then fixed in the supine position to a flat surface couch. Briefly, the irradiation planning was based on a 3D model (Figure 2a), and the dose was delivered to the geometric center of the heart. For better coverage of the heart and lung protection, a 6 MeV electron radiation was given with a circle-shaped aperture with a 2 cm diameter (Figure 2b). The radiation dose was delivered with a Primus linear accelerator (Siemens Healthcare GmbH, Erlangen, Germany) at a dose intensity of 5 Gy/min if the appropriate position of the animal was proven using a built-in electronic portal imaging device (Figure 2c).

3.5. Transthoracic echocardiography

Cardiac morphology and function were assessed by transthoracic echocardiography in both studies as described previously [9], at weeks 1, 3, and 15 or 19 (Figures 2d, 3). Rats were anesthetized with 2% isoflurane (Forane, Aesica, Queenborough Limited, Queenborough, UK). Then, the chest was shaved, and the rat was placed supine on a heating pad. Two-dimensional, M-mode, Doppler, tissue Doppler, and four chamber-view images were performed by the criteria of the American Society of Echocardiography. In the model setup study, a Vivid 7 Dimension ultrasound system (General Electric Medical Systems, New York, NY, USA) was used with a phased array 5.5–12 MHz transducer (General Electric 10S probe, General Electric Medical Systems, New York, NY, USA) as described previously [29,32]. In the treatment study, a Vivid IQ ultrasound system (General Electric Medical Systems, New York, NY, USA) with a phased array 5.0–11 MHz transducer (General Electric 12S-RS probe, General Electric Medical Systems, New York, NY, USA) was used. Data of three consecutive heart cycles were analyzed (EchoPac Dimension, General Electric Medical Systems, New York, NY, USA) by an experienced investigator in a blinded manner. The mean values of three measurements were calculated and used for statistical evaluation. Systolic and diastolic wall thicknesses were obtained from parasternal short-axis view at the papillary muscles (in cases of anterior and inferior walls) and long-axis view at the mitral valve (in cases of septal and posterior walls). The LV diameters were measured using M-mode echocardiography from long-axis and short-axis views between the endocardial borders. The fractional shortening was calculated on M-mode images in the long-axis view. Diastolic function was assessed using pulse-wave Doppler across the mitral valve and tissue Doppler on the septal mitral annulus from the apical four-chamber view. Early (E) flow and septal mitral annulus velocity (e') indicate diastolic function. Ejection fraction was calculated on four-chamber view images using the modified Simpson method (i.e., biplane method of disks) requiring area tracing of LV cavity in end-systole and end-diastole.

3.6. Blood parameters

In the treatment study, blood was collected from the abdominal aorta at weeks 1, 3, and 15 (Figure 3). Total blood count and hematocrit were measured from whole blood by a hematology analyzer (XE-2100, Sysmex Corporation, Kobe, Japan) [33] to characterize

the severity of systemic inflammation and the compensatory increase in red blood cell synthesis associated with lung and heart damage due to RT.

3.7. Tissue harvesting

At weeks 1, 3, and 19 (in the model setup study) or 1, 3, and 15 (in the treatment study), the hearts of the animals of the respective subgroups were isolated under pentobarbital anesthesia (Euthasol, ip. 40 mg/kg, Produlab Pharma b.v., Raamsdonksveer, The Netherlands). The blood was washed out in calcium-containing (model setup study) or calcium-free (treatment study) Krebs-Henseleit solution (Figures 2d, 3). Then the hearts were weighed, left and right ventricles were separated and weighed, and the cross-section of the left ventricle at the ring of the papillae was cut and fixed in 4% buffered formalin for histological analysis. In the case of the model setup study, LV samples were prepared for histological analysis only at week 19 (Figure 2d). In the case of the treatment study, LV samples were prepared for histology at weeks 1, 3, and 15. Other parts of the left ventricles were freshly frozen in liquid nitrogen and stored at -80 °C until further biochemical measurements. Following the removal of the heart, the presence of pleural fluid was checked. Body weight, tibia length, and weights of the lungs were also measured.

3.8. Hematoxylin-eosin and picrosirius red and fast green stainings

Five μm thick transverse cut sections of the formalin-fixed and paraffin-embedded subvalvular areas of the left ventricles were stained with HE or PSFG as described previously [29]. Histological slides were scanned with a Pannoramic P250 scanner (3D-Histech, Budapest, Hungary) in the case of the model setup study and a Pannoramic Midi II scanner (3D-Histech, Budapest, Hungary) in the case of the treatment study. Digital HE- and PSFG-stained slides were captured at the magnification of ×40 and ×100 in Panoramic Viewer 1.15.4 (3DHistech, Budapest, Hungary; https://old.3dhistech.com/pannoramic_viewer).

In the model setup study, transverse transnuclear widths (i.e., cardiomyocyte diameters) were measured of 100 longitudinally oriented, mono-nucleated cardiomyocytes on left ventricle sections cut on the same plane [34,35]. In the treatment study, cardiomyocyte cross-sectional areas were measured to verify the development of LVH at the cellular level. The Biology Image Analysis Software (BIAS) was used for the evaluation [33]. BIAS (internal built, dated December 2019; https://single-cell-technologies.com/bias/) is

developed by Single-Cell Technologies Ltd., Szeged, Hungary. Image pre-processing was followed by deep learning-based cytoplasm segmentation. User-selected objects were forwarded to the feature extraction module, configurable to extract properties from the selected cell components. Here, transverse transnuclear cardiomyocyte cross-sectional areas were measured in 100 (consecutive) cardiomyocytes selected on the basis of longitudinal orientation and mononucleation from a single cut surface (digitalized histological slide) of the LV tissue blocks.

Cardiac fibrosis was assessed on PSFG slides with an in-house developed program [31]. Briefly, this program determines the proportion of red pixels of heart sections using two simple color filters. For each red–green–blue (RGB) pixel, the program calculates the color of the pixel in hue–saturation– luminance (HSL) color space. The first filter is used for detecting red portions of the image. The second filter excludes any white (empty) or light grey (residual dirt on the slide) pixels from further processing using a simple RGB threshold. In this way, the program groups each pixel into one of two sets: pixels considered red and pixels considered green but neither white nor grey. Red pixels in the first set represent collagen content and fibrosis. Green pixels in the second set correspond to cardiac muscle. Medium-size vessels and their perivascular connective tissue sheet, the subepicardial and subendocardial areas were avoided as much as possible. In the model setup study, the number of elements in the first set was divided by the number of elements in both sets, giving the ratio of the connective tissue in the LV slide. In the treatment study, the mean values of 10 representative images were calculated and used for statistical evaluation.

3.9. MicroRNA expression profiling by qRT-PCR

In our model setup study, quantitative RT-PCR was performed with miR-specific primers to monitor miR expression as described earlier (Figure 2d) [19,35]. In the case of miR-212, RNA was isolated using Trizol reagent (Invitrogen, #15596-018) from heart tissue. For quantitative detection of miR-212, TaqMan MicroRNA Reverse Transcription Kit (Applied Biosystems, #4366597), TaqMan miR-212, and snoRNA (U64702) Assays (Applied Biosystems, #A25576 and #4427975), and Absolute Blue qPCR Mix (Abgene, #AB-4136/B) were used according to the manufacturer’s instructions. SnoRNA was used as a control for normalization.

3.10. mRNA expression profiling by qRT-PCR

Quantitative RT-PCR was performed with gene-specific primers to monitor mRNA expression as described previously (Figure 2d) [35,36]. RNA was isolated from LV tissue using Qiagen RNeasy Fibrous Tissue Mini Kit (Qiagen, Hilden, Germany).

In the model set up study, 3 µg of total RNA was reverse transcribed using High-Capacity cDNA Reverse Transcription Kit (Applied Biosystems, #4368814), specific primers for *Foxo3* (forward primer sequence: *gatggtgcgctgtgtgccctac*, reverse primer sequence: *ccaagagctcttgccagtccctt*), and FastStart Essential DNA Green Master (Roche, #06402712001) according to the manufacturer's instructions. Hypoxanthine phosphoribosyl transferase 1 (*Hgprt1*, forward primer sequence: *gaccggttctgtcatgtcg*, reverse primer sequence: *acctggttcatcatcactaatcac*), peptidyl prolyl isomerase A (*Ppia*, forward primer sequence: *tgctggaccaaacacaaatg*, reverse primer sequence: *caccttcccaaagaccacat*) and ribosomal protein lateral stalk subunit P2 (*Rplp2*, forward primer sequence: *agcgccaaagacatcaagaa*, reverse primer sequence: *tcagctcactgatgaccttgtt*) were used as controls for normalization. At week 19, *Foxo3* expression was also measured by another method using iScript™cDNA Synthesis Kit (BioRad Laboratories Inc., Hercules, CA, USA) and Specific primers for forkhead box O3 (*Foxo3*: #qRnoCID0003272) and glyceraldehyde-3-phosphate dehydrogenase (*Gapdh:* #qRnoCID0057018) as a housekeeping gene, SsoAdvanced™ Universal SYBR® Green Supermix (BioRad Laboratories Inc., Hercules, CA, USA) according to the manufacturer's instructions.

In the treatment study, 100 µg of total RNA was reverse transcribed using iScript™cDNA Synthesis Kit (BioRad Laboratories Inc., Hercules, CA, USA). Specific primers (*Agt*: angiotensinogen, #qRnoCED0051666; *Cma1*: chymase, #qRnoCED0005462; *Col1a1*: collagen type 1 alpha 1 chain, #qRnoCED0007857; *Ctgf* : connective tissue growth factor, #qRnoCED0001593; *Il1*: interleukin-1, #qRnoCID0002056; *Il6*: interleukin-6, #qRnoCID0053166; *Mmp2*: matrix metalloproteinase 2, #qRnoCID0002887; *Myh6*: α-myosin heavy chain, #qRnoCID0001766; *Myh7*: β-myosin heavy chain, #qRnoCED0001215; *Tgfb*: transforming growth factor-β, #qRnoCID0009191, *Tnf-a*: tumor necrosis factor-α, #qRnoCED0009117) and SsoAdvanced™ Universal SYBR® Green Supermix (BioRad Laboratories Inc., Hercules, CA, USA) were used according to the manufacturer's instructions. Ribosomal protein lateral stalk subunit P2 (*RpIp2*,

forward primer sequence: *agcgccaaagacatcaagaa* and reverse primer sequence: *tcagctcactgatgaccttgtt*) was used as a housekeeping control gene for normalization.

3.11. Western blot

To investigate gene expression changes at the protein level, standard Western blot techniques were used in both studies [9,33,35,37].

3.11.1. Western blot in the model setup study

Phosphorylated FOXO3 (pFOXO3, 97 kDa) and FOXO3 (82 to 97 kDa) with GAPDH (36 kDa) loading background were assessed at week 19 (Figure 2d). Heart tissue samples (n=7-8) were homogenized with an ultrasonicator (UP100H Hielscher, Teltow, Germany) in RIPA (Radioimmunoassay) buffer [50 mM Tris–HCl (pH 8.0), 150 mM NaCl, 0.5% sodium deoxycholate, 5 mM ethylenediamine tetra-acetic acid (EDTA), 0.1% sodium dodecyl sulfate (SDS), 1% NP-40 (Cell Signaling, Carlsbad, CA, USA)] supplemented with protease inhibitor cocktail and phosphatase inhibitors phenylmethanesulfonyl fluoride (PMSF; Sigma-Aldrich, St. Louis, MO, USA) and sodium fluoride (NaF; Sigma-Aldrich, St. Louis, MO, USA). The crude homogenates were centrifuged at 15 000× g for 30 min at 4°C. After quantification of protein concentrations of the supernatants using BCA Protein Assay Kit (Pierce, Rockford, IL, USA), 25 µg reduced and denatured protein was loaded, and SDS-PAGE (10% gel, 90 V, 2 h) was performed, followed by transfer of proteins onto nitrocellulose membrane (20% methanol, 35 V, 2 h). The efficacy of transfer was checked using Ponceau staining. The membranes were cut horizontally into parts corresponding to the molecular weights of FOXO3, and GAPDH. Then the membranes were blocked for 1 h in 5% (w/v) BSA at room temperature and then incubated with primary antibodies (Cell Signaling, Beverly, MA, USA; overnight, 4°C, 5% BSA) in the concentrations of 1:1000 against pFOXO3 (Ser253; #13129), 1:500 against FOXO3 (#2497) or 1:5000 against GAPDH (#2118 overnight, 4°C, 1% BSA). Then the membranes were incubated with horseradish peroxidase (HRP)-conjugated goat anti-rabbit secondary antibody 1:2000 (1:1000 for FOXO3, 1:5000 for GAPDH) (Dako Corporation, Santa Barbara, CA, USA; 45 min, room temperature, 1% BSA). After the assessment of pFOXO3, the membranes were stripped and reassessed for the total amount of proteins. An enhanced chemiluminescence kit (Cell Signaling, Carlsbad, CA, USA) was used to develop the membranes. The chemiluminescence signals were analyzed and evaluated by Quantity One Software.

3.11.2. Western blot in the treatment study

AT1R (41 kDa), AT2R (41 kDa), SMAD2/3 (52 and 60 kDa), TGF-βRII (85 kDa), STAT3 (79 and 86 kDa), pSTAT3 (79 and 86 kDa), AKT (60 kDa), pAKT (60 kDa), ERK1/2 (42 and 44 kDa), and pERK1/2 (42 and 44 kDa) with GAPDH (36 kDa) loading background were assessed at weeks 1, 3, and 15. Left ventricular samples (n =6–7 in each group, total n = 21 at week 1, total n = 20 at week 3, and total n = 20 at week 15) were homogenized with an ultrasonicator (UP100H, Hielscher, Germany) in Radio-Immunoprecipitation Assay (RIPA) buffer [50mM Tris-HCl (pH 8.0), 150mM NaCl, 0.5% sodium deoxycholate, 5mM EDTA, 0.1% SDS, 1% NP-40 (Cell Signaling Technology Inc., Danvers, MA, USA)] supplemented with PMSF (Sigma-Aldrich, St. Louis, MO, USA) and NaF (Sigma-Aldrich, St. Louis, MO, USA). The crude homogenates were centrifuged at 15,000 x g for 30 min at 4 °C. After quantifying the supernatants' protein concentrations using the BCA Protein Assay Kit (Pierce Thermo Fisher Scientific Inc., Waltham, MA, USA), 25 μg of reduced and denaturized protein was loaded. Then sodium dodecyl-sulfate polyacrylamide gel electrophoresis (SDS-PAGE, 50V, 4 h) was performed (10% gel in case of AT1R, AT2R, SMAD2/3, TGF-βRII, STAT3, pSTAT3, AKT, pAKT, ERK1/2, and pERK1/2) followed by the transfer of proteins onto a nitrocellulose membrane (10% methanol in case of AT1R, AT2R, SMAD2/3, TGF-βRII and 20% methanol in case of STAT, pSTAT, AKT, pAKT, ERK1/2, pERK1/2, 35V, 2 h). The efficacy of transfer was checked using Ponceau staining. The membranes were cut horizontally into parts corresponding to the molecular weights of AT1R, AT2R, SMAD2/3, TGF-βRII, STAT3, pSTAT3, AKT, pAKT, ERK1/2, pERK1/2, and GAPDH. Membranes were blocked for 1 h in 5% (w/v) bovine serum albumin (BSA, Sigma-Aldrich, Saint Louis, MO, USA) and were incubated with primary antibodies in the concentrations of 1:1000 against AT1R (#ab124734, Abcam PLC, Cambridge, UK), AT2R (#ab92445, Abcam PLC, Cambridge, UK), SMAD2/3 (#8685T, Cell Signaling Technology Inc., Danvers, MA, USA), TGF-βRII (#79424T, Cell Signaling Technology Inc., Danvers, MA, USA), STAT3 (#9139, Cell Signaling Technology Inc., Danvers, MA, USA), pSTAT3 (#9145, Cell Signaling Technology Inc., Danvers, MA, USA), AKT (#2920, Cell Signaling Technology Inc., Danvers, MA, USA), pAKT (#4060, Cell Signaling Technology Inc., Danvers, MA, USA), ERK1/2 (#4696, Cell Signaling Technology Inc., Danvers, MA, USA), pERK1/2 (#9101S, Cell Signaling Technology Inc., Danvers, MA, USA), or 1:5000 against GAPDH (#2118, Cell Signaling Technology Inc., Danvers, MA, USA) overnight at 4 °C in 5% BSA. Then the membranes

were incubated with IRDye® 800CW Goat Anti-Rabbit and/or IRDye® 680RD Goat Anti-Mouse secondary antibody (LI-COR Biosciences, Lincoln, NE, USA, in the concentrations of 1:5000) for 1 h at room temperature in 5% BSA antibodies to detect proteins with similar molecular weight on the same membrane where it is applicable. Fluorescent signals were detected by Odyssey CLx machine (LI-COR Biosciences, Lincoln, NE, USA), and digital images were analyzed and evaluated by densitometry with Quantity One Software (Bio-Rad Laboratories Inc., Hercules, CA, USA).

3.12. Statistical analysis

Statistical analysis was performed using Sigmaplot 12.0 for Windows (Systat Software Inc, San Jose, CA, USA). All values are presented as mean±SEM except the gene expression data measured by qRT-PCR in the model setup study. $P < 0.05$ was accepted as a statistically significant difference. Specific sample numbers used for measurements are described in the corresponding figure and table legends. Data showed normal distribution unless otherwise indicated.

In the model setup study, the data measured at different follow-up time points in separate experiments, including body weight, heart weight, heart weight to body weight ratio, lung weight, and echocardiographic parameters, were compared using One-Way ANOVA among the groups. Bonferroni test was used as a *post hoc* test. Two sample t-tests (in case of the normal distribution of the data) or Mann Whitney U tests (in case of the non-normal distribution of the data) were used to determine the effect of RT on all measured parameters within each time point. In the case of target genes, the analysis of relative gene expression data was performed using the $2^{-\Delta\Delta Ct}$ method. Gene expression ratios with a p-value of <0.05 and fold change of <-2.00 or fold change of >2.00 were considered as repression or overexpression respectively in gene activity.

One-Way ANOVA was used in the treatment study to determine the statistical significance between all measured parameters within each time point. A Holm-Sidak test was used as a post hoc test.

4. Results

4.1. Results of the model setup study

4.1.1. Characteristics of the RIHD models

At week 1, there was no difference in the body weight between the control and irradiated groups (Table 1). At week 3, the irradiated animals presented a trend toward a lower body weight as compared to the time-matched controls (Table 1). At week 19, the irradiated rats showed significantly lower body weight as compared to the time-matched controls (Table 1).

Parameter (unit)	week 1		week 3		week 19	
	Control	RT	Control	RT	Control	RT
BW (g)	270±9	254±8	394±11$^{\#}$	366±10$^{\#}$	597±24$^{\#}$	425±43$^{\#}$*
HW (g)	1.21±0.07	1.13±0.05	1.33±0.05	1.45±0.09$^{\#}$	1.74±0.08$^{\#}$	1.34±0.06$^{\#}$*
Lung weight (g)	1.35±0.06	1.64±0.07*	2.01±0.09$^{\#}$	2.72±0.25$^{\#}$*	2.29±0.17$^{\#}$	2.26±0.18$^{\#}$
HW/BW*1000	4.45±0.13	4.44±0.10	3.38±0.10$^{\#}$	3.99±0.32$^{\#}$	2.92±0.09$^{\#}$	3.36±0.35$^{\#}$

Table 1 Characteristics of the RIHD models at weeks 1, 3, and 19, respectively. Values are mean±SEM, n=8, *p<0.05 vs. control, unpaired t-test within the same time points. p-values refer to the unpaired t-test at each time point. $^{\#}$p<0.05 vs. week 1 within the same group (control or RT), One-Way ANOVA, Bonferroni post hoc test. BW, body weight; HW, heart weight; RT, radiotherapy

At weeks 1 and 3, there was no pleural fluid in the irradiated animals at autopsy. At week 19, extensive pleural fluids were found in almost all animals in the irradiated group (data not shown). At the macroscopic level, no major heart pathologies (including the large vessels, the valves, the coronary arteries, etc.) were observed in the irradiated groups at any follow-up time point. At weeks 1 and 3, lung weights were significantly increased in the irradiated groups as compared to the time-matched controls (Table 1). At week 19, no difference was found in lung weights between the groups (Table 1). At weeks 1 and 3, there was no difference in heart weights between the irradiated groups and their time-matched controls (Table 1). However, the heart-to-body weight ratio showed a trend toward an increase in the irradiated group at week 3 (Table 1). At week 19, the tibia length (4.23 ± 0.05 vs.4.46 ± 0.04 cm, $p = 0.003$) and the heart weight was significantly lower in the irradiated group than in the control group, pointing out the growth retardation in these animals (Table 1). At week 19, all of the morphometric parameters (body weight, heart weight, heart rate to body weight ratio, and lung weight) were significantly higher in both the control and irradiated groups as compared to week 1 parameters within the same group, due to the growth of the animals (Table 1). Transthoracic echocardiography was performed at weeks 1, 3, and 19 to investigate whether the development of acute and

chronic RIHD leads to an alteration in myocardial morphology and function (Table 2; Figures 2d, 4).

4.1.2. HFpEF developed in RIHD at week 19

At week 1, the LV wall thicknesses were not different between the irradiated and time-matched control groups (Table 2). In contrast, the left ventricular end-systolic and end-diastolic diameters (LVESD and LVEDD), as well as the volumes (LVESV and LVEDV), were significantly decreased in the irradiated animals, pointing out an acute dysfunction in the contraction and relaxation as well (Table 2).

Parameter (unit)	week 1		week 3		week 19	
	Control	RT	Control	RT	Control	RT
PWTs (mm)	2.78±0.12	2.95±0.11	2.94±0.11	3.16±0.12	3.19±0.16$^{\#}$	3.37±0.24$^{\#}$
PWTd (mm)	1.85±0.07	1.76±0.07	2.01±0.12	1.80±0.13	2.00±0.11	2.44±0.14$^{\#}$*
SWTs (mm)	2.91±0.13	3.06±0.08	3.13±0.08	3.54±0.13*	3.27±0.13$^{\#}$	3.71±0.29$^{\#}$
SWTd (mm)	1.64±0.07	1.79±0.10	1.65±0.05	1.85±0.04*	1.87±0.12$^{\#}$	2.69±0.34$^{\#}$*
LVEDD (mm)	7.73±0.10	7.31±0.15*	7.99±0.13	7.63±0.25	8.55±0.14$^{\#}$	6.04±0.52$^{\#}$*
LVESD (mm)	4.45±0.20	3.76±0.23*	4.37±0.16	3.50±0.26*	4.13±0.23	2.59±0.55$^{\#}$*
FS (%)	43±3	48±3	45±2	54±3*	46±1	63±6$^{\#}$*
LVEDV (µl)	135±15	94±6*	120±9	114±8	262±27$^{\#}$	91±13*
LVESV (µl)	54±6	33±3*	38±3$^{\#}$	37±3	100±17$^{\#}$	36.±5.*
SV (µl)	82±9	61±5	82±6	77±6	162±14$^{\#}$	56±9*
HR (1/min)	349±10	373±6	338±14	352±14	291±7$^{\#}$	279±7$^{\#}$
E/e’	13±1	23±1*	15±1	30±3*	17±1	25±2
e' (m/s)	0.079±0.005	0.042±0.002*	0.071±0.007	0.038±0.003*	0.055±0.004$^{\#}$	0.042±0.005*

Table 2 Effects of radiotherapy on various in vivo LV morphological and functional parameters measured by transthoracic echocardiography at weeks 1, 3, and 19, respectively. Transthoracic echocardiographic measurements were performed 1, 3, and 19 weeks after the selective heart irradiation in separated experiments. Values are mean ±SEM, n=8, *$p<0.05$ vs. control, unpaired t-test within the same time point. p-values refer to the unpaired t-test at each time point. $^{\#}p<0.05$ vs. week 1 within the same group (control or RT), One-Way ANOVA, Bonferroni post hoc test. 2D, two-dimensional; E-wave, early ventricular filling velocity; FS, fractional shortening; HR, heart rate; LV, left ventricular; LVEDD, left ventricular end-diastolic diameter; LVEDV, left ventricular end-diastolic volume; LVESD, left ventricular end-systolic diameter; LVESV, left ventricular end-systolic volume; MM, M (motion) mode; PWTd, posterior wall thickness-diastolic; PWTs, posterior wall thickness-systolic; PW, pulse wave; RT, radiotherapy; SV, stroke volume; SWTd, septal wall thickness-diastolic; SWTs, septal wall thickness-systolic; TD, tissue Doppler.

Stroke volume (SV) showed a statistically nonsignificant trend toward a decrease in the irradiated animals as compared to the time-matched controls (Table 2). There was a trend to an increase in heart rate (HR) in the irradiated animals, likely a compensatory mechanism, to maintain cardiac output (CO) (Table 2). The ratio of the early flow velocity (E) and the septal mitral annulus velocity (e′) significantly increased, and e′ significantly

decreased in irradiated rats indicating the presence of concomitant diastolic dysfunction (Table 2).

At week 3, septal wall-thicknesses in both diastole and systole were significantly increased in the irradiated rats indicating the development of LVH (Table 2). The LVESD was significantly decreased, and fractional shortening (FS) was significantly increased in the irradiated animals in this early phase of hypertrophy (Table 2). DD was also present in the irradiated group characterized by significantly increased E/e′ and significantly decreased e′ (Table 2).

At week 19, LV wall thicknesses, including anterior and inferior walls both in systole and diastole and septal and posterior walls in diastole, significantly increased in irradiated rats, pointing to the presence of a marked concentric LVH (Table 2; Figures 4a–c). In addition, both LVESD and LVEDD significantly decreased in irradiated animals compared to the controls (Figure 4d). Indeed, LVESV and LVEDV decreased in the irradiated group (Table 2). In contrast, ejection fraction (EF) remained unchanged in the irradiated group showing a characteristic feature of HFpEF (Figure 4e).

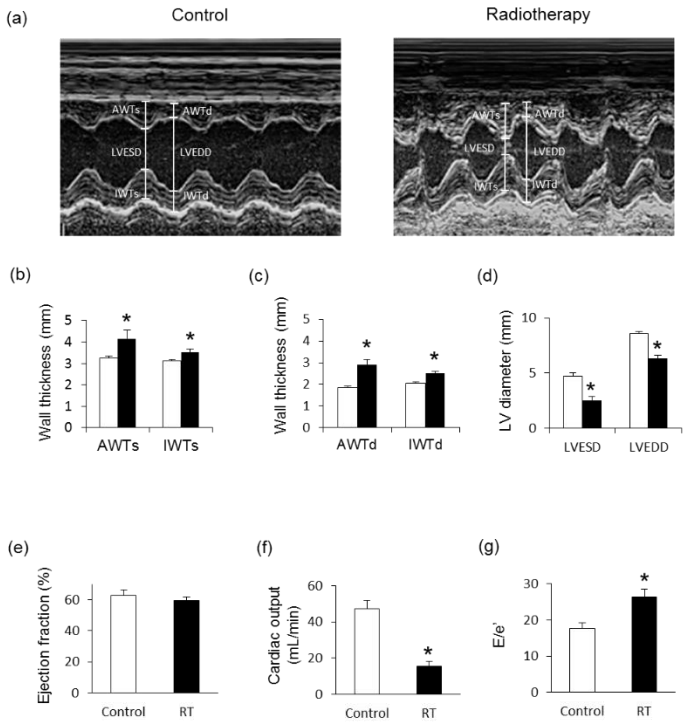

Figure 4 Echocardiographic results at week 19. (a) Representative M-mode images, (b) anterior and inferior wall thicknesses in systole (AWTs and IWTs), (c) anterior and inferior wall thicknesses in diastole (AWTd and IWTd), (d) left ventricular end-systolic diameter (LVESD) and left ventricular end-diastolic diameter (LVEDD), (e) ejection fraction, (f) cardiac output, and (g) E/e' ratio. White bars represent the control group, and black bars represent the irradiated group. RT means radiotherapy. Values are means ± SEM, n = 8, *p< 0.05.

There was no difference in HR between the two groups at this stage (Table 2). SV and CO were significantly reduced in irradiated rats compared to controls (Table 2; Figure 4f). More importantly, e′ was significantly decreased, and E/e′ was significantly increased, indicating DD (Table 2; Figure 4g). Septal and posterior wall thicknesses were

significantly increased both in the control and irradiated groups at week 19 compared to data measured at week 1 in the same group due to the growth of the animals (Table 2). Interestingly, LVEDD and LVESD were significantly decreased in the RIHD group at week 19 compared to week 1 values, indicating the presence of marked concentric hypertrophy (Table 2). In the control group, LVEDD was significantly increased at week 19 compared to week 1 values due to the normal growth of the animals (Table 2). HR was significantly decreased in both the control and irradiated groups at week 19 compared to week 1 values which might be caused by the aging of the animals (Table 2).

4.1.3. Cardiomyocyte hypertrophy and interstitial fibrosis in RIHD at week 19

To verify the development of severe LVH seen on echocardiographic images at week 19, cardiomyocyte diameters were measured histologically (Figures 5a, b). Cross-sectional cardiomyocyte diameters significantly increased in RIHD, proving the presence of LVH at the cellular level at week 19 (Figure 5b). Collagen deposition was assessed to investigate the development of fibrosis in response to selective heart irradiation at week 19 (Figures 5c, d). Significant interstitial fibrosis was found with slight but consistent collagen depositions in all studied segments of the irradiated hearts (Figures 5c, d).

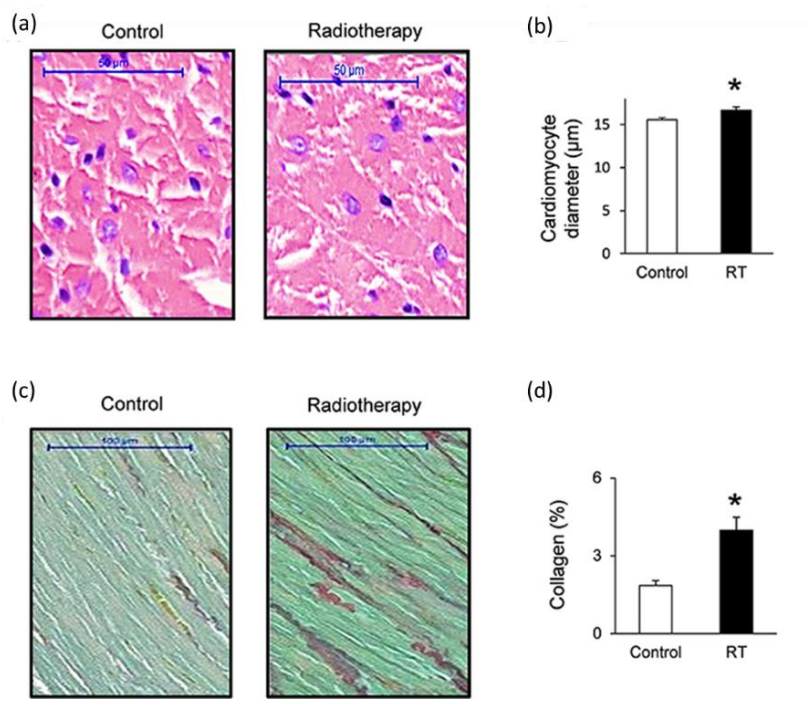

Figure 5 Histology results at week 19. (a) Hematoxylin-eosin stained slides, (b) cardiomyocyte diameter, (c) picrosirius red and fast green stained slides, (d) cardiac collagen content. White bars represent the control group, and black bars represent the irradiated group. RT means radiotherapy. Values are means ± SEM, n = 8, *p < 0.05.

4.1.4. Cardiac overexpression of miR-212 at weeks 3 and 19

At week 1, there was no change in the cardiac expression of miR-212 between the irradiated and control groups (Table 3). Both at weeks 3 and 19, miR-212 was significantly overexpressed in the irradiated hearts compared to the controls (Table 3; Figure 6a).

Gene name	Gene symbol	week 1				week 3			
		log_2 change	SD log_2 change	p-value	Fold change	log_2 change	SD log_2 change	p-value	Fold change
miR-212	*miR-212*	-0.38	0.63	0.183	-1.30	-1.01	0.38	0.000	2.15*
Forkhead box O3	*Foxo3*	-0.02	0.41	0.916	-1.01	-0.19	0.29	0.170	-1.14

Table 3 Cardiac *Foxo3* gene expression changes 1 and 3 weeks after the selective heart irradiation (qRT-PCR results). Gene expression ratios at week 1 and 3, respectively, (radiotherapy vs. control). Fold change of <−2.00 or >2.00 (repression or overexpression, respectively) and a p-value of <0.05 were considered as significant changes*, n=6, unpaired t-test or Mann-Whitney U test.

4.1.5. Repression of the antihypertrophic FOXO3 at the mRNA level in RIHD only at week 19

Both at week 1 and 3, there was no change in the cardiac expression of the antihypertrophic miR-212 target molecule *Foxo3* between the irradiated and time-matched control groups (Table 3). In contrast, cardiac expression of *Foxo3* was significantly decreased at the mRNA level in irradiated hearts as compared to controls at week 19 (Table 3; Figure 6b).

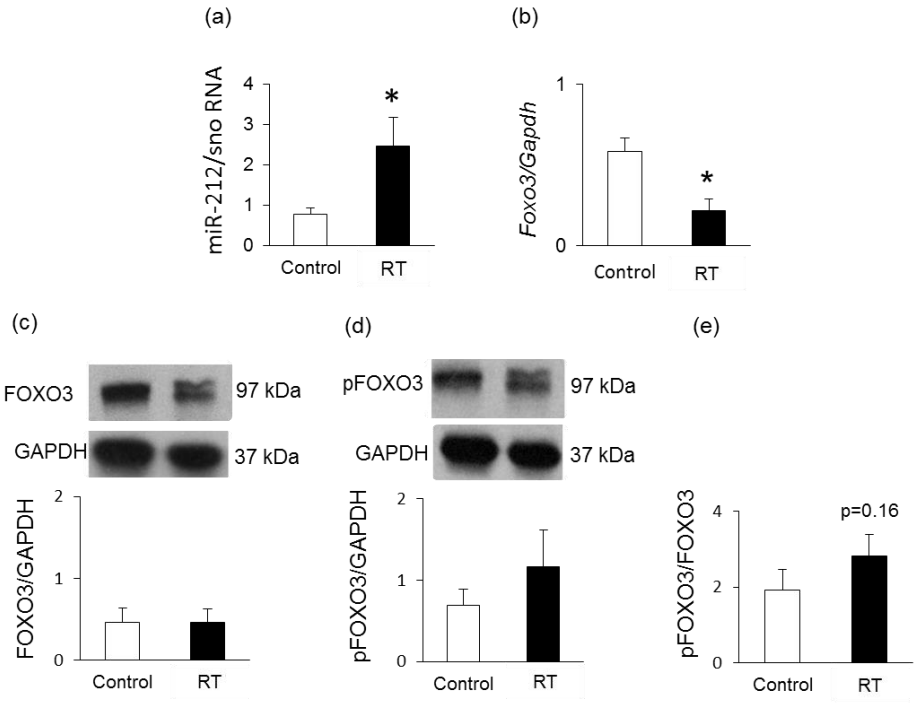

Figure 6 qRT-PCR and Western blot results at week 19. (a) Cardiac miR-212 expression, (b) cardiac *Foxo3* mRNA expression, (c) cardiac FOXO3 expression, (d) cardiac pFOXO3 expression, and (e) cardiac pFOXO3/FOXO3 ratio. White bars represent the control group, and black bars represent the irradiated group. RT means radiotherapy. Values are means ± SEM, n = 7–8, *p < 0.05. In the case of Western blot results, only the representative blot image was shown, and the mean was calculated.

The expression of the antihypertrophic miR-212 target molecule FOXO3 was also investigated at the protein level using a Western blot technique at week 19. FOXO3 protein levels failed to decrease in the irradiated hearts as compared to the controls (Figure 6c). The cardiac pFOXO3 level and the pFOXO3/FOXO3 ratio showed a statistically non-significant trend toward an increase in RIHD as compared to the control group (Figures 6d, e). An increased pFOXO3/FOXO3 ratio is considered to be a characteristic shift in pressure-overload-induced cardiac hypertrophy forms [38]. In our RIHD model, the statistically non-significant trend toward an increase in the pFOXO3/FOXO3 ratio seems to be independent of the effect of miR-212 in RIHD.

4.2. Results of the treatment study

4.2.1. Systemic effects of the radiotherapy in our RT model

Altogether two animals died in the RT only group (in the 3-week and 15-week subgroups). Before the treatments, there were no significant differences in the body weights between the groups in each experiment (Table 4). At week 1, there were no significant differences in the tibia length, heart weight, lung weight, and right ventricular

weight between the groups. In contrast, body weight was significantly lower in the RT plus losartan group as compared to the control group (Table 4). Moreover, LV weight was significantly reduced in both RT groups irrespective of the addition of losartan treatment compared to the control group at week 1 (Table 4). At week 3, there was no significant difference in tibia length, heart weight, or right ventricular weight between the groups (Table 4). However, body weight and LV weight were significantly smaller in the RT groups irrespective of losartan treatment compared to the control group at week 3, probably due to the detrimental effects of ionizing radiation in the RT groups (Table 4). Moreover, lung weights were significantly higher both in the RT only and losartan-treated RT groups compared to the control group, suggesting the presence of pulmonary edema at week 3 (Table 4) (fluid was found in the lungs during the autopsy, data not shown). At week 15, body weight, tibia length, heart weight, and LV weight were significantly smaller in both RT groups, irrespective of losartan treatment, indicating that the irradiated animals had severe developmental retardation in the late chronic phase of RIHD (Table 6). In contrast, right ventricular and lung weights were not significantly different between the groups (Table 4).

Parameter (unit)	Week 1			Week 3			Week 15		
	Control	RT	RT Los	Control	RT	RT Los	Control	RT	RT Los
BW at the beginning (g)	233±8	233±5	232±4*	282±5	281±7	282±6	261±3	263±4	261±5
BW at the endpoint (g)	269±7	258±6	251±5*	382±9.57	338±5.22*	344±8.8*	525±14	377±29*	414±17*
Tibia length (cm)	3.39±0.06	3.36±0.03	3.33±0.04	3.83±0.07	3.73±0.05	3.86±0.09	4.5±0.04	4.25±0.08*	4.28±0.04*
Heart weight (g)	0.91±0.02	0.87±0.03	0.87±0.02	1.16±0.03	1.1±0.04	1.06±0.05	2.24±0.11	1.75±0.04*	1.63±0.11*
LV weight (g)	0.62±0.01	0.57±0.02*	0.55±0.02*	0.77±0.02	0.69±0.02*	0.66±0.02*	1.3±0.05	0.99±0.03*	0.88±0.06*
RV weight (g)	0.17±0.01	0.17±0.01	0.18±0.01	0.24±0.01	0.25±0.01	0.23±0.02	0.35±0.01	0.33±0.01	0.32±0.02
Lung weight (g)	1.3±0.02	1.29±0.05	1.3 ±0.03	1.7±0.12	2.98±0.26*	2.47±0.29*	1.64±0.04	1.88±0.32	1.50±0.1

Table 4 Post-RT body weights, organ weights, and tibia lengths at weeks 1, 3, and 15. Values are presented as mean±S.E.M., *p<0.05 vs. control group, (n=6–7, One-Way ANOVA, Holm-Sidak post hoc test). RT, radiotherapy only group (50 Gy); RT Los, RT plus losartan group; BW, body weight; LV, left ventricle; RV, right ventricle.

Blood counts, hemoglobin concentrations, and hematocrit levels were determined at weeks 1, 3, and 15 to investigate the effects of losartan on the severity of systemic inflammation and the compensatory increase in hemoglobin synthesis associated with radiation-induced lung and heart damage (Table 5). One week post-RT, white blood cell counts were not significantly higher (7% increase, $p = 0.646$) in the RT only group and

significantly increased in the RT plus losartan group compared to that in the control group (Table 5). At week 3, white blood cell counts were significantly increased in the irradiated groups irrespective of losartan treatment, suggesting the presence of systemic inflammation at that time point (Table 5). No such differences were detected between the groups at week 15 (Table 5). RT might lead to the activation of platelets which are considered important sources of pro-thrombotic agents during the inflammatory process [39]. Platelet counts were not significantly different between the groups at weeks 1 and 15. However, platelet counts showed a non-significant increase (16%, p = 0.073) in the RT only group and a significant increase in the losartan-treated RT group as compared to that in the control group at week 3 (Table 5).

Parameter (unit)	Week 1			Week 3			Week 15		
	Control	RT	RT Los	Control	RT	RT Los	Control	RT	RT Los
WBC counts (10^9/L)	5.79±0.43	6.18±0.7	7.15±0.36*	4.44±0.56	6.77±0.8*	7.16±0.7*	6.09±0.58	6±0.39	6.51±0.52
Platelet counts (10^9/L)	569±8	587±20	643±33	559±27	646±35	673±31*	636±17	586±67	736±53
RBC counts (10^{12}/L)	6.69±0.11	7.37±0.29*	7.74±0.2*	7.54±0.15	7.54±0.18	7.95±0.18	8.30±0.15	9.16±0.44	9.50±0.3*
HGB (g/L)	130±3	143±5	146±3*	143±3	142±3	152±3	146±2	165±8*	175±7*
HCT (L/L)	0.41±0.01	0.44±0.02	0.45±0.01	0.44±0.01	0.45±0.01	0.47±0.01	0.43±0.01	0.49±0.02*	0.50±0.02*

Table 5 Post-RT blood cell counts, hemoglobin, and hematocrit values. Values are presented as mean±S.E.M., *p<0.05 vs. control group, #p<0.05 vs. RT group (n=6–7, One-Way ANOVA, Holm-Sidak post hoc test). HGB, hemoglobin; HCT, hematocrit; RBC, red blood cell; RT, radiotherapy only group (50 Gy); RT Los, RT plus losartan group; WBC, white blood cell.

At week 1, red blood cell counts were significantly elevated in both RT groups compared to the control group (Table 5). Hemoglobin level showed a trend to an increase (10%, p = 0.057) in the RT only group and a significant increase in the RT plus losartan group compared to the control group (Table 5). There was no significant difference in the hematocrit levels between the groups (Table 5). At week 3, there were no significant differences in the red blood cell counts, hemoglobin, or hematocrit levels between the groups (Table 5). In contrast, at week 15, red blood cell counts showed a trend to an increase (10%, p = 0.076) in the RT only group and a significant increase in the RT plus losartan group, while hemoglobin concentrations and hematocrit levels were significantly increased in the RT groups irrespective of losartan treatment compared to the control group (Table 5).

4.2.2. Post-RT diastolic dysfunction was alleviated by losartan at weeks 1 and 3 but not at week 15

Transthoracic echocardiography was performed at weeks 1, 3, and 15 to monitor the effects of RT and losartan on cardiac morphology and function (Figure 3). At week 1, the diastolic parameter mitral valve early flow velocity (E) was not significantly different between the groups (Table 6). A sensitive parameter of the diastolic function, the septal mitral annulus velocity (e'), was significantly decreased in the RT only group as compared to the control group, indicating an early-phase DD at week 1 (Table 6; Figure 7a). Septal e' was not significantly different between the control and the losartan-treated RT groups (Table 6; Figure 7a). Another indicator of DD, the E/e' ratio, was not significantly different between the RT only and the control groups. However, the E/e' ratio was significantly reduced in the RT plus losartan group as compared to the RT only or control groups at week 1 (Figure 7b). At week 3, E velocity was not significantly different between the RT only and the control group (Table 6). In contrast, E velocity was significantly lower in the losartan treated RT group than in RT only group at week 3 (Table 6). At week 15, E velocity was significantly lower in both RT groups irrespective of losartan treatment compared to the control group (Table 6). At weeks 3 and 15, the significantly decreased septal e' and significantly increased E/septal e' ratio indicated the presence of DD in the RT only groups compared to the time-matched control groups, respectively (Table 6; Figure 7a, b). Losartan significantly ameliorated these parameters compared to the RT group at week 3 (Table 6; Figure 7a, b). Nonetheless, at week 15, there was a trend to an increase (13.5%, $p = 0.061$) in the septal e' and a trend to decrease (17%, $p = 0.16$) in the E/septal e' parameter in the RT plus losartan group compared to the RT only group (Table 6; Figure 7a, b). Irradiation and cardiac remodeling might lead to HR changes [9]. There were no significant differences in the HR between the groups at weeks 1 and 3 (Figure 7c). In contrast, the HR was significantly decreased in both RT groups irrespective of losartan treatment at week 15 (Figure 7c).

Parameter (unit)	Week 1			Week 3			Week 15		
	Control	RT	RT Los	Control	RT	RT Los	Control	RT	RT Los
E velocity (m/s)	1.00±0.04	0.94±0.05	0.90±0.04	1.00±0.04	1.05±0.03	0.93±0.04#	1.01±0.02	0.81±0.10*	0.75±0.05*
e' (m/s)	0.060±0.002	0.053±0.001*	0.063±0.005	0.066±0.006	0.038±0.002*	0.056±0.005#	0.077±0.007	0.035±0.002*	0.042±0.002*
SWTs (mm)	2.70±0.10	2.84±0.16	2.91±0.10	3.14±0.15	3.47±0.12	3.18±0.14	3.58±0.12	4.64±0.17*	4.29±0.32
SWTd (mm)	1.61±0.10	1.60±0.09	1.90±0.06	1.79±0.12	1.73±0.06	1.77±0.14	1.83±0.04	3.23±0.33*	3.12±0.28
AWTs (mm)	2.64±0.17	2.61±0.09	2.92±0.20	2.85±0.17	3.19±0.18	2.89±0.27	3.3±0.23	4.56±0.28*	4.51±0.17*
AWTd (mm)	1.63±0.17	1.51±0.07	1.75±0.09	1.61±0.07	1.67±0.11	1.67±0.09	1.99±0.13	3.14±0.31*	3.04±0.17*
IWTs (mm)	2.24±0.13	2.47±0.08	2.70±0.10*	2.67±0.07	3.32±0.17*	2.91±0.23	3.44±0.25	4.56±0.09*	3.69±0.31
IWTd (mm)	1.48±0.03	1.51±0.09	1.67±0.09	1.73±0.07	1.98±0.07*	1.90±0.15	2.01±0.12	3.67±0.12*	2.72±0.26*#
LVEDD (mm)	7.73±0.22	7.34±0.27	6.98±0.16*	8.33±0.2	7.4±0.14*	7.11±0.29*	8.44±0.33	4.85±0.17*	5.67±0.29*#
LVESD (mm)	4.75±0.21	4.05±0.28	3.68±0.21*	4.83±0.17	3.40±0.20*	3.25±0.25*	4.26±0.55	0.98±0.15*	1.63±0.16*
FS (%)	39±2	45±2*	48±2*	42±2	54±2*	54±2*	50±5	80±3*	71±3*
EF (%)	56±2	57±3	52±1	53±2	53±3	53±1	53±2	57±2	55±1

Table 6 Echocardiographic parameters according to treatment groups at weeks 1, 3, and 15. Values are presented as mean±S.E.M., *p<0.05 vs. control group, #p<0.05 vs. RT group (n=6–7, One-Way ANOVA, Holm-Sidak post hoc test). RT, radiotherapy only group (50 Gy); RT Los, RT plus losartan group. AWT, anterior wall thickness; d, diastolic; E, early flow velocity; e', the early velocity of the septal mitral annulus during diastole; EF, ejection fraction; FS, fractional shortening; IWT, inferior wall thickness; LVEDD, left ventricular end-diastolic diameter; LVESD, left ventricular end-systolic diameter; s, systolic; SWT, septal wall thickness.

4.2.3. RT-related echocardiographic signs of left ventricular hypertrophy (LVH) were alleviated by losartan at week 15

At week 1, there was no significant difference in wall thicknesses and LV diameters, and EF between the RT only and control groups (Table 6; Figures 7d–f). Nevertheless, in the RT only group, the systolic inferior and posterior wall thicknesses increased in a statistically non-significant manner (10%, p = 0.14 and 7%, p = 0.17, respectively) while the LVESD decreased in comparison with the control group (trend, 15%, p = 0.07), supposing the beginning of the development of LVH at week 1 (Table 6; Figure 7d–f). These echocardiographic signs of a mild LVH resulted in significantly increased FS in the RT only group measured by the Teichholz method in M-mode images at week 1 (Table 6). Interestingly, similar statistically significant changes occurred in the systolic inferior wall thickness and LVESD and LVEDD in the RT plus losartan group compared to the control group at week 1 (Table 6).

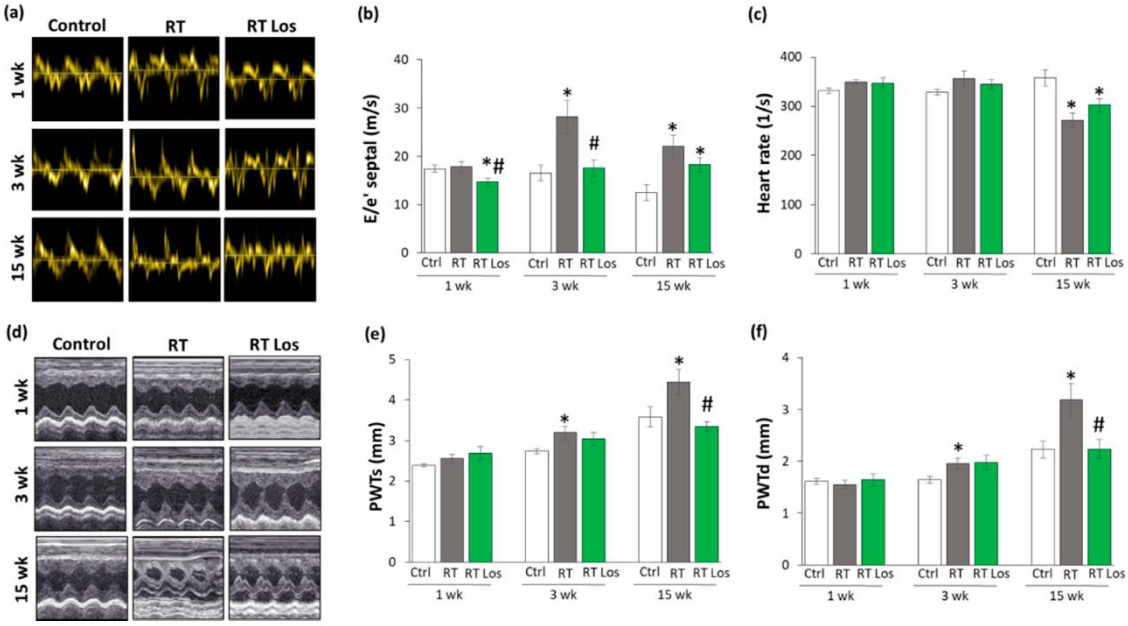

Figure 7 The effects of losartan on the echocardiographic parameters at weeks 1, 3, and 15. (a) Representative tissue Doppler images of diastolic septal mitral annulus velocity e', (b) mitral valve early flow velocity (E)/ e', (c) heart rate, (d) representative M-mode images of wall thicknesses and LV diameters, (e) posterior wall thicknesses in systole (PWTs) and (f) diastole (PWTd). Values are presented as mean±S.E.M., *p<0.05 vs. control group, #p<0.05 vs. RT only group (n=6–7, One-Way ANOVA, Holm-Sidak post hoc test). Ctrl, control group; RT, radiotherapy only group (50 Gy); RT Los, RT plus losartan group. Representative M-mode images were saved from the EchoPac Dimension v201 software.

The systolic posterior wall thickness showed a trend to increase (13%, p = 0.084) in the RT plus losartan group compared to the control group at week 1 (Figure 7e). Notably,

there were no significant differences in the echocardiographic morphological and functional parameters between the RT only and RT plus losartan groups at week 1.

At week 3, inferior and posterior wall thicknesses both in systole and diastole were significantly increased in the RT only group as compared to that in the control group, indicating the development of LVH (Table 6; Figure 7d–f). Accordingly, the LVESD and LVEDD were significantly smaller, and the FS was significantly higher in the RT only group as compared to that in the control group at week 3 (Table 6; Figure 7d). There were no significant differences in the systolic and diastolic inferior and systolic posterior wall thicknesses between the control and RT plus losartan groups (Table 6; Figure 7d–f). However, the LVEDD and LVESD remained significantly smaller, and the FS was significantly higher in the RT plus losartan group compared to those in the control group at week 3 (Table 6; Figure 7c,d). There were no significant differences in the EF between the groups at week 3.

At week 15, severe concentric LVH developed in the RT only group with a significant increase in all wall thicknesses and FS and a marked reduction in the LVEDD and LVESD compared to the control group (Table 6; Figure 7d-f). After losartan therapy, the systolic and diastolic posterior and diastolic inferior wall thicknesses were significantly reduced, and the LVEDD markedly increased as compared to these values in the RT only group suggesting antihypertrophic effects of losartan in our chronic RIHD model at week 15 (Table 6; Figure 7d–f). Moreover, systolic inferior wall thickness and FS showed a trend of being lower (19%, $p = 0.068$ and 13%, $p = 0.098$, respectively), and the LVESD seemed to be higher (66%, $p = 0.063$) in response to losartan compared to the RT only group at week 15 (Table 6). However, there was no significant difference in the EF between the groups at week 15.

4.2.4. Cardiomyocyte hypertrophy and the overexpression of LVH markers were reduced in the losartan-treated animals 3 and 15 weeks after RT

Cardiomyocyte cross-sectional areas were measured on HE-stained histological slides. Additionally, the LV expressions of cardiac hypertrophy markers were measured by qRT-PCR to resolve the contradiction between the autopsy and echocardiography results on heart size and LVH development (Tables 5, 6; Figures 7, 8).

At week 1, there were no significant differences in the cardiomyocyte cross-sectional areas between the groups, supporting the heart weight results (Figure 8a, b; Table 4). In contrast, at week 1, the echocardiographic signs showed the initiation of LVH (Table 6; Figure 7d–f). Therefore, we investigated the expression of the fetal myosin heavy chain β-isoform (i.e., β-MHC or *Myh7*) and the adult myosin heavy chain α-isoform (i.e., α-MHC or *Myh6*), as well as their ratio, in order to use them as molecular markers of LVH (Figure 8c–e). The increased ratio of the β-MHC to the α-MHC is an indicator of the fetal gene reprogramming in LVH in response to tissue hypoxia [20].

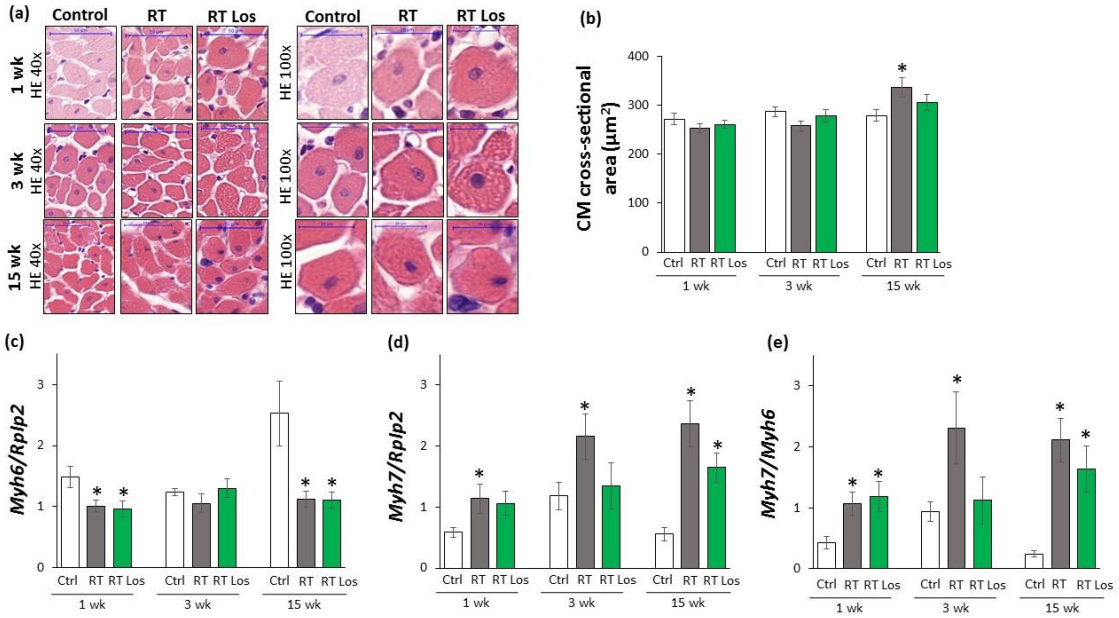

Figure 8 The effects of losartan on left ventricular hypertrophy assessed by histology at weeks 1, 3, and 15. (a) Representative hematoxylin-eosin (HE)-stained sections at 40x and 100× magnification, (b) cardiomyocyte cross-sectional area, (c) alpha-myosin heavy chain (*Myh6*), and (d) beta-myosin heavy chain (*Myh7*) expression in the left ventricle normalized to the ribosomal protein lateral stalk subunit P2 (*RpIp2)* gene expression, (e) *Myh7/Myh6* ratios. On the digital HE images, cardiomyocyte (CM) cross-sectional areas were measured in 100 selected cardiomyocytes in left ventricular tissue sections cut on equivalent planes. Scale bars represent 50 µm in the 40× magnified images and 20 µm in the 100× magnified images. Values are presented as mean±S.E.M., *p<0.05 vs. control group, #p<0.05 vs. RT only group (n=6–7, One-Way ANOVA, Holm-Sidak post hoc test). Ctrl, control group; RT, radiotherapy only group (50 Gy) ; RT Los, RT plus losartan group. Representative HE-stained slides were captured in the Panoramic Viewer 1.15.4 software.

At week 1, the expression of *Myh6* was significantly decreased, and the expression of *Myh7* was tendentiously increased in both RT groups irrespective of losartan treatment (93%, p = 0.061 and 80%, p = 0.067, respectively) (Figure 8c, d). Accordingly, as a compensatory mechanism to cardiac tissue damage due to RT, the *Myh7* to *Myh6* (*Myh7/Myh6*) ratio was significantly increased in both RT groups compared to the control group, supporting the echocardiographic signs of the initiation of compensatory LVH at week 1 (Table 6).

At week 3, the cardiomyocyte cross-sectional area showed a trend toward a decrease (10%, p = 0.08) in the RT only group compared to the control group, paralleling the LV weight results (Figure 8a, b; Table 4). Notably, there were no significant differences in the cardiomyocyte cross-sectional areas between the control and losartan treated RT groups, supposing the protective effects of losartan in our RIHD model at week 3 (Figure 8a, b). At the molecular level, there was no significant difference in the expression of *Myh6* between the groups at week 3 (Figure 8c). In contrast, the *Myh7* expression and the *Myh7* to *Myh6* ratio were significantly higher in the RT only group compared to the control group, supporting the echocardiographic signs of a mild LVH in our RIHD model at week 3 (Figure 8d, e; Table 6). There were no significant differences in the *Myh7* expression and the *Myh7* to *Myh6* ratio between the losartan-treated RT and control groups, similar to the echocardiographic and histologic results in our RIHD model at week 3 (Figure 8d, e; Table 6).

At week 15, the cardiomyocyte cross-sectional area was significantly higher in the RT only group compared to the control group, indicating the development of hypertrophy in the surviving cardiomyocytes as a compensatory mechanism despite the smaller heart size in our RIHD model (Figure 8a, b; Table 6). Moreover, there were no significant differences in the cardiomyocyte cross-sectional areas between the losartan-treated RT and control groups, similarly to the echocardiographic results on the antihypertrophic effects of losartan at week 15 (Figure 8a, b; Table 6). The *Myh6* expressions were markedly decreased, and the *Myh7* expressions with the *Myh7* to *Myh6* ratios were significantly increased in the RT only group as compared to that in the control group, indicating the development of cardiac hypertrophy at the molecular level in consistence with the echocardiographic results (Figures 7, 8c–e; Table 6). Notably, the losartan-treated RT group showed a trend to a decrease (30%, p = 0.139) in *Myh7* expression compared to the RT only group, in accordance with the echocardiographic results and supporting the antihypertrophic effects of losartan in our RIHD model (Figure 8d; Table 6).

4.2.5. Interstitial fibrosis was reduced in the losartan-treated animals 15 weeks after RT

To further characterize the antiremodeling effects of losartan in RIHD, fibrosis was quantified on PSFG-stained sections, and the LV gene expression changes of fibrosis and HF markers were measured by qRT-PCR (Figure 3, 9). At week 1, there was no

significant difference in the collagen content between the groups (Figure 9a, b). Moreover, at week 1, LV expressions of collagen type I alpha 1 (*Col1a1*) and the fibrosis marker connective tissue growth factor (*Ctgf*) showed no significant difference between the control and RT only groups (Figure 9c). Interestingly, losartan significantly reduced the *Ctgf* expression compared to the control group at week 1 (Figure 9c).

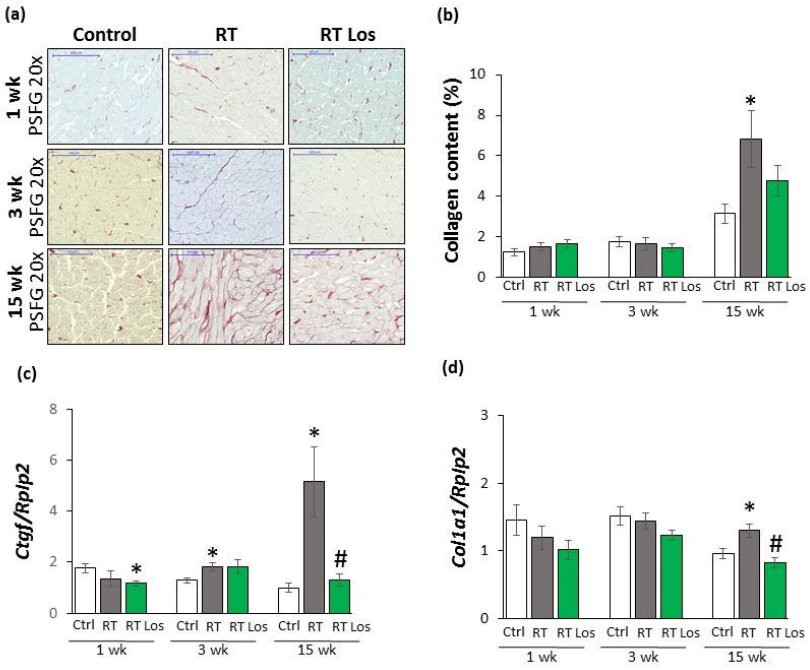

Figure 9 The effects of losartan on left ventricular fibrosis as assessed by histology and qRT-PCR at weeks 1, 3, and 15. (a) Representative picrosirius red and fast green (PSFG)-stained sections at 20x magnification, (b) left ventricular collagen content, left ventricular expression of (c) connective tissue growth factor (*Ctgf*), (d) collagen type I alpha 1 (*Col1a1*) normalized to ribosomal protein lateral stalk subunit P2 (*Rplp2*) gene expression. The mean values of the collagen content of 10 representative PSFG-stained images were calculated and used for statistical evaluation in each left ventricular sample. Scale bars represent 100 µm at the 20× magnified images. Values are presented as mean±S.E.M., *p< 0.05 vs. control group, #p<0.05 vs. RT only group (n=6–7, One-Way ANOVA, Holm-Sidak post hoc test). Ctrl, control group; RT, radiotherapy only group (50 Gy); RT Los, RT plus losartan group. Representative PSFG-stained slides were captured in the Panoramic Viewer 1.15.4 software.2.7.

At week 3, there were no significant differences in the collagen content and *Col1a1* expressions between the groups, suggesting no severe fibrosis in this stage of RIHD (Figure 9a, b, d). Interestingly, the expression of the profibrotic *Ctgf* was significantly increased in the RT only group and tendentiously elevated (43%, p = 0.074) in the losartan-treated RT group compared to the control group (Figure 9c), probably due to initiating wound healing by fibrosis after RT. At week 15, the collagen content and *Col1a1* and *Ctgf*, expressions were significantly increased in the RT only group compared to that in the control group, supporting the development of LV fibrosis (Figure 9a-d). There was no significant difference in the collagen content between the control and the

losartan-treated RT groups, indicating the antifibrotic effects of losartan in RIHD at week 15 (Figure 9a, b). Indeed, losartan significantly reduced the overexpression of *Col1a1* and *Ctgf* compared to the RT only group, showing its antiremodeling effects in our RIHD model at the molecular level (Figure 9c, d).

4.2.6. Losartan reduced the chymase overexpression at weeks 3 and 15 after RT

Inflammatory processes triggered by the overactivation of RAAS are major contributors to the development of cardiac remodeling and fibrosis in RIHD [9]. Therefore, the effects of losartan on the cardiac expression of the inflammatory cytokines interleukin-1 (*Il1*), interleukin-6 (*Il6*), and tumor necrosis factor-α (*Tnf*) were measured by qRT-PCR.

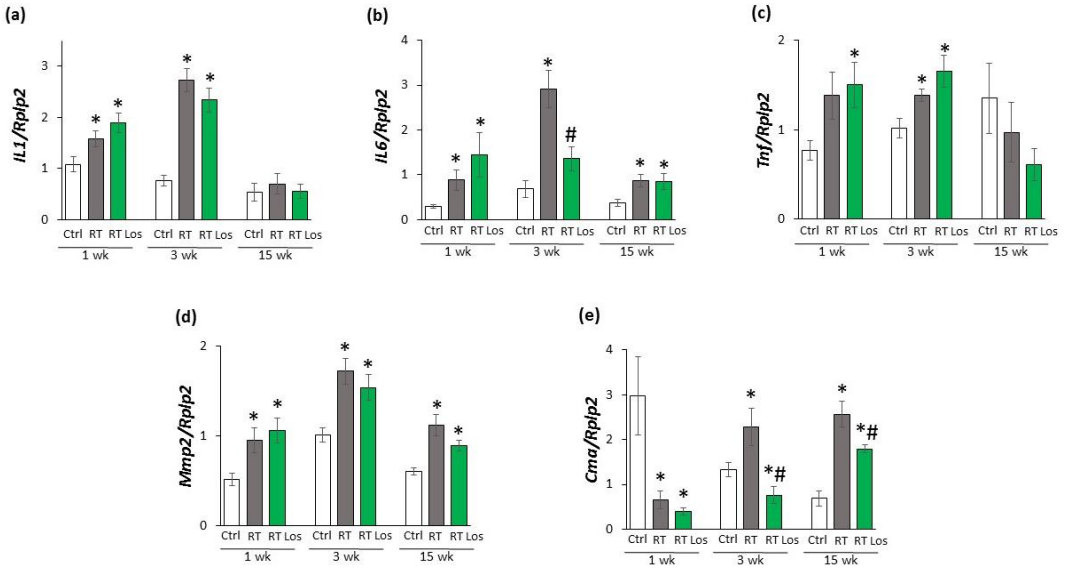

Figure 10 The effects of losartan on inflammatory gene expressions assessed by qRT-PCR at weeks 1, 3, and 15. Expression of (a) interleukin-1 (*Il1*), (b) interleukin-6 (*Il6)*, (c) tumor necrosis factor-alpha (*Tnfα*), (d) matrix metalloprotease-2 (*Mmp2*), and (e) chymase (*Cma*) normalized to ribosomal protein lateral stalk subunit P2 (*RpIp2*) gene expressions were measured in left ventricle samples. Values are presented as mean±S.E.M., *p<0.05 vs. control group, #p<0.05 vs. RT only group (n=6–7, One-Way ANOVA, Holm-Sidak post hoc test). Ctrl, control group; RT, radiotherapy only group (50 Gy); RT Los, RT plus losartan group.

At week 1, the expressions of *Il1* and *Il6* were significantly higher in both RT groups, and the expression of *Tnfa* was tendentiously increased (79%, p = 0.062) in the RT only group and significantly increased in the RT plus losartan group as compared to the control group, indicating tissue inflammation after RT (Figure 10a–c). At week 3, all measured inflammatory markers, including *Il1*, *Il6*, and *Tnfa*, were significantly overexpressed in the RT only group compared to the control group, pointing out the presence of tissue inflammation at week 3 (Figure 10a–c). Nevertheless, losartan significantly reduced the overexpression of *Il6* at week 3 (Figure 10b). In contrast, the expression of *Il1* and *Tnf*

remained significantly higher in the RT plus losartan group compared to the control group at week 3 (Figure 10a, c). At week 15, there were no significant differences in the *Il1* and *Tnf* expressions between the groups (Figure 10a, c). However, it should be mentioned that losartan reduced the *Tnf* expression in a non-significant manner (45%, p = 0.348) compared to the control group. Only *Il6* was significantly overexpressed in the RT groups irrespective of losartan treatment compared to the control group (Figure 10b). Mast cell chymase is an alternative activator of tissue AngII in the heart under inflammatory conditions [40,41]. The collagenase matrix metalloprotease 2 (*Mmp2*) and the mast cell chymase (*Cma*) could be activated by each other in the heart under inflammatory conditions [42]. Indeed, due to the cardiac inflammation in or RIHD model, *Mmp2* was overexpressed in the RT groups irrespective of losartan treatment compared to the time-matched control groups at weeks 1, 3, and 15, respectively (Figure 10d). In contrast, *Cma* was significantly repressed in both RT groups irrespective of losartan treatment compared to the control group at week 1 (Figure 10e). At weeks 3 and 15, the significant overexpression of *Cma* due to RT was markedly reduced in the RT plus losartan group (Figure 10e).

4.2.7. Losartan alleviated the cardiac fibrosis via inhibiting the TGF-β-mediated SMAD-dependent pathway in our RIHD model at weeks 3 and 15

To further characterize the antiremodeling effects of the AT1R blocker losartan in RIHD, the expression of angiotensinogen (*Agt*) and transforming growth factor-β (*Tgfb*) was measured by qRT-PCR. In addition, the expression of the main AngII receptors, including the pro-inflammatory, prohypertrophic, and profibrotic AT1R, and the anti-inflammatory, antihypertrophic and antifibrotic AT2R were studied at the protein level [22,23] (Figure 11b, c). AT1R was described to activate TGF-β, which can induce fibrosis via the canonical SMAD-dependent and the non-canonical SMAD-independent signaling pathways [22,23,43].

At week 1, there was no significant difference in *Agt* expression between the control and RT only groups. However, in the RT plus losartan group, significantly increased *Agt* expression was found as compared to the control group at week 1 (Figure 11a). No significant differences were detected in the expression of AT1R and AT2R, TGF-βRII, and SMAD2/3 levels between the groups at week 1, in consistence with the histology results on either collagen content or cardiomyocyte cross-sectional areas at week 1

(Figure 11b, c, e, f). Interestingly, *Tgfb* was significantly repressed in both RT groups irrespective of losartan compared to the control group at week 1 (Figure 11d).

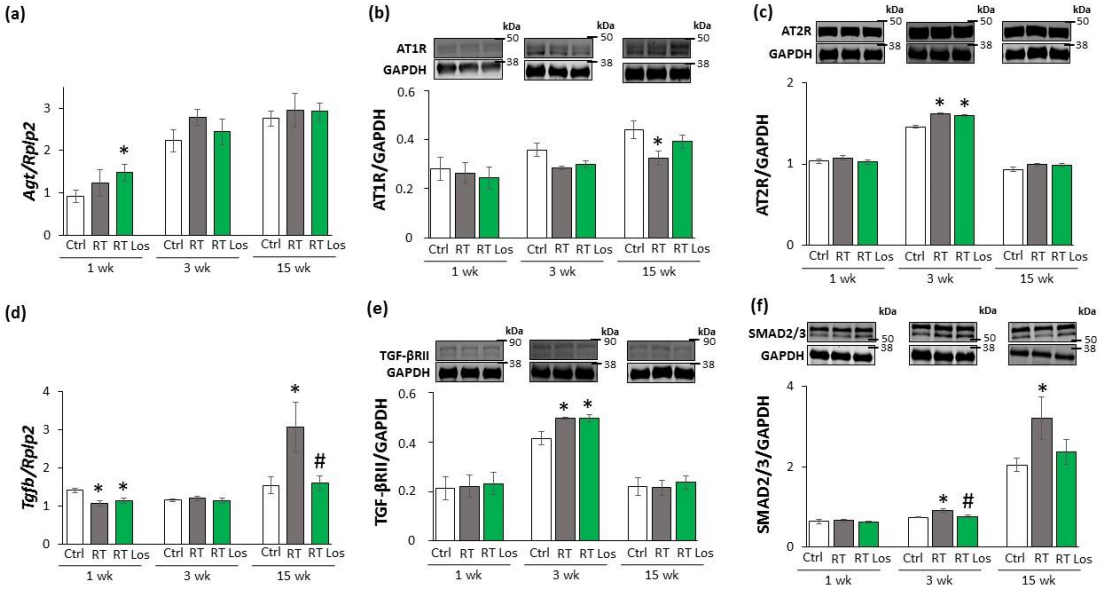

Figure 11 The effects of losartan on the expression of genes and proteins related to the cardiac RAAS and canonical SMAD-dependent pathway at weeks 1, 3, and 15. Left ventricular expression of (a) angiotensinogen (*Agt*) normalized to ribosomal protein lateral stalk subunit P2 (*RpIp2*) gene expression, left ventricular protein expression and cropped representative images of (b) angiotensin II type 1 receptor (AT1R, 41 kDa), and (c) angiotensin II type 2 receptor (AT2R, 41 kDa), (d) left ventricular expression of transforming growth factor-beta (*Tgfb*) normalized to *RpIp2* gene expression, left ventricular expression and cropped representative images of (e) TGF-β receptor II (TGF-βRII, 85 kDa) and (f) SMAD2/3 (52 and 60 kDa). Values are presented as mean±S.E.M., *p< 0.05 vs. control group, #p<0.05 vs. RT only group (n=6–7, One-Way ANOVA, Holm-Sidak post hoc test). Ctrl, control group; RT, radiotherapy only group (50 Gy); RT Los, RT plus losartan group. Glyceraldehyde-3-phosphate dehydrogenase (GAPDH, 36 kDa) was used as a loading control in protein expression changes assessed by Western blot. Images were captured with the Odyssey CLx machine and exported with Image Studio 5.2.5 software. Black lines next to the Western blot images represent the position of protein markers with corresponding molecular weights.

At week 3, the *Agt* expression was tendentiously increased (40%, p = 0.118) in the RT only group compared to the control group, which may suggest a mild activation of tissue RAAS (Figure 11a). In both RT groups, the AT1R protein levels showed a trend to decrease (19%, p = 0.054 and 16%, p = 0.090, respectively) compared to the control group (Figure 11b). Moreover, in both RT groups, the AT2R protein expressions were significantly increased as compared to the control group (Figure 11c). There was no significant difference in the cardiac *Tgfb* expression between the groups (Figure 11d). In contrast, TGF-βRII and SMAD2/3 protein levels were significantly increased in the RT only group compared to the control group (Figure 11e, f). Losartan significantly reduced the SMAD2/3 levels but not the TGF-βRII level compared to the RT only group at week 3 (Figure 11e, f).

At week 15, there was no significant difference in *Agt* expression between the groups (Figure 11a). The AT1R protein level was significantly decreased in the RT only group compared to the control group at week 15, supposedly, in response to the overactivation of AngII (Figure 11b). There was no significant difference in the AT1R protein levels between the control and losartan-treated RT groups at week 15 (Figure 12b). There were no significant differences between the AT2R protein levels between the groups (Figure 11c). Interestingly, the significant overexpression of *Tgfb* was markedly reduced by losartan at week 15 (Figure 11d). Accordingly, SMAD2/3 protein levels were significantly increased in the RT only group compared to the control group at week 15, suggesting that the canonical SMAD-dependent signaling pathway might play a crucial role in the development of fibrosis in RIHD (Figure 11f). Interestingly, there were no significant differences between the AT2R and TGF-βRII levels between the groups at week 15 (Figure 11c, e). In accordance with the echocardiography and histology results, there was no significant difference in the SMAD2/3 protein level between the losartan-treated RT and the control groups at week 15 (Figure 11f).

4.2.8. ERK1,2- and AKT-mediated pathways might be involved in compensatory hypertrophy after RT at week 15

The non-canonical SMAD-independent signaling pathways include ERK1,2, AKT, and STAT3-mediated fibrotic and hypertrophic pathways beyond other mediators [44].

At week 1, there was no significant difference in the expression of the pERK1,2/tERK1,2, pAKT/tAKT, and pSTAT3/STAT3 ratios between the groups (Figure 12a-d). At week 3, there were no significant differences in the pERK1/tERK1 and pERK2/tERK2 ratios between the RT only and control groups (Figure 12a, b). In contrast, after losartan treatment at week 3, the pERK1/tERK1 ratio was significantly increased, and a trend to an increase (60%, p=0.072) was seen in the case of the pERK2/tERK2 ratio (Figure 12a, b). The higher pERK1 and pERK2 protein levels led to the increased pERK1/tERK1 and pERK2/tERK2 ratios in the losartan-treated RT group compared to the control group at week 3.

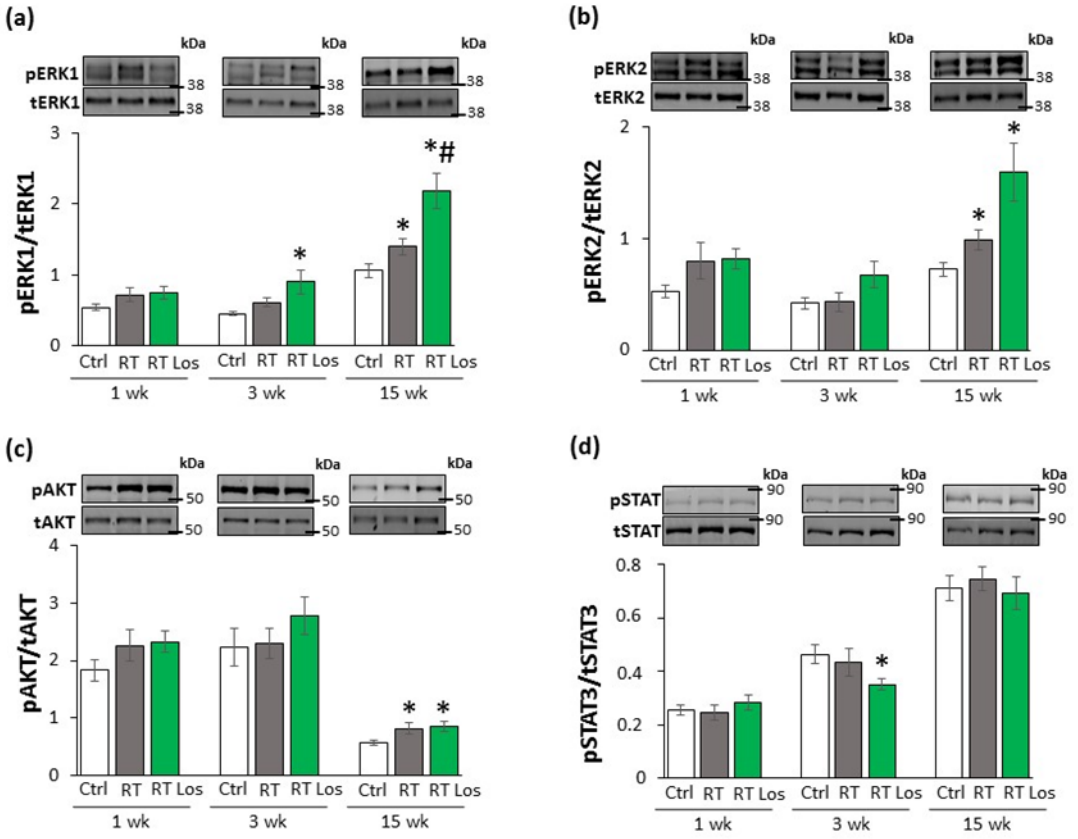

Figure 12 The effects of losartan on the expression of proteins associated with the non-canonical SMAD-independent fibrotic pathway at weeks 1, 3, and 15. Left ventricular expression and cropped representative images of (a) phospho-ERK1/total- ERK1 ratio (pERK1/tERK1 42 and 44 kDa), (b) phospho-ERK2/total-ERK2 ratio (pERK2/tERK2, 42 and 44 kDa), (c) phospho-AKT/total-AKT ratio (pAKT/tAKT, 60 kDa), (d) phospho-STAT3/total-STAT3 ratio (pSTAT3/tSTAT3, 79 and 86 kDa). Values are presented as mean±S.E.M., *p< 0.05 vs. control group, #p<0.05 vs. RT only group (n=6–7, One-Way ANOVA, Holm-Sidak post hoc test). Ctrl, control group; RT, radiotherapy only group (50 Gy); RT Los, RT plus losartan group. Images were captured with the Odyssey CLx machine and exported with Image Studio 5.2.5 software. Black lines next to the Western blot images represent the position of protein markers with corresponding molecular weights.

At week 15, pERK1/tERK1 and pERK2/tERK2 ratios were significantly increased in the RT groups irrespective of losartan treatment as compared to the control group (Figure 12a, b). Moreover, in response to losartan, the pERK1/tERK1 ratio was significantly elevated, and the pERK2/tERK2 ratio showed a trend to an increase (61%, p = 0.063) as compared to the RT only group (Figure 12a, b). The pERK1 and pERK2 protein levels showed a similar pattern to the pERK/tERK ratios. At weeks 1 and 3, there were no significant differences in the pAKT/tAKT ratios between the groups (Figures 12c). At week 15, the pAKT/tAKT ratio was significantly higher in both RT groups irrespective of losartan treatment compared to that in the control group (Figures 12c). STAT3 could be activated not only via TGF-β on the non-canonical non-SMAD-dependent fibrotic pathway but also by AngII [45].

There were no significant differences in the pSTAT3/tSTAT3 ratios between the groups at weeks 1 and 15 (Figure 12d). However, in the RT plus losartan group at week 3, the pSTAT3/tSTAT3 ratio was significantly reduced as compared to the control group at week 3 (Figures 12d).

5. Discussion

RT-induced diffuse myocardial injury, leading to the clinical entity of cardiomyopathy and HF, is a progressive disease ending in cardiac fibrosis, which might develop over several years post-RT depending primarily on RT dose in humans [9,12]. RT-induced cardiomyopathy and HF cover a spectrum of functional abnormalities. Among them, a typical initial phase is HFpEF characterized by DD and compensatory LVH [46-48]. Later on, due to the progression of interstitial fibrosis and loss of cardiomyocytes, the clinical entity of HFrEF develops [49,50]. Regarding the underlying pathomechanisms, in humans, radiation injury affects two important systems: one is blood circulation, and the other is the system of cardiomyocytes. Radiation exposure of the coronary arteries and microvasculature results in endothelial cell damage and disturbed circulation. Hypoxia and the injury of the endothelial cells aggravate chronic/progressive inflammation and fibrosis which are essential components of RIHD. In fact, in humans, this component is of utmost significance because RIHD manifests mainly as a potentially fatal coronary event. Concerning radiogenic cardiomyopathy, a fractionated RT dose of 40 Gy to the heart has been found to induce diffuse myocardial injury in patients that may be revealed early by serial follow-up tests [9,49]. Diffuse myocardial injury presents more commonly in patients who received higher RT doses (>60 Gy) and/or anthracycline chemotherapy [50,51]. In most RIHD animal models, exclusively cardiac fibrosis could be studied due to the difficulties in developing radiation-induced arteriosclerosis in rodents [11,12,52,53]. This is why most animal studies, including ours, focus on the effects of radiation-induced diffuse myocardial injury and consequential interstitial inflammation and fibrosis only. In our previous studies, including the model setup study, we developed a rat model of high dose radiation-induced heart damage using a single dose (50 Gy) of heart irradiation to investigate diffuse myocardial injury [29,31]. In the treatment study, we used this rat model of RIHD to investigate the effects of losartan.

The presented echocardiography and histology findings in both studies are consistent with the literature data [46,48,54] and our previous results on developing a rat model of chronic

RIHD [29]. We detected DD in the irradiated animals at every pre-specified follow-up time point in our rat model of RIHD. In fact, the molecular markers (the expression of *Myh7* and *Myh6* in the LV and their ratios), echocardiography findings, and histological signs of LVH became more severe over time. Interestingly, the weights of the left ventricles were significantly lower in the RT groups as compared to that in the control group throughout the experiment, probably due to the cell death and developmental retardation caused by the RT. Despite the smaller LV weights, the surviving cardiomyocytes might develop compensatory LVH to maintain the EF and sufficient oxygen supply to the whole body.

In the treatment study, a compensatory increase in the red blood cell counts at week 1 might be related to the hypoxia caused by radiation-induced heart and lung damage. Indeed, at week 1, *Il1* was significantly overexpressed in the left ventricles, pointing to the development of tissue inflammation in RIHD. The systemic inflammatory marker white blood cell count was significantly increased at week 3 in the irradiated animals. Accordingly, at week 3, the LV expression of all investigated inflammatory markers, including *Il1*, *Il6*, and *Tnfα*, were significantly higher post-RT, indicating a more severe tissue inflammation at this phase. At week 15, *Il6* expression (which is a well-known mediator of myocardial fibrosis leading to concentric hypertrophy and secondary DD [55]) remained high. In the fibrotic phase with severe concentric LVH at week 15, hemoglobin and hematocrit levels significantly increased, probably, in response to the chronic hypoxia caused by radiogenic HF and lung fibrosis.

In both studies, picrosirius red staining indicated interstitial fibrosis in response to RT at the endpoints (19 and 15 weeks). Generally, the increased collagen deposition could be explained by either the stimulation of production or the reduced turnover of the mRNAs and/or proteins of different collagen types. The key molecular mechanism of radiation-induced cardiac fibrosis is thought to be the TGF-β/SMAD2/3-mediated fibrotic pathway [12,39,56,57]. In our previous experiments, increased plasma levels of TGF-β1 and growth differentiation factor 15 (GDF-15) were shown 12 weeks after the selective heart irradiation with 50 Gy [29]. According to our experimental data, the heart at 19 weeks following irradiation is best characterized by hypertrophy, mild interstitial fibrosis, and DD, demonstrating characteristic HFpEF. In our treatment study, molecular signs (i.e., overexpression of *Ctgf*, TGF-βRII, and SMAD2/3) preceded the histologic signs of fibrosis 3 weeks after the irradiation, showing the initiation of fibrotic remodeling in the heart in our RIHD model. At week 15, left ventricular *Ctgf* and SMAD2/3 expressions

remained high with the overexpression of *Tgfb* and *Col1a1*. At week 15, the significantly increased interstitial collagen content of the left ventricle revealed the presence of fibrosis in RIHD. These molecular, morphological, and functional changes were similar to those reported in other studies [46,48].

A number of studies demonstrated that miRs are critical contributors to cardiovascular biology and disease development [15-18,58]. MicroRNA-212 was shown to be a key regulator in the development of LVH and HF via the repression of the antihypertrophic transcription factor FOXO3 and overactivation of the calcineurin/NFAT signaling during HF development [19]. In our model setup study, LVH was accompanied by the overexpression of miR-212 3 and 19 weeks after the selective heart irradiation. Interestingly, the repression of *Foxo3* at the mRNA level was present in cardiac tissue samples in RIHD only at week 19 (Figure 6). In contrast, the FOXO3 protein level failed to decrease, and the pFOXO3/FOXO3 ratio showed a non-significant trend toward an increase in RIHD at week 19 (Figure 6). Although the increased pFOXO3/FOXO3 ratio is a characteristic shift in cardiac hypertrophy forms [38], it seems to be independent of the effect of miR-212 in chronic RIHD. It has also been demonstrated in other LVH models that the repression of the FOXO3 level could indirectly lead to the overactivity of the hypertrophic calcineurin/NFAT pathway [59]. In our model setup study, cardiac mRNA levels of calcineurin A-alpha and calcineurin A-beta showed a statistically non-significant decrease in the irradiated hearts as compared to the controls. The development of the LVH and HFpEF in RIHD seems to be unique and very different from other forms of cardiac hypertrophies, such as the commonly studied pressure-overload-induced compensatory hypertrophy and subsequent HF.

In our treatment study, we also investigated selected molecules, including AKT, ERK1,2, and STAT3 and their phosphorylated forms, in the non-canonical non-SMAD-dependent fibrotic pathway. Significantly increased pERK1,2/tERK1,2 and pAKT/tAKT ratios were detected after the RT at week 15. Since the ERK-mediated pathways are also considered survival pathways regulating cell death and hypertrophy [60], the increased pERK1,2/tERK1,2 ratios in the RT groups could be explained as compensatory defense mechanisms against cell death. AKT was also described as a molecule mediating cardiomyocyte survival and hypertrophy [44], and this, in fact, might explain the higher pAKT/tAKT ratios in the RT groups at week 15. In summary, the canonical SMAD-dependent TGF-β pathway seems to be responsible for the cardiac fibrosis in our RIHD model. The non-canonical SMAD-independent pathways, including the AKT and

ERK1,2-mediated mechanisms, seem to be involved in cell survival and compensatory hypertrophy in RIHD.

It has been reported that irradiation could induce AngII overexpression in the rat heart [24] and lung [25] in a dose-dependent manner [26]. AngII can be cleaved from AngI by several proteases, of which angiotensin-converting enzyme (ACE), and alternatively, under inflammatory conditions, mast cell chymase are the primary converters [40,61,62]. Chymase overexpression seems to be particularly important in the cardiac generation of AngII in RIHD [40,63,64]. Interestingly, the cardiac RAAS interacts with many other systems in the heart, including the endothelin system and cardiac sympathetic nervous systems. The locally generated AngII appears to contribute to LVH and fibrosis via different mechanisms [40]. AngII has been reported to activate cardiac NADPH-oxidase via AT1R, and subsequently, the over-production of reactive oxygen and nitrogen species leads to increased nitro-oxidative stress [65,66]. This could trigger the production of pro-inflammatory mediators, such as IL1, IL6, TNF-α, and TGF-β, contributing to cardiac remodeling and HF [65,66]. The AT1R is mainly involved in pro-inflammatory, prohypertrophic, and profibrotic mechanisms, whereas the AT2R is associated with counter-regulatory anti-inflammatory, antihypertrophic and antifibrotic pathways in the cardiovascular system [22,23]. Therefore, selective AT1 blockade by losartan seems to be a rational therapeutic option to ameliorate cardiac remodeling by reducing nitro-oxidative stress and inflammatory mechanisms in RIHD. However, to our best knowledge, there are no experimental data on the antiremodeling effects of ARBs in RIHD. Interestingly, two clinical trials investigated the effects of ARBs after RT; however, their results were controversial.

In the treatment study, at week 1, losartan-treatment did not influence the early molecular (i.e., left ventricular expressional changes of *Myh7* and *Myh6* and their ratios) and echocardiographic signs of LVH as assessed by M-mode echocardiography, probably due to the acute compensatory and surviving mechanisms in response to tissue damage caused by RT. At week 3, in the losartan-treated animals, various experimental parameters improved as compared to that in the RT only group, such as several echocardiographic signs of LVH and consequential DD together with the overexpression of *Myh7* and SMAD2/3 in the left ventricle indicating a possible antihypertrophic and antifibrotic effect of losartan in the early chronic phase of RIHD. In contrast, white blood cell counts remained elevated irrespective of losartan treatment in RIHD at week 3, supposing the presence of systemic inflammation. At week 15, losartan treatment did not reduce the

molecular signs of LVH (the changes in the expression of *Myh7* and *Myh6* and their ratios), suggesting that the hypertrophic process is also active in this late chronic phase of RIHD as a compensatory mechanism to cardiomyocyte loss after RT and secondary hypoxia. However, according to the echocardiography and histology findings at week 15, losartan reduced the severity of LVH. Losartan reduced the interstitial collagen content by reducing the *Ctgf, Tgfb,* and *Col1a1* overexpression and SMAD2/3 levels in RIHD. Similar to our results, losartan reduced cardiac fibrosis in HF by reducing the CTGF and SMAD2/3 expression in other studies [67,68]. We also investigated molecules in the non-canonical SMAD-independent fibrotic pathway and found that pERK1,2/tERK1,2 ratios were significantly increased in the RT groups and were further increased by losartan at week 15. In contrast, several studies found that losartan reduced the pERK1,2/tERK1,2 ratio in HF [69,70]. Our result could be explained by the fact that ERK1,2 phosphorylation can be increased by MMP2 [71]. Indeed, losartan failed to significantly reduce the overexpression of *Mmp2* in our RIHD model.

Interestingly, at weeks 3 and 15, *Agt* expression was not significantly different between the groups, but the AT1R levels were decreased, probably, due to increased AngII levels after RT. This finding is in accordance with human data showing that AT1Rs are selectively downregulated in HF depending on the severity of ventricular dysfunction [72]. At week 15, the repression of the AT1R was weakened by losartan, supposedly via blocking the cleavage of AngII from AngI. Indeed, the LV expression of the mast cell *Cma* was higher both at week 3 and 15 in RIHD, likely mediated by cardiac inflammation and *Mmp2* overexpression [73]. Chymase overexpression was reduced by losartan at weeks 3 and 15, possibly explained by its mild anti-inflammatory effects in RIHD [74](i.e., repression of *Il6* at week 3, and decreased expression of *Tnfα* at week 15). Indeed, it has been described that losartan was more effective than the ACE-inhibitor captopril in controlling ongoing vascular inflammation if AngII-dependent components of atherogenesis were present in mice [61]. However, DD was not improved by losartan in our RIHD model at week 15, which may have been due to the presence of local inflammation (i.e., *Il6* overexpression) and more severe LVH and fibrosis at this late chronic stage of RIHD.

Our studies are not without limitations, similar to other experimental works. In the model setup study, the results regarding altered cardiac gene expression due to RIHD are based on selected miRNAs and mRNA target molecules; however, measurement of the full rat transcriptome and proteome should be performed in the future. In the treatment study, we

intended to test losartan for controlling HF related to RIHD. Nevertheless, significant differences exist between the pathomechanisms in the model used vs. that in patients. (i) While, in humans, radiogenic coronary artery damage is an essential component of the radiation damage, in most murine models, no similar alterations evolve unless specific genetically modified animal strains are used [8,11,12,57,63]. In our experiments, RT-induced diffuse myocardial injury and consequential interstitial inflammation and fibrosis were the basis of the HF studied [29]. (ii) In order to obtain the measurable end-points of HF and interstitial fibrosis in the myocardium [9,12,50,57] within a reasonable timeframe, we used a very high biological dose with drastic consequences to which a similar one is never applied in conventional RT. Nevertheless, in modern RT practice, the use of very large doses (stereotactic radiosurgery delivered with precision selectivity) is widely utilized [75]. (iii) In patients, the effects of various risk factors (such as hyperlipidemia, diabetes, hypertension, aging, sex hormonal differences, individual radiosensitivity, etc.) may modulate radiation-induced changes, which are less pronounced in most animal models. (iv) Finally, while in the animal model, a relatively short follow-up time was used post-RT, in patients, about 10 years elapse until the recognition of RIHD, although the presence of manifest heart disease or other risk factors may advance its diagnosis [6, 7,11,53]. Moreover, we used only one dose of losartan which is comparable to the human therapeutic doses and widely used in HF models of other etiologies. The demonstration of molecular mechanisms of how losartan interacts with tissue remodeling was out of the scope of our present descriptive study. We found here antiremodeling effects of losartan and hypothesized that losartan could have antifibrotic effects by ameliorating the TGF-β/SMAD2/3-mediated pathway and reducing the overexpression of chymase. Moreover, the non-canonical SMAD-independent pathways, including the AKT and ERK1,2-mediated mechanisms, seem to be involved in maintaining compensatory hypertrophy in our chronic RIHD model.

Inhibition of the TGF-β /SMAD2/3-pathway or the non-SMAD-dependent pathways in further experiments is needed to determine their exact role in losartan-mediated antiremodeling effects in RIHD.

6. Conclusion

The purpose of the studies was to i) set up a rat model of RIHD in the acute, early chronic, and late chronic phases, ii) investigate the potential role of miR-212 and iii) its hypertrophy-associated target FOXO3, and iv) test the effects of the ARB losartan on the development of RIHD in our rat model. In summary, our model setup experiment is the first study to report that LVH is accompanied by characteristic overexpression of miR-212 in the heart, both in the early and late chronic phases of RIHD. Our results suggest that miR-212 might play a significant role in the development of RIHD via FOXO3 independent mechanisms, and the molecular mechanism of RIHD development is distinct from other forms of hypertrophy and pathological remodeling. In our treatment study, we reported that the selective AT1R blocker losartan alleviates the radiation-induced LVH and fibrosis. The antiremodeling effects of losartan seem to be associated with the repression of chymase and several elements of the canonical TGF-β/SMAD2/3 fibrotic pathway in our RIHD model. Moreover, the non-canonical SMAD-independent pathways, including the AKT and ERK1,2-mediated mechanisms, seem to be involved in the maintenance of compensatory hypertrophy in the late chronic phase of RIHD.

7. Funding

This research was funded by the projects NKFIH FK129094 (to M.S.), GINOP-2.3.2-15-2016-00040, GINOP-2.3.2-15-2016-00034, EFOP-3.6.2-16-2017-00006 (LIVE LONGER) and by the Ministry of Human Capacities (20391-3/2018/FEKUSTRAT). M.G.K., Z.Z.A.K., and M.S. were supported by the New National Excellence Program of the Ministry of Human Capacities. MS was supported by the János Bolyai Research Fellowship of the Hungarian Academy of Sciences. Z.Z.A.K. and M.G.K. were supported by the EFOP-3.6.3-VEKOP-16-2017-00009 project.

8. Acknowledgements

There are so many to whom I would like to acknowledge for their contribution and support during my scientific work.

Most importantly, I would like to express my thanks to Professor László Dux, the Head of the Multidisciplinary Doctoral School and former Head of the Department of Biochemistry, as well as to Tamás Csont, the Head of the Department of Biochemistry, who gave me the possibility to work at the Institute in the past several years.

I would like to thank my supervisor, Márta Sárközy, for the continuous help and enthusiasm throughout these years in the Department.

I am grateful for the enormous amount of help of Professor Zsuzsanna Kahán, Zoltán Varga, Gabriella Fábián and Laura Kiscsatári at the Department of Oncotherapy.

I would like to express my thanks to Imre Földesi and Katalin Farkas at the Department of Laboratory Medicine, as well as to Professor Gábor Cserni, Bálint Gábor Cserni, Bence Kővári and Krisztián Daru at the Department of Pathology.

I am grateful for the help of the CEO of Single-Cell Technologies Ltd., Péter Horváth as well as Ferenc Kovács, software engineer, and András Kriston, software architect for the use of Biology Image Analysis Software (BIAS) before its public release.

I would also like to thank Ágnes Zvara and László Puskás at the Laboratory for Functional Genomics, Biological Research Center of the Hungarian Academy of Sciences and to Thomas Thum and Sándor Bátkai at the Institute of Molecular and Translational Therapeutic Strategies (IMTTS), Hanover Medical School.

I would like to express my gratitude to my best friend at work, „twin sister", Zsuzsanna Kovács, who was always there with (for) me. You supported me throughout our often challenging periods of time. I am also grateful to Gergő Szűcs, Marah Freiwan, Klaudia Kupecz, Réka Losonczi, Merse Kiss, and Ilona Ungi for their demanding work in these projects. I would like to thank all my laboratory colleagues for their support.

Above all, I owe special gratitude to my whole family and my significant other half because, without you, none of this would indeed have been possible.

9. References

[1] ‘Cancer’. https://www.who.int/news-room/fact-sheets/detail/cancer (accessed Jan. 12, 2022).

[2] ‘Cardiovascular diseases (CVDs)’. https://www.who.int/news-room/fact-sheets/detail/cardiovascular-diseases-(cvds) (accessed Jan. 12, 2022).

[3] R. Baskar and K. Itahana, ‘Radiation therapy and cancer control in developing countries: Can we save more lives?’, *Int. J. Med. Sci.*, vol. 14, no. 1, pp. 13–17, 2017, doi: 10.7150/ijms.17288.

[4] K. D. Miller *et al.*, ‘Cancer treatment and survivorship statistics, 2019’, *CA. Cancer J. Clin.*, vol. 69, no. 5, pp. 363–385, 2019, doi: 10.3322/caac.21565.

[5] K. M. Menezes, H. Wang, M. Hada, and P. B. Saganti, ‘Radiation Matters of the Heart: A Mini Review’, *Front. Cardiovasc. Med.*, vol. 5, p. 83, 2018, doi: 10.3389/fcvm.2018.00083.

[6] C. Taylor *et al.*, ‘Estimating the Risks of Breast Cancer Radiotherapy: Evidence From Modern Radiation Doses to the Lungs and Heart and From Previous Randomized Trials’, *J. Clin. Oncol.*, vol. 35, no. 15, pp. 1641–1649, 0 2017, doi: 10.1200/JCO.2016.72.0722.

[7] F. A. van Nimwegen *et al.*, ‘Radiation Dose-Response Relationship for Risk of Coronary Heart Disease in Survivors of Hodgkin Lymphoma’, *J. Clin. Oncol.*, vol. 34, no. 3, pp. 235–243, 0 2016, doi: 10.1200/JCO.2015.63.4444.

[8] T. Rassaf *et al.*, ‘Onco-Cardiology: Consensus Paper of the German Cardiac Society, the German Society for Pediatric Cardiology and Congenital Heart Defects and the German Society for Hematology and Medical Oncology’, *Clin. Res. Cardiol.*, vol. 109, no. 10, pp. 1197–1222, 2020, doi: 10.1007/s00392-020-01636-7.

[9] M. Sárközy *et al.*, ‘Pathomechanisms and therapeutic opportunities in radiation-induced heart disease: from bench to bedside’, *Clin. Res. Cardiol.*, vol. 110, no. 4, pp. 507–531, 2021, doi: 10.1007/s00392-021-01809-y.

[10] J. L. Zamorano *et al.*, ‘2016 ESC Position Paper on cancer treatments and cardiovascular toxicity developed under the auspices of the ESC Committee for Practice Guidelines: The Task Force for cancer treatments and cardiovascular toxicity of the

European Society of Cardiology (ESC)', *Eur. Heart J.*, vol. 37, no. 36, pp. 2768–2801, 0 2016, doi: 10.1093/eurheartj/ehw211.

[11] N. Andratschke, J. Maurer, M. Molls, and K.-R. Trott, 'Late radiation-induced heart disease after radiotherapy. Clinical importance, radiobiological mechanisms and strategies of prevention', *Radiother. Oncol.*, vol. 100, no. 2, pp. 160–166, Aug. 2011, doi: 10.1016/j.radonc.2010.08.010.

[12] N. K. Taunk, B. G. Haffty, J. B. Kostis, and S. Goyal, 'Radiation-Induced Heart Disease: Pathologic Abnormalities and Putative Mechanisms', *Front. Oncol.*, vol. 5, p. 39, 2015, doi: 10.3389/fonc.2015.00039.

[13] S. Tapio, 'Pathology and biology of radiation-induced cardiac disease', *J. Radiat. Res. (Tokyo)*, vol. 57, no. 5, pp. 439–448, 0 2016, doi: 10.1093/jrr/rrw064.

[14] M. Ha and V. N. Kim, 'Regulation of microRNA biogenesis', *Nat. Rev. Mol. Cell Biol.*, vol. 15, no. 8, pp. 509–524, 0 2014, doi: 10.1038/nrm3838.

[15] S. Bátkai and T. Thum, 'MicroRNAs in hypertension: mechanisms and therapeutic targets', *Curr. Hypertens. Rep.*, vol. 14, no. 1, pp. 79–87, Feb. 2012, doi: 10.1007/s11906-011-0235-6.

[16] R. Kumarswamy and T. Thum, 'Non-coding RNAs in cardiac remodeling and heart failure', *Circ. Res.*, vol. 113, no. 6, pp. 676–689, 0 2013, doi: 10.1161/CIRCRESAHA.113.300226.

[17] J. Viereck, C. Bang, A. Foinquinos, and T. Thum, 'Regulatory RNAs and paracrine networks in the heart', *Cardiovasc. Res.*, vol. 102, no. 2, pp. 290–301, May 2014, doi: 10.1093/cvr/cvu039.

[18] J. Viereck and T. Thum, 'Circulating Noncoding RNAs as Biomarkers of Cardiovascular Disease and Injury', *Circ. Res.*, vol. 120, no. 2, pp. 381–399, 0 2017, doi: 10.1161/CIRCRESAHA.116.308434.

[19] A. Ucar *et al.*, 'The miRNA-212/132 family regulates both cardiac hypertrophy and cardiomyocyte autophagy', *Nat. Commun.*, vol. 3, p. 1078, 2012, doi: 10.1038/ncomms2090.

[20] T. Thum *et al.*, 'MicroRNAs in the Human Heart', *Circulation*, vol. 116, no. 3, pp. 258–267, 0 2007, doi: 10.1161/CIRCULATIONAHA.107.687947.

[21] C. Jentzsch *et al.*, ‘A phenotypic screen to identify hypertrophy-modulating microRNAs in primary cardiomyocytes’, *J. Mol. Cell. Cardiol.*, vol. 52, no. 1, pp. 13–20, Jan. 2012, doi: 10.1016/j.yjmcc.2011.07.010.

[22] S. J. Forrester *et al.*, ‘Angiotensin II Signal Transduction: An Update on Mechanisms of Physiology and Pathophysiology’, *Physiol. Rev.*, vol. 98, no. 3, pp. 1627–1738, 0 2018, doi: 10.1152/physrev.00038.2017.

[23] M. Paz Ocaranza *et al.*, ‘Counter-regulatory renin–angiotensin system in cardiovascular disease’, *Nat. Rev. Cardiol.*, vol. 17, no. 2, pp. 116–129, Feb. 2020, doi: 10.1038/s41569-019-0244-8.

[24] R. Wu and Y. Zeng, ‘Does angiotensin II–aldosterone have a role in radiation-induced heart disease?’, *Med. Hypotheses*, vol. 72, no. 3, pp. 263–266, 0 2009, doi: 10.1016/j.mehy.2008.09.051.

[25] S. Cao and R. Wu, ‘Expression of Angiotensin II and Aldosterone in Radiation-induced Lung Injury’, *Cancer Biol. Med.*, vol. 9, no. 4, pp. 254–260, Dec. 2012.

[26] M. Pinter, W. J. Kwanten, and R. K. Jain, ‘Renin–Angiotensin System Inhibitors to Mitigate Cancer Treatment–Related Adverse Events’, *Clin. Cancer Res.*, vol. 24, no. 16, pp. 3803–3812, Aug. 2018, doi: 10.1158/1078-0432.CCR-18-0236.

[27] G. Gulati *et al.*, ‘Prevention of cardiac dysfunction during adjuvant breast cancer therapy (PRADA): a 2 × 2 factorial, randomized, placebo-controlled, double-blind clinical trial of candesartan and metoprolol’, *Eur. Heart J.*, vol. 37, no. 21, pp. 1671–1680, 0 2016, doi: 10.1093/eurheartj/ehw022.

[28] T. T. Sio *et al.*, ‘Dosimetric Correlate of Cardiac-Specific Survival Among Patients Undergoing Coronary Artery Stenting After Thoracic Radiotherapy for Cancer’, *Am. J. Clin. Oncol.*, vol. 40, no. 2, pp. 133–139, Apr. 2017, doi: 10.1097/COC.0000000000000135.

[29] L. Kiscsatári *et al.*, ‘High-dose Radiation Induced Heart Damage in a Rat Model’, *Vivo Athens Greece*, vol. 30, no. 5, pp. 623–631, 10 2016.

[30] M. G. Kovács *et al.*, ‘Investigation of the Antihypertrophic and Antifibrotic Effects of Losartan in a Rat Model of Radiation-Induced Heart Disease’, *Int. J. Mol. Sci.*, vol. 22, no. 23, p. 12963, Jan. 2021, doi: 10.3390/ijms222312963.

[31] M. Sárközy *et al.*, ‘Selective Heart Irradiation Induces Cardiac Overexpression of the Pro-hypertrophic miR-212’, *Front. Oncol.*, vol. 9, p. 598, 2019, doi: 10.3389/fonc.2019.00598.

[32] G. F. Kocsis *et al.*, ‘Preconditioning protects the heart in a prolonged uremic condition’, *Am. J. Physiol. Heart Circ. Physiol.*, vol. 303, no. 10, pp. H1229-1236, 0 2012, doi: 10.1152/ajpheart.00379.2012.

[33] Z. Z. A. Kovács *et al.*, ‘Comparison of the antiremodeling effects of losartan and mirabegron in a rat model of uremic cardiomyopathy’, *Sci. Rep.*, vol. 11, no. 1, p. 17495, 2021, doi: 10.1038/s41598-021-96815-5.

[34] C. Mátyás *et al.*, ‘The soluble guanylate cyclase activator cinaciguat prevents cardiac dysfunction in a rat model of type-1 diabetes mellitus’, *Cardiovasc. Diabetol.*, vol. 14, p. 145, Oct. 2015, doi: 10.1186/s12933-015-0309-x.

[35] M. Sárközy *et al.*, ‘Chronic kidney disease induces left ventricular overexpression of the pro-hypertrophic microRNA-212’, *Sci. Rep.*, vol. 9, no. 1, p. 1302, Feb. 2019, doi: 10.1038/s41598-018-37690-5.

[36] M. Sárközy *et al.*, ‘Metabolic syndrome influences cardiac gene expression pattern at the transcript level in male ZDF rats’, *Cardiovasc. Diabetol.*, vol. 12, p. 16, 0 2013, doi: 10.1186/1475-2840-12-16.

[37] R. Gáspár *et al.*, ‘The cytoprotective effect of biglycan core protein involves Toll-like receptor 4 signaling in cardiomyocytes’, *J. Mol. Cell. Cardiol.*, vol. 99, pp. 138–150, Oct. 2016, doi: 10.1016/j.yjmcc.2016.08.006.

[38] Y. G. Ni *et al.*, ‘Foxo Transcription Factors Blunt Cardiac Hypertrophy by Inhibiting Calcineurin Signaling’, *Circulation*, vol. 114, no. 11, pp. 1159–1168, 0 2006, doi: 10.1161/CIRCULATIONAHA.106.637124.

[39] J. Ahamed and J. Laurence, ‘Role of Platelet-Derived Transforming Growth Factor-β1 and Reactive Oxygen Species in Radiation-Induced Organ Fibrosis’, *Antioxid. Redox Signal.*, vol. 27, no. 13, pp. 977–988, 0 2017, doi: 10.1089/ars.2017.7064.

[40] M. Boerma and M. Hauer-Jensen, ‘Potential Targets for Intervention in Radiation-Induced Heart Disease’, *Curr. Drug Targets*, vol. 11, no. 11, pp. 1405–1412.

[41] G. Froogh *et al.*, ‘Chymase-dependent production of angiotensin II: an old enzyme in old hearts’, *Am. J. Physiol.-Heart Circ. Physiol.*, vol. 312, no. 2, pp. H223–H231, 0 2017, doi: 10.1152/ajpheart.00534.2016.

[42] P. Liu, M. Sun, and S. Sader, ‘Matrix metalloproteinases in cardiovascular disease’, *Can. J. Cardiol.*, vol. 22, pp. 25B-30B, Feb. 2006, doi: 10.1016/S0828-282X(06)70983-7.

[43] S. Saadat *et al.*, ‘Pivotal Role of TGF-β/Smad Signaling in Cardiac Fibrosis: Non-coding RNAs as Effectual Players’, *Front. Cardiovasc. Med.*, vol. 7, p. 256, 2021, doi: 10.3389/fcvm.2020.588347.

[44] K. W. Finnson, Y. Almadani, and A. Philip, ‘Non-canonical (non-SMAD2/3) TGF-β signaling in fibrosis: Mechanisms and targets’, *Semin. Cell Dev. Biol.*, vol. 101, pp. 115–122, 0 2020, doi: 10.1016/j.semcdb.2019.11.013.

[45] S. Ye *et al.*, ‘Celastrol Attenuates Angiotensin II–Induced Cardiac Remodeling by Targeting STAT3’, *Circ. Res.*, vol. 126, no. 8, pp. 1007–1023, prilis 2020, doi: 10.1161/CIRCRESAHA.119.315861.

[46] V. Monceau *et al.*, ‘Epac contributes to cardiac hypertrophy and amyloidosis induced by radiotherapy but not fibrosis’, *Radiother. Oncol.*, vol. 111, no. 1, pp. 63–71, Apr. 2014, doi: 10.1016/j.radonc.2014.01.025.

[47] L. O’Donnell, T. O’Neill, M. Toner, S. O’Briain, and I. Graham, ‘Myocardial hypertrophy, fibrosis and infarction following exposure of the heart to radiation for Hodgkin’s disease.’, *Postgrad. Med. J.*, vol. 62, no. 733, pp. 1055–1058, Nov. 1986, doi: 10.1136/pgmj.62.733.1055.

[48] H. Saiki *et al.*, ‘Experimental cardiac radiation exposure induces ventricular diastolic dysfunction with preserved ejection fraction’, *Am. J. Physiol.-Heart Circ. Physiol.*, vol. 313, no. 2, pp. H392–H407, 0 2017, doi: 10.1152/ajpheart.00124.2017.

[49] J. R. Cuomo, G. K. Sharma, P. D. Conger, and N. L. Weintraub, ‘Novel concepts in radiation-induced cardiovascular disease’, *World J. Cardiol.*, vol. 8, no. 9, pp. 504–519, Sep. 2016, doi: 10.4330/wjc.v8.i9.504.

[50] H. Wang *et al.*, ‘Radiation-induced heart disease: a review of classification, mechanism and prevention’, *Int. J. Biol. Sci.*, vol. 15, no. 10, pp. 2128–2138, 2019, doi: 10.7150/ijbs.35460.

[51] D. Hardy, C.-C. Liu, J. N. Cormier, R. Xia, and X. L. Du, ‘Cardiac toxicity in association with chemotherapy and radiation therapy in a large cohort of older patients with non-small-cell lung cancer’, *Ann. Oncol.*, vol. 21, no. 9, pp. 1825–1833, Sep. 2010, doi: 10.1093/annonc/mdq042.

[52] M. Boerma, K. A. Roberto, and M. Hauer-Jensen, ‘Prevention and Treatment of Functional and Structural Radiation Injury in the Rat Heart by Pentoxifylline and Alpha-Tocopherol’, *Int. J. Radiat. Oncol. Biol. Phys.*, vol. 72, no. 1, pp. 170–177, Sep. 2008, doi: 10.1016/j.ijrobp.2008.04.042.

[53] V. A. B. van den Bogaard *et al.*, ‘Validation and Modification of a Prediction Model for Acute Cardiac Events in Patients With Breast Cancer Treated With Radiotherapy Based on Three-Dimensional Dose Distributions to Cardiac Substructures’, *J. Clin. Oncol.*, vol. 35, no. 11, pp. 1171–1178, prilis 2017, doi: 10.1200/JCO.2016.69.8480.

[54] M. Boerma *et al.*, ‘Influence of Endothelin 1 Receptor Inhibition on Functional, Structural and Molecular Changes in the Rat Heart after Irradiation’, *Radiat. Res.*, vol. 170, no. 3, pp. 275–283, Sep. 2008, doi: 10.1667/RR1093.1.

[55] G. C. Meléndez, J. L. McLarty, S. P. Levick, Y. Du, J. S. Janicki, and G. L. Brower, ‘Interleukin 6 Mediates Myocardial Fibrosis, Concentric Hypertrophy, and Diastolic Dysfunction in Rats’, *Hypertension*, vol. 56, no. 2, pp. 225–231, 0 2010, doi: 10.1161/HYPERTENSIONAHA.109.148635.

[56] B. Farhood *et al.*, ‘TGF-β in radiotherapy: Mechanisms of tumor resistance and normal tissues injury’, *Pharmacol. Res.*, vol. 155, p. 104745, 0 2020, doi: 10.1016/j.phrs.2020.104745.

[57] S. Schultz-Hector, ‘Radiation-induced Heart Disease: Review of Experimental Data on Dose Reponse and Pathogenesis’, *Int. J. Radiat. Biol.*, vol. 61, no. 2, pp. 149–160, 0 1992, doi: 10.1080/09553009214550761.

[58] M. Sárközy, Z. Kahán, and T. Csont, ‘A myriad of roles of miR-25 in health and disease’, *Oncotarget*, vol. 9, no. 30, pp. 21580–21612, Apr. 2018, doi: 10.18632/oncotarget.24662.

[59] K. N. Papanicolaou, Y. Izumiya, and K. Walsh, ‘Forkhead Transcription Factors and Cardiovascular Biology’, *Circ. Res.*, vol. 102, no. 1, pp. 16–31, 0 2008, doi: 10.1161/CIRCRESAHA.107.164186.

[60] Z. Lu and S. Xu, ‘ERK1/2 MAP kinases in cell survival and apoptosis’, *IUBMB Life*, vol. 58, no. 11, pp. 621–631, 2006, doi: 10.1080/15216540600957438.

[61] C. Company *et al.*, ‘Contributions of ACE and mast cell chymase to endogenous angiotensin II generation and leucocyte recruitment in vivo’, *Cardiovasc. Res.*, vol. 92, no. 1, pp. 48–56, 0 2011, doi: 10.1093/cvr/cvr147.

[62] M. Miyazaki and S. Takai, ‘Tissue Angiotensin II Generating System by Angiotensin-Converting Enzyme and Chymase’, *J. Pharmacol. Sci.*, vol. 100, no. 5, pp. 391–397, 2006, doi: 10.1254/jphs.CPJ06008X.

[63] M. Boerma, C. Zurcher, I. Esveldt, C. I. Schutte-Bart, and J. Wondergem, ‘Histopathology of ventricles, coronary arteries and mast cell accumulation in transverse and longitudinal sections of the rat heart after irradiation’, *Oncol. Rep.*, vol. 12, no. 2, pp. 213–219, Aug. 2004, doi: 10.3892/or.12.2.213.

[64] R. Yarom *et al.*, ‘Effect of Captopril on Changes in Rats’ Hearts Induced by Long-Term Irradiation’, *Radiat. Res.*, vol. 133, no. 2, pp. 187–197, 1993, doi: 10.2307/3578356.

[65] J. E. J. Schultz *et al.*, ‘TGF-β1 mediates the hypertrophic cardiomyocyte growth induced by angiotensin II’, *J. Clin. Invest.*, vol. 109, no. 6, pp. 787–796, Mar. 2002, doi: 10.1172/JCI14190.

[66] S. Wassmann *et al.*, ‘Interleukin-6 Induces Oxidative Stress and Endothelial Dysfunction by Overexpression of the Angiotensin II Type 1 Receptor’, *Circ. Res.*, vol. 94, no. 4, pp. 534–541, 0 2004, doi: 10.1161/01.RES.0000115557.25127.8D.

[67] J. L. Miguel-Carrasco *et al.*, ‘Mechanisms underlying the cardiac antifibrotic effects of losartan metabolites’, *Sci. Rep.*, vol. 7, no. 1, p. 41865, 2017, doi: 10.1038/srep41865.

[68] M. Wu *et al.*, ‘Losartan Attenuates Myocardial Endothelial-To-Mesenchymal Transition in Spontaneous Hypertensive Rats via Inhibiting TGF-β/Smad Signaling’, *PLOS ONE*, vol. 11, no. 5, p. e0155730, May 2016, doi: 10.1371/journal.pone.0155730.

[69] W. Yang *et al.*, ‘Angiotensin II downregulates catalase expression and activity in vascular adventitial fibroblasts through an AT1R/ERK1/2-dependent pathway’, *Mol. Cell. Biochem.*, vol. 358, no. 1, p. 21, 2011, doi: 10.1007/s11010-011-0915-1.

[70] W. Zhang, V. Elimban, Y. J. Xu, M. Zhang, M. S. Nijjar, and N. S. Dhalla, ‘Alterations of Cardiac ERK1/2 Expression and Activity Due to Volume Overload Were Attenuated by the Blockade of RAS’, *J. Cardiovasc. Pharmacol. Ther.*, vol. 15, no. 1, pp. 84–92, 0 2010, doi: 10.1177/1074248409356430.

[71] W. Xiong, T. Meisinger, R. Knispel, J. M. Worth, and B. T. Baxter, ‘MMP-2 Regulates Erk1/2 Phosphorylation and Aortic Dilatation in Marfan Syndrome’, *Circ. Res.*, vol. 110, no. 12, pp. e92–e101, 0 2012, doi: 10.1161/CIRCRESAHA.112.268268.

[72] K. Asano *et al.*, ‘Selective Downregulation of the Angiotensin II AT1-Receptor Subtype in Failing Human Ventricular Myocardium’, *Circulation*, vol. 95, no. 5, pp. 1193–1200, 0 1997, doi: 10.1161/01.CIR.95.5.1193.

[73] M. a. W. Hermans, J. E. Roeters van Lennep, P. L. A. van Daele, and I. Bot, ‘Mast Cells in Cardiovascular Disease: From Bench to Bedside’, *Int. J. Mol. Sci.*, vol. 20, no. 14, p. 3395, Jan. 2019, doi: 10.3390/ijms20143395.

[74] T. Wang, W. Gao, K. Xiao, Q. Liu, and R. Jia, ‘Interaction between interleukin‐6 and angiotensin II receptor 1 in the hypothalamic paraventricular nucleus contributes to progression of heart failure’, *Mol. Med. Rep.*, vol. 15, no. 6, pp. 4259–4265, Jun. 2017, doi: 10.3892/mmr.2017.6495.

[75] H. Chen, A. V. Louie, D. S. Higginson, D. A. Palma, R. Colaco, and A. Sahgal, ‘Stereotactic Radiosurgery and Stereotactic Body Radiotherapy in the Management of Oligometastatic Disease’, *Clin. Oncol.*, vol. 32, no. 11, pp. 713–727, Nov. 2020, doi: 10.1016/j.clon.2020.06.018.

I.

International Journal of
Molecular Sciences

MDPI

Article

Investigation of the Antihypertrophic and Antifibrotic Effects of Losartan in a Rat Model of Radiation-Induced Heart Disease

Mónika Gabriella Kovács [1], Zsuzsanna Z. A. Kovács [1], Zoltán Varga [2], Gergő Szűcs [1], Marah Freiwan [1], Katalin Farkas [3], Bence Kővári [4], Gábor Cserni [4], András Kriston [5,6,7], Ferenc Kovács [5,6,7], Péter Horváth [5,6,7], Imre Földesi [3], Tamás Csont [1,*], Zsuzsanna Kahán [2,†] and Márta Sárközy [1,*,†]

1 Interdisciplinary Center of Excellence and MEDICS Research Group, Department of Biochemistry, Albert Szent-Györgyi Medical School, University of Szeged, H-6720 Szeged, Hungary; kovacs.monika.gabriella@med.u-szeged.hu (M.G.K.); kovacs.zsuzsanna@med.u-szeged.hu (Z.Z.A.K.); szucs.gergo@med.u-szeged.hu (G.S.); marah.mf.94@gmail.com (M.F.)
2 Department of Oncotherapy, Albert Szent-Györgyi Medical School, University of Szeged, H-6720 Szeged, Hungary; varga.zoltan@med.u-szeged.hu (Z.V.); kahan.zsuzsanna@med.u-szeged.hu (Z.K.)
3 Department of Laboratory Medicine, Albert Szent-Györgyi Medical School, University of Szeged, H-6720 Szeged, Hungary; lokine.farkas.katalin@med.u-szeged.hu (K.F.); foldesi.imre@med.u-szeged.hu (I.F.)
4 Department of Pathology, Albert Szent-Györgyi Medical School, University of Szeged, H-6720 Szeged, Hungary; kovari.bence@med.u-szeged.hu (B.K.); cserni.gabor@med.u-szeged.hu (G.C.)
5 Synthetic and Systems Biology Unit, Biological Research Centre, Eötvös Loránd Research Network, H-6726 Szeged, Hungary; kriston.andras@single-cell-technologies.com (A.K.); kovacs.ferenc@single-cell-technologies.com (F.K.); peter.horvath@brc.hu (P.H.)
6 Single-Cell Technologies Ltd., H-6726 Szeged, Hungary
7 Institute for Molecular Medicine Finland (FIMM), University of Helsinki, FIN-00014 Helsinki, Finland
* Correspondence: csont.tamas@med.u-szeged.hu (T.C.); sarkozy.marta@med.u-szeged.hu (M.S.)
† These authors contributed to the work equally.

Abstract: Radiation-induced heart disease (RIHD) is a potential late side-effect of thoracic radiotherapy resulting in left ventricular hypertrophy (LVH) and fibrosis due to a complex pathomechanism leading to heart failure. Angiotensin-II receptor blockers (ARBs), including losartan, are frequently used to control heart failure of various etiologies. Preclinical evidence is lacking on the anti-remodeling effects of ARBs in RIHD, while the results of clinical studies are controversial. We aimed at investigating the effects of losartan in a rat model of RIHD. Male Sprague-Dawley rats were studied in three groups: (1) control, (2) radiotherapy (RT) only, (3) RT treated with losartan (per os 10 mg/kg/day), and were followed for 1, 3, or 15 weeks. At 15 weeks post-irradiation, losartan alleviated the echocardiographic and histological signs of LVH and fibrosis and reduced the overexpression of chymase, connective tissue growth factor, and transforming growth factor-beta in the myocardium measured by qPCR; likewise, the level of the SMAD2/3 protein determined by Western blot decreased. In both RT groups, the pro-survival phospho-AKT/AKT and the phospho-ERK1,2/ERK1,2 ratios were increased at week 15. The antiremodeling effects of losartan seem to be associated with the repression of chymase and several elements of the TGF-β/SMAD signaling pathway in our RIHD model.

Keywords: onco-cardiology; radiation-induced heart disease; diastolic dysfunction; left ventricular hypertrophy; fibrosis; heart failure; angiotensin-II receptor blocker (ARB); losartan; chymase; TGF-β/SMAD signaling pathway

Citation: Kovács, M.G.; Kovács, Z.Z.A.; Varga, Z.; Szűcs, G.; Freiwan, M.; Farkas, K.; Kővári, B.; Cserni, G.; Kriston, A.; Kovács, F.; et al. Investigation of the Antihypertrophic and Antifibrotic Effects of Losartan in a Rat Model of Radiation-Induced Heart Disease. *Int. J. Mol. Sci.* **2021**, *22*, 12963. https://doi.org/10.3390/ijms222312963

Academic Editors: Francesco Fedele and Paul J. Mather

Received: 31 October 2021
Accepted: 26 November 2021
Published: 30 November 2021

1. Introduction

Cardiovascular diseases and cancer are the leading causes of morbidity and mortality worldwide [1,2]. The most common cancerous diseases are breast and lung cancers in women and men, respectively [2]. Cancer therapy has undergone significant improvement, which led to increased long-term survival rates among cancer patients [3]. About

50% of cancer patients receive radiotherapy (RT), which also has an important role in the treatment of malignancies superposed on the chest wall, such as breast cancer and thoracic malignancies including lung, and esophageal cancers, Hodgkin's lymphoma, and thymoma [3,4]. While high-energy ionizing radiation (i.e., RT) successfully kills tumor cells, it could have harmful effects on the surrounding healthy tissues [5]. Depending on the RT technique and dose used in thoracic and breast malignancies, the heart can be at risk of being exposed to ionizing radiation resulting in radiogenic sequelae in a dose-dependent manner [6,7]. The syndrome of unwanted cardiovascular side effects of thoracic RT is termed radiation-induced heart disease (RIHD), which is a critical concern in current oncology and cardiology practice [8–10].

RIHD is a progressive multifactorial disease that covers a broad spectrum of cardiac pathology [8–10]. Its clinical manifestation includes acute and chronic pericarditis, conduction system abnormalities, ischemic heart disease, cardiomyopathy, heart failure with preserved ejection fraction (HFpEF) or reduced ejection fraction (HFrEF), and valvular heart disease [8–10]. RT simultaneously causes damage to the cardiac macrovasculature (i.e., coronary arteries) and microvasculature, as well as the myocardium (i.e., diffuse injury), leading to the complex pathomechanism of RIHD [11,12]. However, the precise molecular mechanisms in the progression of RIHD from acute to chronic heart diseases are not clearly understood yet. Evidence suggests that RT-induced direct nitro-oxidative damage of macromolecules, including DNA, proteins, and lipids, initiates the development of RIHD. At this acute phase of RIHD, the elevated nitro-oxidative stress causes injury to the endothelial and other cells, eventually leading to various forms of cell death and acute inflammation [8,12,13]. In the early chronic phase of RIHD, the sublethally damaged surviving cardiomyocytes develop hypertrophy accompanied by endothelial cell proliferation as a compensatory mechanism [8,12,13]. If these compensatory mechanisms are exhausted, chronic inflammatory processes, fibrosis, and endothelial senescence play the primary role in the progression of RIHD [8,12,13]. Several pathomechanisms, including nitro-oxidative stress, cell death, and inflammatory processes, overlap in the acute and chronic phases of RIHD [8]. The injury of the capillaries or coronary arteries disturbs circulation and leads to hypoxia which aggravates tissue damage [8]. These mechanisms seem to activate and potentiate each other leading to a vicious cycle in the progression of RIHD [8]. Unfortunately, therapeutic options for RIHD are currently insufficient. Therefore, understanding the exact molecular mechanisms in the progression of RIHD is essential for developing preventive and therapeutic strategies together with testing drugs that do not interfere with the anti-cancer effects of RT.

Chronic activation of the renin-angiotensin-aldosterone system (RAAS) plays a pivotal role in cardiovascular pathophysiology, including hypertension, cardiac hypertrophy, and heart failure via different systemic and tissue-specific mechanisms such as elevated nitro-oxidative and endoplasmic reticulum stress, inflammation, apoptosis, and fibrosis via transforming growth factor-β (TGF-β) signaling, and the transactivation of various intracellular protein kinases such as ERKs and AKT [14,15]. There is some preclinical evidence that irradiation could upregulate angiotensin-II (AngII) expression in the rat heart [16] and lungs [17] in a dose-dependent manner [18]. Interestingly, preclinical studies evaluating the cardiac effects of the widely used selective AngII type 1 (AT1) receptor blockers in RIHD are lacking in the literature. Only two clinical studies investigated the effects of ARBs in cancer patients treated with thoracic RT, and their results were controversial [19,20]. In the present study, we aimed at investigating the effects of the ARB losartan (widely used in standard heart failure therapy) in a rat model of RIHD.

2. Results

2.1. Systemic Effects of the Radiotherapy in Our RIHD Model

An overview of the experimental setup is shown in Figure 1. Altogether two animals died in the RT only group (in the 3-week and 15-week subgroups).

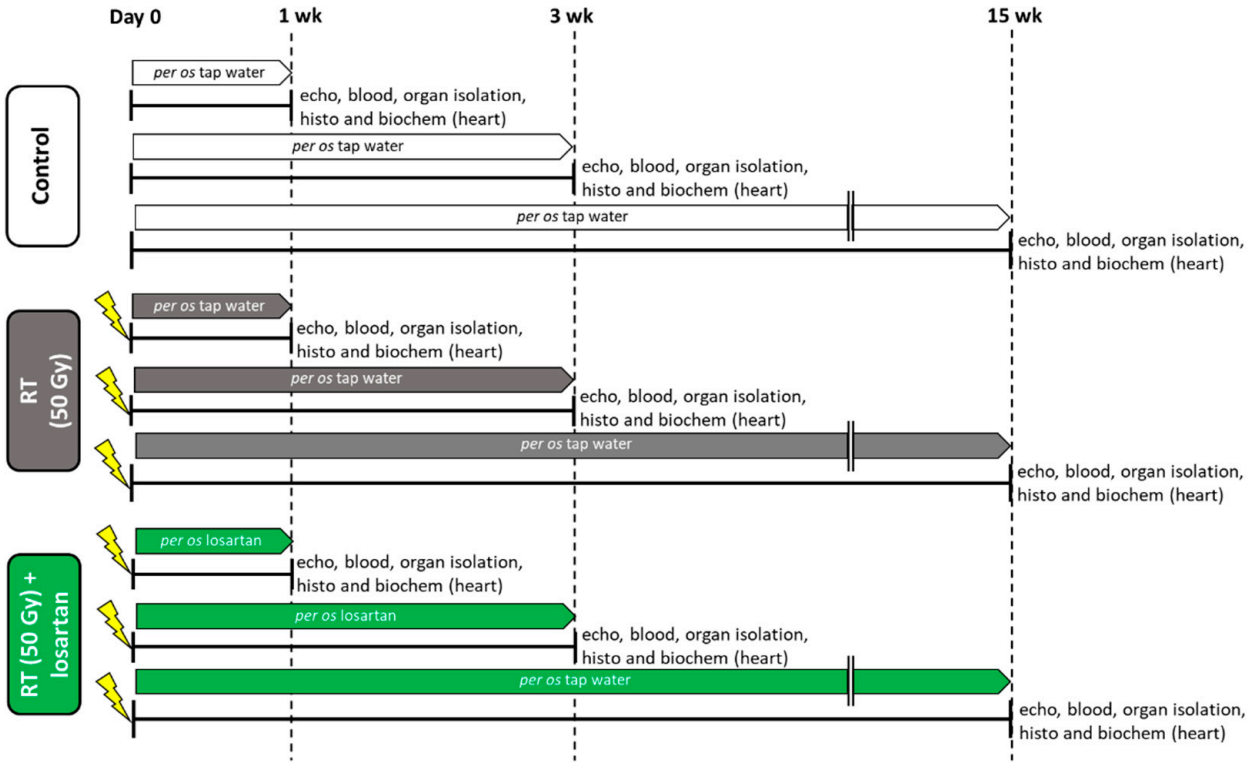

Figure 1. Experimental setup. Rats (n = 63) were divided into three groups (n = 6–9) and treated via oral gavage daily for 1, 3, or 15 weeks, respectively, as follows: (i) control group treated with tap water, (ii) radiotherapy (RT) only group treated with tap water, and (iii) RT plus losartan group treated with losartan (per os 10 mg/kg/day) dissolved in tap water. Cardiac morphology and function were assessed by transthoracic echocardiography (echo) at the end-points of each experiment under anesthesia. Then, blood was collected from the abdominal aorta to measure routine laboratory parameters, and hearts, lungs, and tibias were isolated. Left and right ventricles were separated, and left ventricular samples were prepared for histology (histo) and biochemical measurements (biochem). The development of LVH and fibrosis in the irradiated groups were investigated by the measurement of cardiomyocyte cross-sectional areas on hematoxylin-eosin-stained slides and picrosirius red/fast green-stained slides. The expression of selected genes related to LVH and fibrosis, heart failure, renin-angiotensin-aldosterone system (RAAS), and inflammation were measured at the transcript level by qRT-PCR. Left ventricular levels of selected proteins related to the RAAS, cardiac hypertrophy, and fibrosis pathways were measured by Western blot.

At weeks 1, 3, and 15, hearts, lungs, and tibias were isolated, then left and right ventricles were separated, and the organ weights and tibia lengths were measured (Figure 1 and Table 1). Before the treatments, there were no significant differences in the body weights between the groups in each experiment (Table 1). At week 1, there were no significant differences in the tibia length, heart weight, lung weight, and right ventricular weight between the groups. In contrast, body weight was significantly lower in the RT plus losartan group as compared to the control group (Table 1). Moreover, left ventricular weight was significantly reduced in both RT groups irrespective of the addition of losartan treatment as compared to the control group at week 1 (Table 1). At week 3, there was no significant difference in tibia length, heart weight, or right ventricular weight between the groups (Table 1). However, body weight and left ventricular weight were significantly smaller in the RT groups irrespective of losartan treatment compared to the control group at week 3, probably due to the detrimental effects of ionizing radiation in the RT groups (Table 1). Moreover, lung weights were significantly higher both in the RT only and losartan-treated RT groups compared to the control group, suggesting the presence of pulmonary edema at week 3 (Table 1) (Fluid was found in the lungs during the autopsy, data not shown). At week 15, body weight, tibia length, heart weight, and left ventricular weight were significantly smaller in both RT groups, irrespective of losartan treatment,

indicating that the irradiated animals had severe developmental retardation in the late chronic phase of RIHD (Table 1). In contrast, right ventricular and lung weights were not significantly different between the groups (Table 1).

Blood counts, hemoglobin concentrations, and hematocrit levels were determined at weeks 1, 3, and 15 to investigate the effects of losartan on the severity of systemic inflammation and the compensatory increase in hemoglobin synthesis associated with radiation-induced lung and heart damage (Figure 1). One week post-RT, white blood cell counts were not significantly higher (7% increase, $p = 0.646$) in the RT only group and significantly increased in the RT plus losartan group as compared to that in the control group (Table 2). At week 3, white blood cell counts were significantly increased in the irradiated groups irrespective of losartan treatment, suggesting the presence of systemic inflammation at that time point (Table 2). No such differences were detected between the groups at week 15 (Table 2). RT might lead to the activation of platelets which are considered important sources of pro-thrombotic agents during the inflammatory process [21]. Platelet counts were not significantly different between the groups at weeks 1 and 15. However, platelet counts showed a non-significant increase (16%, $p = 0.073$) in the RT only group and a significant increase in the losartan-treated RT group as compared to that in the control group at week 3 (Table 2).

At week 1, red blood cell counts were significantly elevated in both RT groups compared to the control group (Table 2). Hemoglobin level showed a trend to an increase (10%, $p = 0.057$) in the RT only group and a significant increase in the RT plus losartan group compared to the control group (Table 2). There was no significant difference in the hematocrit levels between the groups (Table 2). At week 3, there were no significant differences in the red blood cell counts, hemoglobin, or hematocrit levels between the groups (Table 2). In contrast, at week 15, red blood cell counts showed a trend to an increase (10%, $p = 0.076$) in the RT only group, and a significant increase in the RT plus losartan group, while hemoglobin concentrations and hematocrit levels were significantly increased in the RT groups irrespective of losartan treatment compared to the control group (Table 2).

2.2. Post-RT Diastolic Dysfunction Was Alleviated by Losartan at Weeks 1 and 3 but Not at Week 15

Transthoracic echocardiography was performed at weeks 1, 3, and 15 to monitor the effects of RT and losartan on cardiac morphology and function (Figure 1). At week 1, the diastolic parameter mitral valve early flow velocity (E) was not significantly different between the groups (Table 3). A sensitive parameter of the diastolic function, the septal mitral annulus velocity (e'), was significantly decreased in the RT only group as compared to the control group, indicating an early-phase diastolic dysfunction (DD) at week 1 (Table 3, Figure 2a). Septal e' was not significantly different between the control and the losartan-treated RT groups (Table 3, Figure 2a). Another indicator of DD, the E/e' ratio, was not significantly different between the RT only group and the control group. However, the E/e' ratio was significantly reduced in the RT plus losartan group as compared to the RT only or control groups at week 1 (Figure 2b).

At week 3, E velocity was not significantly different between the RT only and the control group (Table 3). In contrast, E velocity was significantly lower in the losartan-treated RT group than in RT only group at week 3 (Table 3). At week 15, E velocity was significantly lower in both RT groups irrespective of losartan treatment compared to the control group (Table 3). At weeks 3 and 15, the significantly decreased septal e' and significantly increased E/septal e' ratio indicated the presence of DD in the RT only groups compared to the time-matched control groups, respectively (Table 2, Figure 2a,b). Losartan significantly ameliorated these parameters compared to the RT group at week 3 (Table 2, Figure 2a,b). Nonetheless, at week 15, there was a trend to an increase (13.5%, $p = 0.061$) in the septal e' and a trend to decrease (17%, $p = 0.16$) in the E/septal e' parameter in the RT plus losartan group compared to the RT only group (Table 2, Figure 2a,b).

Table 1. Post-RT body weights, organ weights, and tibia lengths at weeks 1, 3, and 15.

Parameter (Unit)	Week 1			Week 3			Week 15		
	Control	RT	RT Los	Control	RT	RT Los	Control	RT	RT Los
Body weight at the beginning (g)	233 ± 8	233 ± 5	232 ± 4 *	282 ± 5	281 ± 7	282 ± 6	261 ± 3	263 ± 4	261 ± 5
Body weight at the endpoint (g)	269 ± 7	258 ± 6	251 ± 5 *	382 ± 9.57	338 ± 5.22 *	344 ± 8.8 *	525 ± 14	377 ± 29 *	414 ± 17 *
Tibia length (cm)	3.39 ± 0.06	3.36 ± 0.03	3.33 ± 0.04	3.83 ± 0.07	3.73 ± 0.05	3.86 ± 0.09	4.5 ± 0.04	4.25 ± 0.08 *	4.28 ± 0.04 *
Heart weight (g)	0.91 ± 0.02	0.87 ± 0.03	0.87 ± 0.02	1.16 ± 0.03	1.1 ± 0.04	1.06 ± 0.05	2.24 ± 0.11	1.75 ± 0.04 *	1.63 ± 0.11 *
Left ventricle weight (g)	0.62 ± 0.01	0.57 ± 0.02 *	0.55 ± 0.02 *	0.77 ± 0.02	0.69 ± 0.02 *	0.66 ± 0.02 *	1.3 ± 0.05	0.99 ± 0.03 *	0.88 ± 0.06 *
Right ventricle weight (g)	0.17 ± 0.01	0.17 ± 0.01	0.18 ± 0.01	0.24 ± 0.01	0.25 ± 0.01	0.23 ± 0.02	0.35 ± 0.01	0.33 ± 0.01	0.32 ± 0.02
Lung weight (g)	1.3 ± 0.02	1.29 ± 0.05	1.3 ±0.03	1.7 ± 0.12	2.98 ± 0.26 *	2.47 ± 0.29 *	1.64 ± 0.04	1.88 ± 0.32	1.50 ± 0.1

Values are presented as mean ± S.E.M., * $p < 0.05$ vs. control group, (n = 6–7, One-Way ANOVA, Holm-Sidak post hoc test). RT: radiotherapy only group (50 Gy), RT Los: RT plus losartan group.

Table 2. Post-RT blood cell counts, hemoglobin, and hematocrit values.

Parameter (Unit)	Week 1			Week 3			Week 15		
	Control	RT	RT Los	Control	RT	RT Los	Control	RT	RT Los
White blood cell counts (10^9/L)	5.79 ± 0.43	6.18 ± 0.7	7.15 ± 0.36 *	4.44 ± 0.56	6.77 ± 0.8 *	7.16 ± 0.7 *	6.09 ± 0.58	6 ± 0.39	6.51 ± 0.52
Platelet counts (10^9/L)	569 ± 8	587 ± 20	643 ± 33	559 ± 27	646 ± 35	673 ± 31 *	636 ± 17	586 ± 67	736 ± 53
Red blood cell counts (10^{12}/L)	6.69 ± 0.11	7.37 ± 0.29 *	7.74 ± 0.2 *	7.54 ± 0.15	7.54 ± 0.18	7.95 ± 0.18	8.30 ± 0.15	9.16 ± 0.44	9.50 ± 0.3 *
Hemoglobin (g/L)	130 ± 3	143 ± 5	146 ± 3 *	143 ± 3	142 ± 3	152 ± 3	146 ± 2	165 ± 8 *	175 ± 7 *
Hematocrit (L/L)	0.41 ± 0.01	0.44 ± 0.02	0.45 ± 0.01	0.44 ± 0.01	0.45 ± 0.01	0.47 ± 0.01	0.43 ± 0.01	0.49 ± 0.02 *	0.50 ± 0.02 *

Values are presented as mean ± S.E.M., * $p < 0.05$ vs. control group, (n = 6–7, One-Way ANOVA, Holm-Sidak post hoc test). RT: radiotherapy only group (50 Gy), RT Los: RT plus losartan group.

Table 3. Echocardiographic parameters according to treatment groups at weeks 1, 3, and 15.

Parameter (Unit)	Week 1			Week 3			Week 15		
	Control	RT	RT Los	Control	RT	RT Los	Control	RT	RT Los
E velocity (m/s)	1.00 ± 0.04	0.94 ± 0.05	0.90 ± 0.04	1.00 ± 0.04	1.05 ± 0.03	0.93 ± 0.04 #	1.01 ± 0.02	0.81 ± 0.10 *	0.75 ± 0.05 *
e′ (m/s)	0.060 ± 0.002	0.053 ± 0.001 *	0.063 ± 0.005	0.066 ± 0.006	0.038 ± 0.002 *	0.056 ± 0.005 #	0.077 ± 0.007	0.035 ± 0.002 *	0.042 ± 0.002 *
SWTs (mm)	2.70 ± 0.10	2.84 ± 0.16	2.91 ± 0.10	3.14 ± 0.15	3.47 ± 0.12	3.18 ± 0.14	3.58 ± 0.12	4.64 ± 0.17 *	4.29 ± 0.32
SWTd (mm)	1.61 ± 0.10	1.60 ± 0.09	1.90 ± 0.06	1.79 ± 0.12	1.73 ± 0.06	1.77 ± 0.14	1.83 ± 0.04	3.23 ± 0.33*	3.12 ± 0.28
AWTs (mm)	2.64 ± 0.17	2.61 ± 0.09	2.92 ± 0.20	2.85 ± 0.17	3.19 ± 0.18	2.89 ± 0.27	3.3 ± 0.23	4.56 ± 0.28 *	4.51 ± 0.17 *
AWTd (mm)	1.63 ± 0.17	1.51 ± 0.07	1.75 ± 0.09	1.61 ± 0.07	1.67 ± 0.11	1.67 ± 0.09	1.99 ± 0.13	3.14 ± 0.31 *	3.04 ± 0.17 *
IWTs (mm)	2.24 ± 0.13	2.47 ± 0.08	2.70 ± 0.10 *	2.67 ± 0.07	3.32 ± 0.17 *	2.91 ± 0.23	3.44 ± 0.25	4.56 ± 0.09 *	3.69 ± 0.31
IWTd (mm)	1.48 ± 0.03	1.51 ± 0.09	1.67 ± 0.09	1.73 ± 0.07	1.98 ± 0.07 *	1.90 ± 0.15	2.01 ± 0.12	3.67 ± 0.12 *	2.72 ± 0.26 *#
LVEDD (mm)	7.73 ± 0.22	7.34 ± 0.27	6.98 ± 0.16 *	8.33 ± 0.2	7.4 ± 0.14 *	7.11 ± 0.29 *	8.44 ± 0.33	4.85 ± 0.17 *	5.67 ± 0.29 *#
LVESD (mm)	4.75 ± 0.21	4.05 ± 0.28	3.68 ± 0.21 *	4.83 ± 0.17	3.40 ± 0.20 *	3.25 ± 0.25 *	4.26 ± 0.55	0.98 ± 0.15 *	1.63 ± 0.16 *
FS (%)	39 ± 2	45 ± 2 *	48 ± 2 *	42 ± 2	54 ± 2 *	54 ± 2 *	50 ± 5	80 ± 3 *	71 ± 3 *
EF (%)	56 ± 2	57 ± 3	52 ± 1	53 ± 2	53 ± 3	53 ± 1	53 ± 2	57 ± 2	55 ± 1

Values are presented as mean ± S.E.M., * $p < 0.05$ vs. control group, # $p < 0.05$ vs. RT group (n = 6–7, One-Way ANOVA, Holm-Sidak post hoc test). RT: radiotherapy only group (50 Gy), RT Los: RT plus losartan group. AWT: anterior wall thickness, d: diastolic, E: early flow velocity, e′: velocity of the septal mitral annulus, EF: ejection fraction, FS: fractional shortening, IWT: inferior wall thickness, LVEDD: left ventricular end-diastolic diameter, LVESD: left ventricular end-diastolic diameter, s: systolic, SWT: septal wall thickness.

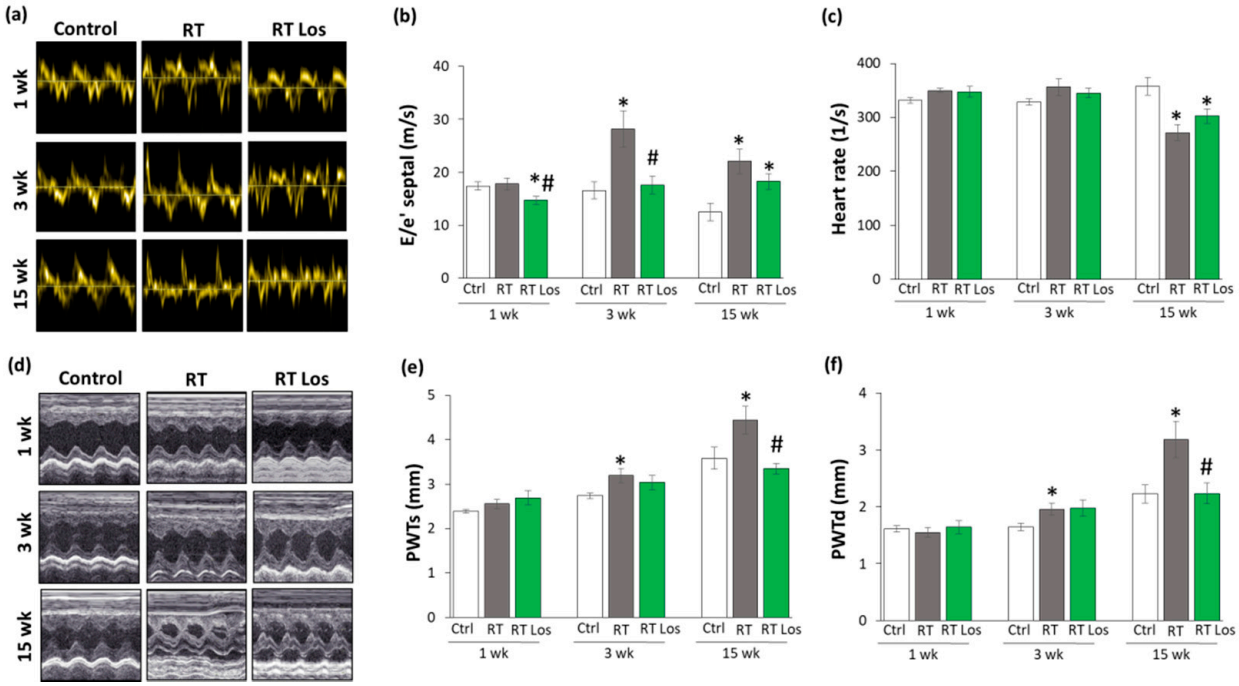

Figure 2. The effects of losartan on the echocardiographic parameters at weeks 1, 3, and 15. (**a**) Representative tissue Doppler images of diastolic septal mitral annulus velocity e', (**b**) mitral valve early flow velocity (E)/ e', (**c**) heart rate, (**d**) representative M-mode images of wall thicknesses and left ventricular diameters, (**e**) posterior wall thicknesses in systole (PWTs) and (**f**) diastole (PWTd). Values are presented as mean ± S.E.M., * $p < 0.05$ vs. control group, # $p < 0.05$ vs. RT only group (n = 6–7, One-Way ANOVA, Holm-Sidak post hoc test). Ctrl: control group, RT: radiotherapy only group (50 Gy), RT Los: RT plus losartan group. Representative M-mode images were saved from the Echo- Pac Dimension v201 software.

Irradiation and cardiac remodeling might lead to heart rate changes [8]. There were no significant differences in the heart rate between the groups at weeks 1 and 3 (Figure 2c). In contrast, the heart rate was significantly decreased in both RT groups irrespective of losartan treatment at week 15 (Figure 2c).

2.3. RT-Related Echocardiographic Signs of Left Ventricular Hypertrophy (LVH) Were Alleviated by Losartan at Week 15

At week 1, there was no significant difference in wall thicknesses and left ventricular diameters, and ejection fraction between the RT only and control groups (Table 3, Figure 2d–f). Nevertheless, in the RT only group, the systolic inferior and posterior wall thicknesses increased in a statistically non-significant manner (10%, p = 0.14 and 7%, p = 0.17, respectively) while the left ventricular end-systolic diameter decreased in comparison with the control group (trend, 15%, p = 0.07), supposing the beginning of the development of LVH at week 1 (Table 3, Figure 2d–f). These echocardiographic signs of a mild LVH resulted in significantly increased fractional shortening in the RT only group measured by the Teichholz method in M-mode images at week 1 (Table 3). Interestingly, similar statistically significant changes occurred in the systolic inferior wall thickness and left ventricular end-systolic and end-diastolic diameters in the RT plus losartan group compared to the control group at week 1 (Table 3). The systolic posterior wall thickness showed a trend to increase (13%, p = 0.084) in the RT plus losartan group compared to the control group at week 1 (Figure 2e). Notably, there were no significant differences in the echocardiographic morphologic and functional parameters between the RT only and RT plus losartan groups at week 1.

At week 3, inferior and posterior wall thicknesses both in systole and diastole were significantly increased in the RT only group as compared to that in the control group,

indicating the development of LVH (Table 3, Figure 2d–f). Accordingly, the left ventricular end-systolic and end-diastolic diameters were significantly smaller, and the fractional shortening was significantly higher in the RT only group as compared to that in the control group at week 3 (Table 3, Figure 2d). There were no significant differences in the systolic and diastolic inferior and systolic posterior wall thicknesses between the control and RT plus losartan groups (Table 3, Figure 2d–f). However, the left ventricular end-diastolic and end-systolic diameters remained significantly smaller, and the fractional shortening was significantly higher in the RT plus losartan group compared to those in the control group at week 3 (Table 3, Figure 2c,d). There were no significant differences in the ejection fraction between the groups at week 3.

At week 15, severe concentric LVH developed in the RT only group with a significant increase in all wall thicknesses and fractional shortening and a marked reduction in the left ventricular end-diastolic and end-systolic diameters compared to the control group (Table 3, Figure 2d–f). After losartan therapy, the systolic and diastolic posterior and diastolic inferior wall thicknesses were significantly reduced, and the left ventricular end-diastolic diameter markedly increased as compared to these values in the RT only group suggesting anti-hypertrophic effects of losartan in our chronic RIHD model at week 15 (Table 3, Figure 2d–f). Moreover, systolic inferior wall thickness and fractional shortening showed a trend of being lower (19%, $p = 0.068$ and 13%, $p = 0.098$, respectively), and the left ventricular end-systolic diameter seemed to be higher (66%, $p = 0.063$) in response to losartan compared to the RT only group at week 15 (Table 3). However, there was no significant difference in the ejection fraction between the groups at week 15.

2.4. Cardiomyocyte Hypertrophy and the Overexpression of LVH Markers Were Reduced in the Losartan-Treated Animals 3 and 15 Weeks after RT

Cardiomyocyte cross-sectional areas were measured on hematoxylin–eosin-stained histological slides. Additionally, the left ventricular expressions of cardiac hypertrophy markers were measured by qRT-PCR to resolve the contradiction between the autopsy and echocardiography results on heart size and LVH development (Tables 1 and 3, Figures 2 and 3).

At week 1, there were no significant differences in the cardiomyocyte cross-sectional areas between the groups, supporting the heart weight results (Figure 3a,b, and Table 1). In contrast, at week 1, the echocardiographic signs showed the initiation of LVH (Table 3 and Figure 2d–f). Therefore, we investigated the expression of the fetal myosin heavy chain β-isoform (i.e., β-MHC or *Myh7*) and the adult myosin heavy chain α-isoform (i.e., α-MHC or *Myh6*), as well as their ratio, in order to use them as molecular markers of LVH (Figure 3c–e). The increased ratio of the β-MHC to the α-MHC is an indicator of the fetal gene reprogramming in LVH in response to tissue hypoxia [22]. At week 1, the expression of α-MHC was significantly decreased, and the expression of β-MHC was tendentiously increased in both RT groups irrespective of losartan treatment (93%, $p = 0.061$ and 80%, $p = 0.067$, respectively, Figure 3c,d). Accordingly, as a compensatory mechanism to cardiac tissue damage due to RT, the β-MHC to α-MHC (*Myh7/Myh6*) ratio was significantly increased in both RT groups compared to the control group, supporting the echocardiographic signs of the initiation of compensatory LVH at week 1 (Table 2).

At week 3, the cardiomyocyte cross-sectional area showed a trend toward a decrease (10%, $p = 0.08$) in the RT only group compared to the control group, paralleling the left ventricular weight results (Figure 3a,b, Table 1). Notably, there were no significant differences in the cardiomyocyte cross-sectional areas between the control and losartan-treated RT groups, supposing the protective effects of losartan in our RIHD model at week 3 (Figure 3a,b). At the molecular level, there was no significant difference in the expression of α-MHC between the groups at week 3 (Figure 3c). In contrast, the β-MHC expression and the β-MHC to α-MHC ratio were significantly higher in the RT only group compared to the control group, supporting the echocardiographic signs of a mild LVH in our RIHD model at week 3 (Figure 3d,e, Table 1). There were no significant differences in the β-MHC expression and the β-MHC to α-MHC ratio between the losartan-treated RT and control

groups, similar to the echocardiographic and histologic results in our RIHD model at week 3 (Figure 3d,e, Table 1).

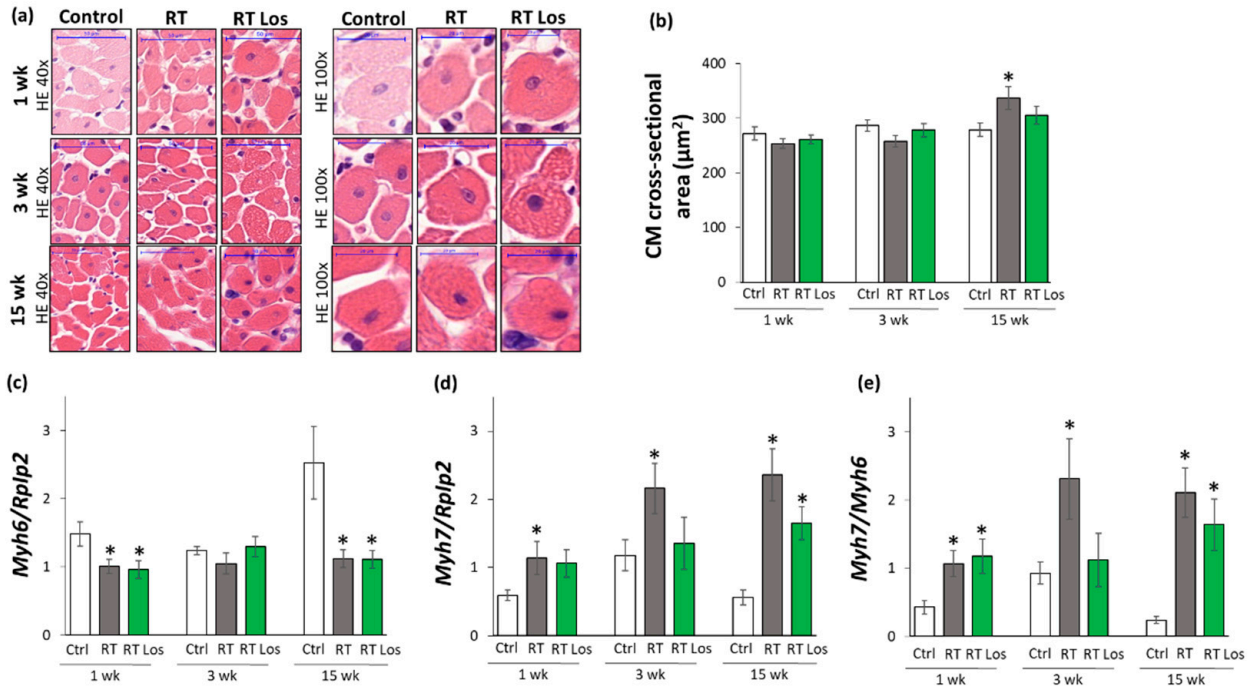

Figure 3. The effects of losartan on left ventricular hypertrophy assessed by histology at weeks 1, 3, and 15. (**a**) Representative hematoxylin-eosin (HE)-stained sections at 40× and 100× magnification, (**b**) cardiomyocyte cross-sectional area, (**c**) alpha-myosin heavy chain (*Myh6*), and (**d**) beta-myosin heavy chain (*Myh7*) expression in the left ventricle normalized to the ribosomal protein lateral stalk subunit P2 (*RpIp2)* gene expression, (**e**) *Myh7/Myh6* ratios. On the digital HE images, cardiomyocyte (CM) cross-sectional areas were measured in 100 selected cardiomyocytes in left ventricular tissue sections cut on equivalent planes. Scale bars represent 50 µm in the 40× magnified images and 20 µm in the 100× magnified images. Values are presented as mean ± S.E.M., * $p < 0.05$ vs. control group, (n = 6–7, One-Way ANOVA, Holm-Sidak post hoc test). Ctrl: control group, RT: radiotherapy only group (50 Gy), RT Los: RT plus losartan group. Representative HE-stained slides were captured in the Panoramic Viewer 1.15.4 software.

At week 15, the cardiomyocyte cross-sectional area was significantly higher in the RT only group compared to the control group, indicating the development of hypertrophy in the surviving cardiomyocytes as a compensatory mechanism despite the smaller heart size in our RIHD model (Figure 3a,b, Table 1). Moreover, there were no significant differences in the cardiomyocyte cross-sectional areas between the losartan-treated RT and control groups, similarly to the echocardiographic results on the anti-hypertrophic effects of losartan at week 15 (Figure 3a,b, Table 1). The α-MHC expressions were markedly decreased, and the β-MHC expressions with the β-MHC to α-MHC ratios were significantly increased in the RT only group as compared to that in the control group, indicating the development of cardiac hypertrophy at the molecular level in consistence with the echocardiographic results (Figures 2 and 3c–e, Table 3). Notably, the losartan-treated RT group showed a trend to a decrease (30%, p = 0.139) in β-MHC expression compared to the RT only group, in accordance with the echocardiographic results and supporting the anti-hypertrophic effects of losartan in our RIHD model (Figure 3d and Table 3).

2.5. Interstitial Fibrosis Was Reduced in the Losartan-Treated Animals 15 Weeks after RT

To further characterize the anti-remodeling effects of losartan in RIHD, fibrosis was quantified on picrosirius red and fast green-stained sections, and the left ventricular gene expression changes of fibrosis and heart failure markers were measured by qRT-PCR (Figures 1 and 4).

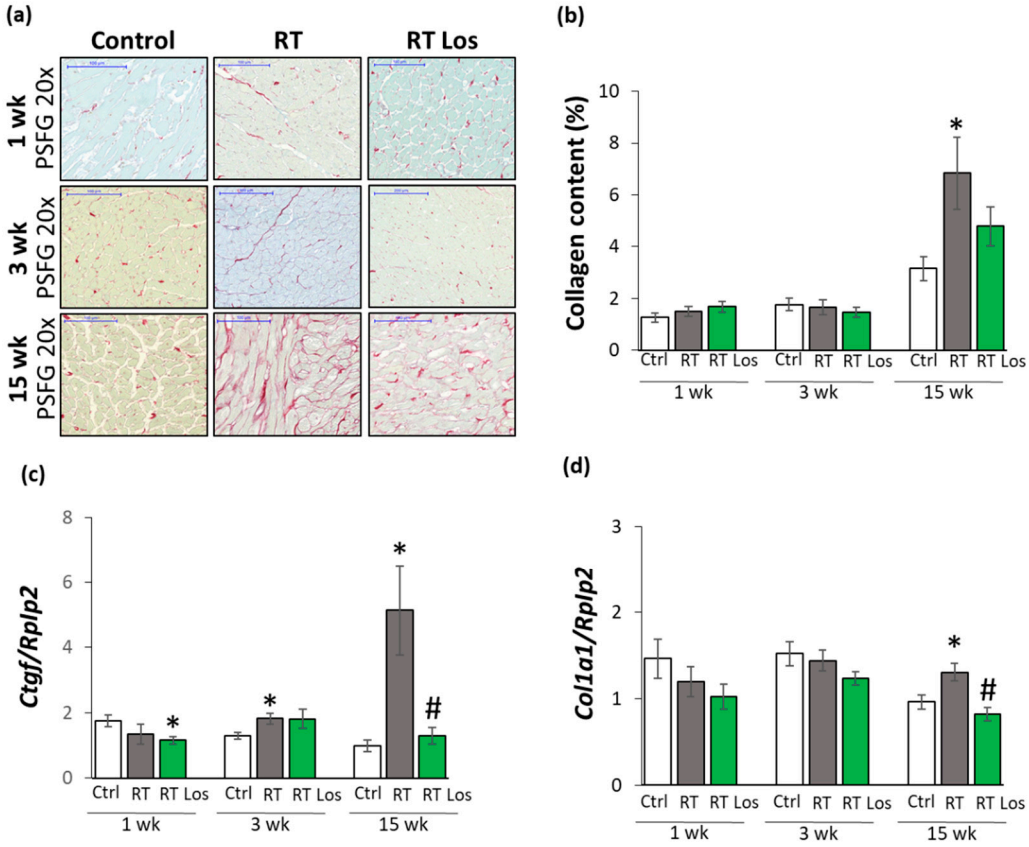

Figure 4. The effects of losartan on left ventricular fibrosis as assessed by histology and qRT-PCR at weeks 1, 3, and 15. (**a**) Representative picrosirius red and fast green (PSFG)-stained sections at 20× magnification, (**b**) left ventricular collagen content, left ventricular expression of (**c**) connective tissue growth factor (*Ctgf*), (**d**) collagen 1a1 (*Col1a1*) normalized to ribosomal protein lateral stalk subunit P2 (*Rplp2*) gene expression. The mean values of the collagen content of 10 representative PSFG-stained images were calculated and used for statistical evaluation in each left ventricular sample. Scale bars represent 100 μm at the 20× magnified images. Values are presented as mean ± S.E.M., * $p < 0.05$ vs. control group, # $p < 0.05$ vs. RT only group (n = 6–7, One-Way ANOVA, Holm-Sidak post hoc test). Ctrl: control group, RT: radiotherapy only group (50 Gy), RT Los: RT plus losartan group. Representative PSFG-stained slides were captured in the Panoramic Viewer 1.15.4 software.2.7.

At week 1, there was no significant difference in the collagen content between the groups (Figure 4a,b). Moreover, at week 1, left ventricular expressions of collagen type I alpha 1 (*Col1a1*) and the fibrosis marker connective tissue growth factor (*Ctgf*) showed no significant difference between the control and RT only groups (Figure 4c). Interestingly, losartan significantly reduced the *Ctgf* expression compared to the control group at week 1 (Figure 4c).

At week 3, there were no significant differences in the collagen content and *Col1a1* expressions between the groups, suggesting no severe fibrosis in this stage of RIHD (Figure 4a,b,d). Interestingly, the expression of the pro-fibrotic *Ctgf* was significantly increased in the RT only group and tendentiously elevated (43%, $p = 0.074$) in the losartan-treated RT group compared to the control group (Figure 4d), probably due to initiating wound healing by fibrosis after RT.

At week 15, the collagen content and *Col1a1* and *Ctgf*, expressions were significantly increased in the RT only group compared to that in the control group, supporting the development of left ventricular fibrosis (Figure 4a–d). There was no significant difference in the collagen content between the control and the losartan-treated RT groups, indicating the anti-fibrotic effects of losartan in RIHD at week 15 (Figure 4a,b). Indeed, losartan

significantly reduced the overexpression Col1a1 and Ctgf compared to the RT only group, showing its anti-remodeling effects in our RIHD model at the molecular level (Figure 4c–f).

2.6. Losartan Reduced the Chymase Overexpression at Weeks 3 and 15 after RT

Inflammatory processes triggered by the over-activation of RAAS are major contributors to the development of cardiac remodeling and fibrosis in RIHD [8]. Therefore, the effects of losartan on the cardiac expression of the inflammatory cytokines interleukin-1 (*Il1*), interleukin-6 (*Il6*), and tumor necrosis factor-α (*Tnfα*) were measured by qRT-PCR.

At week 1, the expressions of *Il1* and *Il6* were significantly higher in both RT groups, and the expression of *Tnfα* was tendentiously increased (79%, $p = 0.062$) in the RT only group and significantly increased in the RT plus losartan group as compared to the control group, indicating tissue inflammation after RT (Figure 5a–c). At week 3, all measured inflammatory markers, including *Il1*, *Il6*, and *Tnfα*, were significantly overexpressed in the RT only group compared to the control group, pointing out the presence of tissue inflammation at week 3 also (Figure 5a–c). Nevertheless, losartan significantly reduced the overexpression of Il6 at week 3 (Figure 5b). In contrast, the expression of *Il1* and *Tnfα* remained significantly higher in the RT plus losartan group compared to the control group at week 3 (Figure 5a,c). At week 15, there were no significant differences in the *Il1* and *Tnfα* expressions between the groups (Figure 5a–c). However, it should be mentioned that losartan reduced the Tnfα expression in a non-significant manner (45%, $p = 0.348$) compared to the control group. Only *Il6* was significantly overexpressed in the RT groups irrespective of losartan treatment compared to the control group (Figure 5b). Mast cell chymase is an alternative activator of tissue AngII in the heart under inflammatory conditions [23,24]. The collagenase matrix metalloprotease 2 (*Mmp2*) and the mast cell chymase (*Cma*) could be activated by each other in the heart under inflammatory conditions [25]. Indeed, due to the cardiac inflammation in or RIHD model, *Mmp2* was overexpressed in the RT groups irrespective of losartan treatment compared to the time-matched control groups at weeks 1, 3, and 15, respectively (Figure 5d). In contrast, *Cma* was significantly repressed in both RT groups irrespective of losartan treatment compared to the control group at week 1 (Figure 5e). At weeks 3 and 15, the significant overexpression of *Cma* due to RT was markedly reduced in the RT plus losartan group (Figure 5e).

2.7. Losartan Alleviated the Cardiac Fibrosis via Inhibiting the TGF-β-Mediated SMAD-Dependent Pathway in Our RIHD Model at Weeks 3 and 15

To further characterize the anti-remodeling effects of the AT1 receptor blocker losartan in RIHD, the expression of angiotensinogen (*Agt*) and transforming growth factor-β (*Tgfb*) was measured by qRT-PCR. In addition, the expression of the main AngII receptors, including the pro-inflammatory, pro-hypertrophic, and pro-fibrotic AT1 receptor, and the anti-inflammatory, anti-hypertrophic and anti-fibrotic type 2 (AT2) receptor were studied at the protein level [14,15] (Figure 6a–f). AT1 receptor was described to activate TGF-β, which can induce fibrosis via the canonical SMAD-dependent and the non-canonical SMAD-independent signaling pathways [14,15,26].

At week 1, there was no significant difference in *Agt* expression between the control and RT only groups. However, in the RT plus losartan group, significantly increased *Agt* expression was found as compared to the control group at week 1 (Figure 6a). No significant differences were detected in the expression of AT1 and AT2 receptors, TGF-β receptor type II (TGF-βRII) and SMAD2/3 levels between the groups at week 1, in consistence with the histology results on either collagen content or cardiomyocyte cross-sectional areas at week 1 (Figure 6b,c,e,f). Interestingly, *Tgfb* was significantly repressed in both RT groups irrespective of losartan compared to the control group at week 1 (Figures 4 and 6d).

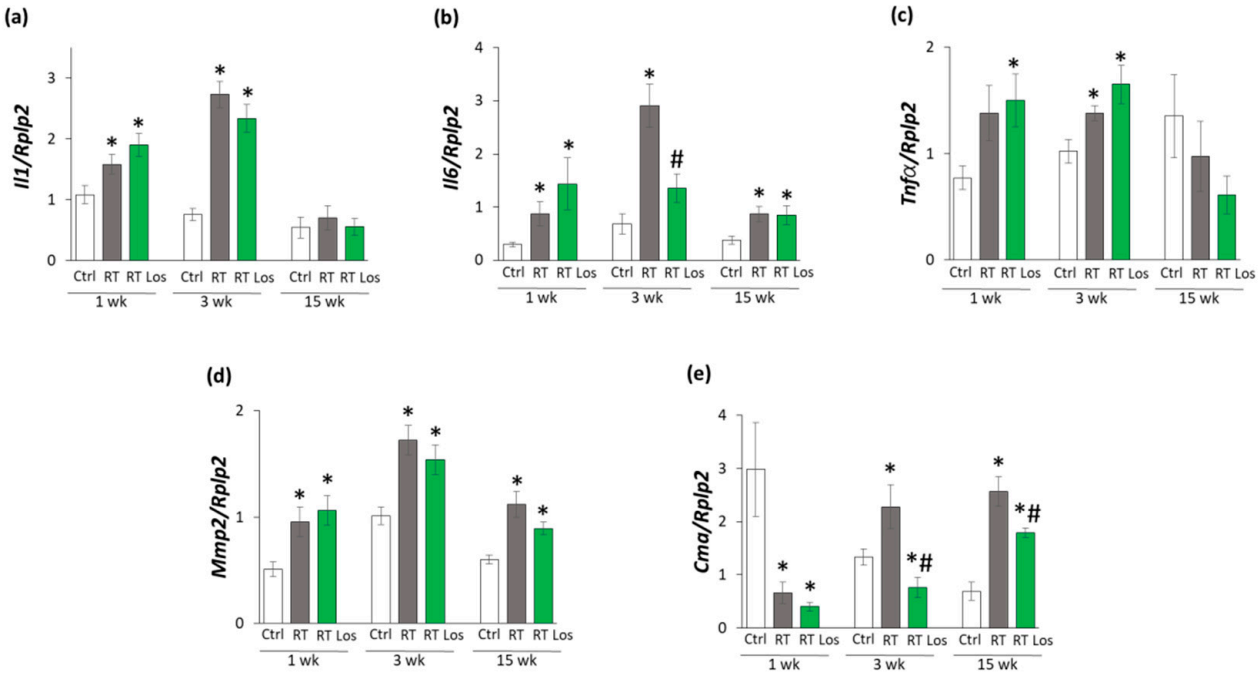

Figure 5. The effects of losartan on inflammatory gene expressions assessed by qRT-PCR at weeks 1, 3, and 15. Expression of (**a**) interleukin-1 (*Il1*), (**b**) interleukin-6 (Il6), (**c**) tumor necrosis factor-alpha (*Tnfα*), (**d**) matrix metalloprotease-2 (*Mmp2*), and (**e**) chymase (*Cma*) normalized to ribosomal protein lateral stalk subunit P2 (*Rplp2*) gene expression were measured in left ventricle samples. Values are presented as mean ± S.E.M., * $p < 0.05$ vs. control group, # $p < 0.05$ vs. RT only group (n = 6–7, One-Way ANOVA, Holm-Sidak post hoc test). Ctrl: control group, RT: radiotherapy only group (50 Gy), RT Los: RT plus losartan group.

At week 3, the *Agt* expression was tendentiously increased (40%, $p = 0.118$) in the RT only group compared to the control group, which may suggest a mild activation of tissue RAAS (Figure 6a). In both RT groups, the AT1 receptor protein levels showed a trend to decrease (19%, $p = 0.054$ and 16%, $p = 0.090$, respectively) compared to the control group (Figure 6b,c). Moreover, in both RT groups, the AT2 receptor protein expressions were significantly increased as compared to the control group (Figure 6c). There was no significant difference in the cardiac *Tgfb* expression between the groups (Figure 6d). In contrast, TGF-βRII and SMAD2/3 protein levels were significantly increased in the RT only group compared to the control group (Figure 6e,f). Losartan significantly reduced the SMAD2/3 levels but not the TGF-βRII level compared to the RT only group at week 3 (Figure 6e,f).

At week 15, there was no significant difference in *Agt* expression between the groups (Figure 6a). The AT1 receptor protein level was significantly decreased in the RT only group compared to the control group at week 15, supposedly, in response to the over-activation of AngII (Figure 6b). There was no significant difference in the AT1 receptor protein levels between the control and losartan-treated RT groups at week 15 (Figure 6b). There were no significant differences between the AT2 protein levels between the groups (Figure 6c). Interestingly, the significant overexpression of *Tgfb* was markedly reduced by losartan at week 15 (Figure 6d). Accordingly, SMAD2/3 protein levels were significantly increased in the RT only group compared to the control group at week 15, suggesting that the canonical SMAD-dependent signaling pathway might play a crucial role in the development of fibrosis in RIHD (Figure 6f). Interestingly, there were no significant differences between the AT2 receptor and TGF-βRII levels between the groups at week 15 (Figure 6c,e). In accordance with the echocardiography and histology results, there was no significant difference in the SMAD2/3 protein level between the losartan-treated RT and the control groups at week 15.

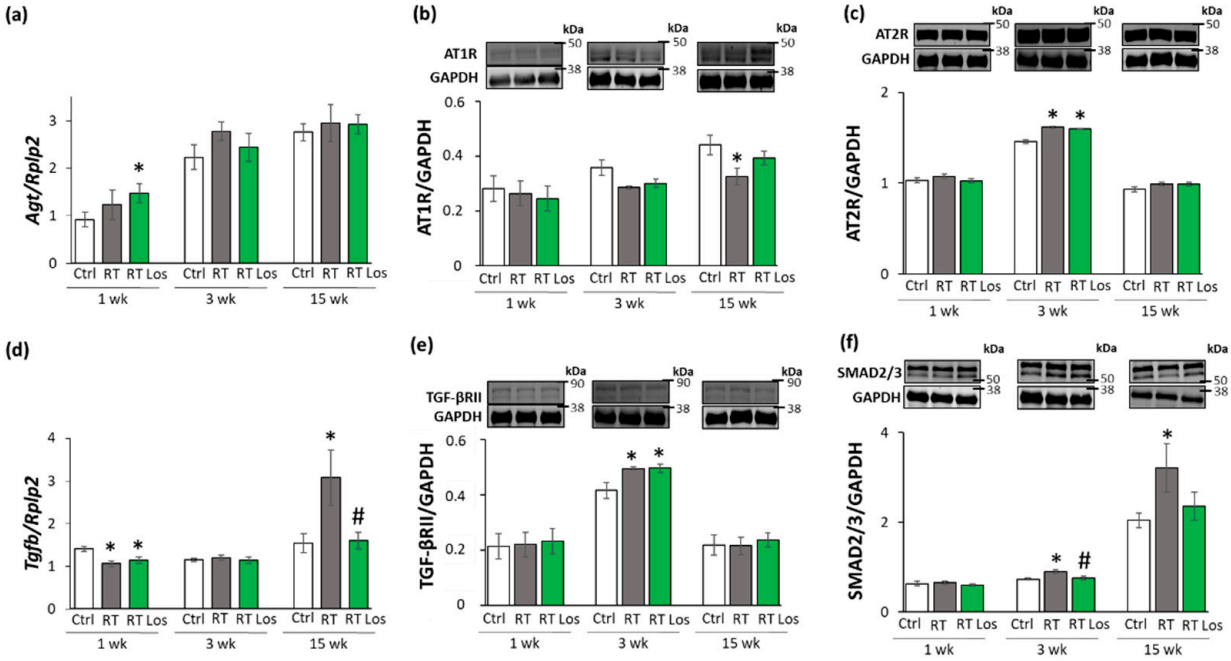

Figure 6. The effects of losartan on the expression of genes and proteins related to the cardiac renin-angiotensin-aldosterone system and canonical SMAD-dependent pathway at weeks 1, 3, and 15. Left ventricular expression of (**a**) angiotensinogen (*Agt*) normalized to ribosomal protein lateral stalk subunit P2 (*RpIp2*) gene expression, left ventricular protein expression and cropped representative images of (**b**) angiotensin II type 1 receptor (AT1R, 41 kDa), and (**c**) angiotensin II type 2 receptor (AT2R, 41 kDa), (**d**) left ventricular expression of transforming growth factor-beta (*Tgfb*) normalized to *RpIp2* gene expression, left ventricular expression and cropped representative images of (**e**) TGF-β receptor II (TGF-βRII, 85 kDa) and (**f**) SMAD2/3 (52 and 60 kDa). Values are presented as mean ± S.E.M., * $p < 0.05$ vs. control group, # $p < 0.05$ vs. RT only group (n = 6–7, One-Way ANOVA, Holm-Sidak post hoc test). Ctrl: control group, RT: radiotherapy only group (50 Gy), RT Los: RT plus losartan group. Glyceraldehyde-3-phosphate dehydrogenase (GAPDH, 37 kDa) was used as a loading control in protein expression changes assessed by Western blot. Images were captured with the Odyssey CLx machine and exported with Image Studio 5.2.5 software. Black lines next to the Western blot images represent the position of protein markers with corresponding molecular weights. The uncropped Ponceau-stained membranes and the full-length Western blot images with the protein ladders are presented in Figures S1–S9.

2.8. ERK1,2- and AKT-Mediated Pathways Might Be Involved in Compensatory Hypertrophy after RT at Week 15

The non-canonical SMAD-independent signaling pathways include ERK1,2, AKT, and STAT3-mediated fibrotic and hypertrophic pathways beyond other mediators [27]. The levels of total (t)ERK1,2, AKT, and STAT3 as well as their phosphorylated (p) forms are presented in the Figures S10 and S11.

At week 1, there was no significant difference in the expression of the pERK1,2/tERK1,2, pAKT/tAKT, and pSTAT3/STAT3 ratios between the groups (Figure 7a–d). At week 3, there were no significant differences in the pERK1/tERK1 and pERK2/tERK2 ratios between the RT only and control groups (Figure 7a,b). In contrast, after losartan treatment at week 3, the pERK1/tERK1 ratio was significantly increased, and a trend to an increase (60%, $p = 0.072$) was seen in the case of the pERK2/tERK2 ratio (Figure 7a,b). The higher pERK1 and pERK2 protein levels led to the increased pERK1/tERK1 and pERK2/tERK2 ratios in the losartan-treated RT group compared to the control group at week 3 (Figure S10). At week 15, pERK1/tERK1 and pERK2/tERK2 ratios were significantly increased in the RT groups irrespective of losartan treatment as compared to the control group (Figure 7a,b). Moreover, in response to losartan, the pERK1/tERK1 ratio was significantly elevated, and the pERK2/tERK2 ratio showed a trend to an increase (61%, $p = 0.063$) as compared to the RT only group (Figure 7a,b). The pERK1 and pERK2 protein levels showed a similar pattern to the pERK/tERK ratios (Figure S10). At weeks 1 and 3, there were no

significant differences in the pAKT/tAKT ratios, pAKT, or tAKT levels between the groups (Figures 7c and S11). At week 15, the pAKT/tAKT ratio was significantly higher in both RT groups irrespective of losartan treatment due to the higher pAKT levels compared to that in the control group (Figures 7c and S11).

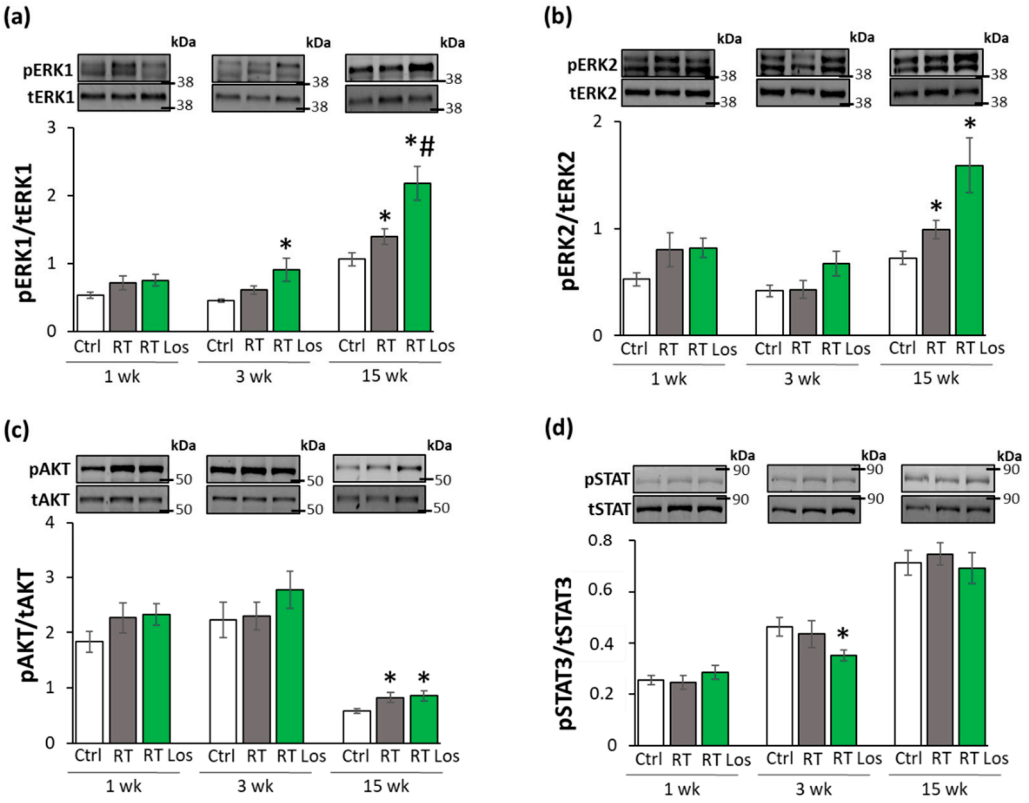

Figure 7. The effects of losartan on the expression of proteins associated with the non-canonical SMAD-independent fibrotic pathway at weeks 1, 3, and 15. Left ventricular expression and cropped representative images of (**a**) phospho-ERK1/total-ERK1 ratio (pERK1/tERK1 42 and 44 kDa), (**b**) phospho-ERK2/total-ERK2 ratio (pERK2/tERK2, 42 and 44 kDa), (**c**) phospho-AKT/total-AKT ratio (pAKT/tAKT, 60 kDa), (**d**) phospho-STAT3/total-STAT3 ratio (pSTAT3/tSTAT3, 79 and 86 kDa). Values are presented as mean ± S.E.M., * $p < 0.05$ vs. control group, # $p < 0.05$ vs. RT only group (n = 6–7, One-Way ANOVA, Holm-Sidak post hoc test). Ctrl: control group, RT: radiotherapy only group (50 Gy), RT Los: RT plus losartan group. Images were captured with the Odyssey CLx machine and exported with Image Studio 5.2.5 software. The phospho-protein and total protein levels are represented in Figures S10 and S11. Black lines next to the Western blot images represent the position of protein markers with corresponding molecular weights. The uncropped Ponceau-stained membranes and the full-length Western blot images with the protein ladders are presented in Figures S12–S17.

STAT3 could be activated not only via TGF-β on the non-canonical non-SMAD-dependent fibrotic pathway but also by AngII [28]. There were no significant differences in the pSTAT3/tSTAT3 ratios between the groups at weeks 1 and 15 (Figure 6d). However, in the RT plus losartan group at week 3, the pSTAT3/tSTAT3 ratio was significantly reduced as compared to the control group at week 3 (Figures 7d and S11). Notably, there was no significant difference in pSTAT3 levels between the losartan-treated RT and control groups at week 15, supporting the anti-remodeling effects of losartan in our RIHD model (Figure S11).

3. Discussion

Here we report that the selective AT1 receptor blocker losartan alleviates the radiation-induced left ventricular hypertrophy and fibrosis. The antiremodeling effects of losartan

seem to be associated with the repression of chymase and several elements of the canonical TGF-β/SMAD2/3 fibrotic pathway in our RIHD model. Moreover, the non-canonical SMAD-independent pathways, including the AKT and ERK1,2-mediated mechanisms, seem to be involved in the maintenance of compensatory hypertrophy in the late phase of RIHD.

RT-induced diffuse myocardial injury, leading to the clinical entity of cardiomyopathy and HF, is a progressive disease ending in cardiac fibrosis, which might develop over several years post-RT depending primarily on RT dose [8,12]. RT-induced cardiomyopathy and HF cover a spectrum of functional abnormalities. Among them, a typical initial phase is HFpEF characterized by DD and compensatory LVH [29–31]. Later on, due to the progression of interstitial fibrosis and loss of cardiomyocytes, the clinical entity of HFrEF develops [32,33]. Regarding the underlying pathomechanisms, in humans, radiation injury affects two important systems: one is blood circulation, and the other is the system of cardiomyocytes. Radiation exposure of the coronary arteries and microvasculature results in endothelial cell damage and disturbed circulation. Hypoxia and the injury of the endothelial cells aggravate chronic/progressive inflammation and fibrosis which are essential components of RIHD. In fact, in humans, this component is of utmost significance because RIHD manifests mostly as a potentially fatal coronary event. Concerning radiogenic cardiomyopathy, a fractionated RT dose of 40 Gy to the heart has been found to induce diffuse myocardial injury in patients that may be revealed early by serial follow-up tests [8,32]. Diffuse myocardial injury presents more commonly in patients who received higher RT doses (>60 Gy) and/or anthracycline chemotherapy [33,34]. In most RIHD animal models, exclusively cardiac fibrosis could be studied due to the difficulties in developing radiation-induced arteriosclerosis in rodents [11,12,35,36]. This is why most animal studies, including ours, focus on the effects of radiation-induced diffuse myocardial injury and consequential interstitial inflammation and fibrosis only. Previously, we developed a rat model of high dose radiation-induced heart damage using a single shot of selective heart irradiation of 50 Gy to investigate diffuse myocardial injury [37,38]. In the present study, we used this rat model of RIHD to investigate the effects of losartan.

The presented echocardiography and histology findings are consistent with the literature data [30,31,39] and the previous results in our rat model of RIHD [37,38]. We detected DD in the irradiated animals at every pre-specified follow-up time point in our rat model of RIHD. In fact, the molecular markers (of the expression of β-MHC and α-MHC in the LV and their ratios), echocardiography findings, and histological signs of LVH became more severe over time. Interestingly, the weights of the left ventricles were significantly lower in the RT groups as compared to that in the control group throughout the experiment, probably due to the cell death and developmental retardation caused by the RT. Despite the smaller left ventricular weights, the surviving cardiomyocytes might develop compensatory LVH to maintain the ejection fraction and sufficient oxygen supply to the whole body. Compensatory increase in the red blood cell counts at week 1 might be related to the hypoxia caused by radiation-induced heart and lung damage. Indeed, at week 1, *Il1* was significantly overexpressed in the left ventricles, pointing to the development of tissue inflammation in RIHD. The systemic inflammatory marker white blood cell count was significantly increased at week 3 in the irradiated animals. Accordingly, at week 3, the left ventricular expression of all investigated inflammatory markers, including *Il1*, *Il6*, and *Tnfα*, were significantly higher post-RT, indicating a more severe tissue inflammation at this phase. At week 15, *Il6* expression (which is a well-known mediator of myocardial fibrosis leading to concentric hypertrophy and secondary DD [40]) remained high. In the fibrotic phase with severe concentric LVH at week 15, hemoglobin and hematocrit levels significantly increased, probably, in response to the chronic hypoxia caused by radiogenic heart failure and lung fibrosis.

The key molecular mechanism of radiation-induced cardiac fibrosis is thought to be the TGF-β/SMAD2/3-mediated fibrotic pathway [12,21,41,42]. Indeed, molecular signs (i.e., overexpression of *Ctgf*, TGF-βRII, and SMAD2/3) preceded the histologic signs of fibrosis

3 weeks after the irradiation, showing the initiation of fibrotic remodeling in the heart in our RIHD model. At week 15, left ventricular *Ctgf* and SMAD2/3 expressions remained high with the overexpression of *Tgfb* and *Col1a1*. At week 15, the significantly increased interstitial collagen content of the left ventricle revealed the presence of fibrosis in RIHD. These molecular, morphological, and functional changes were similar to those reported in other studies [30,31]. We also investigated selected molecules, including AKT, ERK1,2, and STAT3 and their phosphorylated forms, in the non-canonical non-SMAD-dependent fibrotic pathway. Significantly increased pERK1,2/tERK1,2 and pAKT/tAKT ratios were detected after the RT at week 15. Since the ERK-mediated pathways are also considered survival pathways regulating cell death and hypertrophy [43], the increased pERK1,2/tERK1,2 ratios in the RT groups could be explained as compensatory defense mechanisms against cell death. AKT was also described as a molecule mediating cardiomyocyte survival and hypertrophy [27], and this, in fact, might explain the higher pAKT/tAKT ratios in the RT groups at week 15. In summary, the canonical SMAD-dependent TGF-β pathway seems to be responsible for the cardiac fibrosis in our RIHD model. The non-canonical SMAD-independent pathways, including the AKT and ERK1,2-mediated mechanisms, seem to be involved in cell survival and compensatory hypertrophy in RIHD.

It has been reported that irradiation could induce AngII overexpression in the rat heart [16] and lung [17] in a dose-dependent manner [18]. AngII can be cleaved from AngI by several proteases, of which angiotensin-converting enzyme (ACE), and alternatively, under inflammatory conditions, mast cell chymase are the primary converters [23,44,45]. Chymase overexpression seems to be particularly important in the cardiac generation of AngII in RIHD [23,46,47]. Interestingly, the cardiac RAAS interacts with many other systems in the heart, including the endothelin system and cardiac sympathetic nervous systems. The locally generated AngII appears to contribute to LVH and fibrosis via different mechanisms [23]. AngII has been reported to activate cardiac NADPH-oxidase via AT1 receptor, and subsequently, the over-production of reactive oxygen and nitrogen species leads to increased nitro-oxidative stress [48,49]. This could trigger the production of pro-inflammatory mediators, such as IL1, IL6, TNF-α, and TGF-β, contributing to cardiac remodeling and heart failure [48,49]. The AT1 receptor is mainly involved in pro-inflammatory, pro-hypertrophic, and pro-fibrotic mechanisms, whereas the AT2 receptor is associated with counter-regulatory anti-inflammatory, anti-hypertrophic and anti-fibrotic pathways in the cardiovascular system [14,15]. Therefore, selective AT1 blockade by losartan seems to be a rational therapeutic option to ameliorate cardiac remodeling by reducing nitro-oxidative stress and inflammatory mechanisms in RIHD. However, to our best knowledge, there are no experimental data on the anti-remodeling effects of ARBs in RIHD. Interestingly, two clinical trials investigated the effects of ARBs after RT; however, their results were controversial. The PRADA clinical trial demonstrated that administration of the ARB candesartan improved the reduced ejection fraction in early breast cancer patients treated with anthracycline-containing regimens with or without trastuzumab and RT [19]. In contrast, a retrospective clinical study found that ACE inhibitors or ARBs and higher RT doses were related to lower overall survival after the diagnosis of cancer in those patients who were treated with thoracic RT and later underwent percutaneous coronary interventions [20].

In the present study, at week 1, losartan-treatment did not influence the early molecular (i.e., left ventricular expressional changes of β-MHC and α-MHC and their ratios) and echocardiographic signs of LVH as assessed by M-mode echocardiography, probably due to the acute compensatory and surviving mechanisms in response to tissue damage caused by RT. At week 3, in the losartan-treated animals, various experimental parameters improved as compared to that in the RT only group, such as several echocardiographic signs of LVH and consequential DD together with the overexpression of β-MHC and SMAD2/3 in the left ventricle indicating a possible anti-hypertrophic and anti-fibrotic effect of losartan in the early chronic phase of RIHD. In contrast, white blood cell counts remained elevated irrespective of losartan treatment in RIHD at week 3, supposing the

presence of systemic inflammation. At week 15, losartan treatment did not reduce the molecular signs of LVH (the changes in the expression of β-MHC and α-MHC and their ratios), suggesting that the hypertrophic process is also active in this late chronic phase of RIHD as a compensatory mechanism to cardiomyocyte loss after RT and secondary hypoxia. However, according to the echocardiography and histology findings at week 15, losartan reduced the severity of LVH. Losartan reduced the interstitial collagen content by reducing the *Ctgf, Tgfb,* and *Col1a1* overexpression and SMAD2/3 levels in RIHD. Similar to our results, losartan reduced cardiac fibrosis in heart failure by reducing the CTGF and SMAD2/3 expression in other studies [50,51]. We also investigated molecules in the non-canonical SMAD-independent fibrotic pathway and found that pERK1,2/tERK1,2 ratios were significantly increased in the RT groups and were further increased by losartan at week 15. In contrast, several studies found that losartan reduced the pERK1,2/tERK1,2 ratio in heart failure [52,53]. Our result could be explained by the fact that ERK1,2 phosphorylation can be increased by MMP2 [54]. Indeed, losartan failed to significantly reduce the overexpression of *Mmp2* in our RIHD model.

Interestingly, at weeks 3 and 15, angiotensinogen expression was not significantly different between the groups, but the AT1 receptor levels were decreased, probably, due to increased AngII levels after RT. This finding is in accordance with human data showing that AT1 receptors are selectively downregulated in heart failure depending on the severity of ventricular dysfunction [55]. At week 15, the repression of the AT1 receptor was weakened by losartan, supposedly via blocking the cleavage of AngII from AngI. Indeed, the left ventricular expression of the mast cell chymase was higher both at week 3 and 15 in RIHD, likely mediated by cardiac inflammation and *Mmp2* overexpression [56]. Chymase overexpression was reduced by losartan at weeks 3 and 15, possibly explained by its mild anti-inflammatory effects in RIHD [57] (i.e., repression of *Il6* at week 3, and decreased expression of *Tnfα* at week 15). Indeed, it has been described that losartan was more effective than the ACE-inhibitor captopril in controlling ongoing vascular inflammation if AngII-dependent components of atherogenesis were present in mice [45]. However, DD was not improved by losartan in our RIHD model at week 15, which may have been due to the presence of local inflammation (i.e., *Il6* overexpression) and more severe LVH and fibrosis at this late chronic stage of RIHD.

Our study is not without limitations, similar to other experimental works. We intended to test losartan for controlling heart failure related to RIHD. Nevertheless, significant differences exist between the pathomechanisms in the model used vs. that in patients. (i) While, in humans, radiogenic coronary artery damage is an essential component of the radiation damage, in most murine models, no similar alterations evolve unless specific genetically modified animal strains are used [10–12,41,46]. In our experiments, RT-induced diffuse myocardial injury and consequential interstitial inflammation and fibrosis were the basis of the heart failure studied [37]. (ii) In order to obtain the measurable endpoints of heart failure and interstitial fibrosis in the myocardium [8,12,33,41] within a reasonable timeframe, we used a very high biological dose with drastic consequences to which a similar one is never applied in conventional radiotherapy. Nevertheless, in modern radiotherapy practice, the use of very large doses (stereotactic radiosurgery delivered with precision selectivity) is widely utilized [58]. (iii) In patients, the effects of various risk factors (such as hyperlipidemia, diabetes, hypertension, aging, sex hormonal differences, individual radiosensitivity, etc.) may modulate radiation-induced changes, which are less pronounced in most animal models. (iv) Finally, while in the animal model, a relatively short follow-up time was used post-radiotherapy, in patients, about 10 years elapse until the recognition of RIHD, although the presence of manifest heart disease or other risk factors may advance its diagnosis [6,7,11,35]. Moreover, we used only one dose of losartan which is comparable to the human therapeutic doses and widely used in heart failure models of other etiologies. The demonstration of molecular mechanisms of how losartan interacts with tissue remodeling was out of the scope of our present descriptive study. We found here anti-remodeling effects of losartan and hypothesized that losartan could

have anti-fibrotic effects by ameliorating the TGF-β, /SMAD-mediated pathway and reducing the overexpression of chymase. Moreover, the non-canonical SMAD-independent pathways, including the AKT and ERK1,2-mediated mechanisms, seem to be involved in maintaining compensatory hypertrophy in our chronic RIHD model. Inhibition of the TGF-β /SMAD pathway or the non-SMAD-dependent pathways in further experiments is needed to determine their exact role in losartan-mediated anti-remodeling effects in RIHD.

4. Materials and Methods

4.1. Ethics Approval

The study was conducted according to the guidelines of the Declaration of Helsinki, and approved by the University of Szeged and the regional Animal Research Ethics Committee of Csongrád County (Csongrád county, Hungary; project license: XV./800/2019, date of approval: 30 May 2019). All institutional and national guidelines for the care and use of laboratory animals were followed.

4.2. Animals

A total of 63 male Sprague-Dawley rats (220–300 g, 6–7 weeks old) were used in three separate experiments (n = 6–9 in each group). After 1 week of acclimatization in a temperature-controlled room (22 ± 2 °C; relative humidity 55 ± 10%), the animals were randomly assigned to the control or the two RT groups and into 3 subgroups, each with 1, 3, or 15 weeks follow-up times, respectively. A total of 21 animals served as controls, and a total of 42 animals received a single dose of 50 Gy delivered to the whole heart to induce RIHD as described previously [37,38]. The animals were housed in pairs in individually ventilated cages (Sealsafe IVC system, Buguggiate, Italy) in a temperature-controlled room with a 12 h:12 h light/dark cycle. Standard rat chow and tap water were supplied ad libitum.

4.3. Experimental Setup

Rats were divided into three groups (n = 6–9 in each group, Figure 1) and treated via oral gavage daily for 1, 3, and 15 weeks, respectively, as follows: (i) control group: treated with tap water (per os 2 mL/kg/day, n = 7), (ii) RT only group: treated with tap water (per os 2 mL/kg/day, n = 6–7), and (iii) RT plus losartan group: treated with losartan (per os 10 mg/kg/day dissolved in tap water in 2 mL/kg end volume, Arbartan 50 mg film-coated tablets, Teva Pharmaceutical Industries Ltd., Debrecen, Hungary, n = 7–9). Cardiac morphology and function were assessed by transthoracic echocardiography at the end-point of each experiment (Figure 1). At the end of the different follow-up times, rats were anesthetized with sodium pentobarbital (Euthasol, ip. 40 mg/kg Produlab Pharma b.v., Raamsdonksveer, The Netherlands). Then blood was collected from the abdominal aorta to measure routine laboratory parameters (Figure 1). After the blood sampling, hearts, lungs, and tibias were isolated, and the blood was washed out from the heart in calcium-free Krebs-Henseleit solution. Then left and right ventricles were separated, and left ventricular samples were prepared for histology and biochemical measurements. The development of LVH and fibrosis in the irradiated groups were verified by the measurement of cardiomyocyte cross-sectional areas on hematoxylin-eosin (HE)-stained slides and picrosirius red/fast green-stained (PSFG) slides (Figure 1). Total RNA was isolated from the left ventricles, and the expression of hypertrophy and fibrosis (i.e., *Myh6*, *Myh7*, *Ctgf*, *Tgfb*, *Col1a1*, and *Mmp2*), RAAS-associated (i.e., *Cma* and *Agt*), inflammatory (i.e., *Il1*, *Il6*, and *Tnf*) markers were measured at the transcript level by qRT-PCR in every time point (Figure 1). Moreover, left ventricular protein levels of AT1R, AT2R, TGF-βRII, SMAD2/3, STAT3, pSTAT3, AKT, pAKT, ERK1, ERK2, pERK1, pERK2 were measured by using Western blot technique at weeks 1, 3, and 15.

4.4. Heart Irradiation

Heart irradiation with a single dose of 50 Gy in the groups of RT and RT plus losartan was carried out as described previously [37,38]. Before the irradiation, rats were anesthetized with sodium pentobarbital (Euthasol, *ip*. 40 mg/kg, Produlab Pharma b.v., Raamsdonksveer, The Netherlands), then fixed in the supine position to a flat surface couch. Briefly, the planning of the irradiation was based on a 3D model, and the dose was delivered to the geometric centre of the heart. For better coverage of the heart and lung protection, a 6 MeV electron radiation was given with a circle-shaped aperture with a 2 cm diameter. The radiation dose was delivered with a Primus linear accelerator (Siemens Healthcare GmbH, Erlangen, Germany) at a dose intensity of 5 Gy/min if the appropriate position of the animal was proven using a built-in electronic portal imaging device.

4.5. Transthoracic Echocardiography

Cardiac morphology and function were assessed by transthoracic echocardiography as described previously [59,60], at weeks 1, 3, and 15 to monitor the development of RIHD. Rats were anesthetized with 2% isoflurane (Forane, Aesica, Queenborough Limited, Queenborough, UK). Two-dimensional, M-mode, Doppler, tissue Doppler, and four chamber-view images were performed by the criteria of the American Society of Echocardiography with a Vivid IQ ultrasound system (General Electric Medical Systems, New York, NY, USA) using a phased array 5.0–11 MHz transducer (General Electric 12S-RS probe, General Electric Medical Systems, New York, NY, USA). Data of three consecutive heart cycles were analyzed (EchoPac Dimension v201, General Electric Medical Systems, USA; https://www.gehealthcare.com/products/ultrasound/vivid/echopac, accessed on 29 November 2021) by an experienced investigator in a blinded manner. The mean values of three measurements were calculated and used for statistical evaluation. Systolic and diastolic wall thicknesses were obtained from parasternal short-axis view at the level of the papillary muscles (in cases of anterior and inferior walls) and long-axis view at the level of the mitral valve (in cases of septal and posterior walls). The left ventricular diameters were measured by means of M-mode echocardiography from long-axis and short-axis views between the endocardial borders. The fractional shortening was calculated on M-mode images in the long-axis view. Diastolic function was assessed using pulse-wave Doppler across the mitral valve and tissue Doppler on the septal mitral annulus from the apical four-chamber view. Early (E) flow and septal mitral annulus velocity (e') indicate diastolic function. Ejection fraction was calculated on four-chamber view images using the modified Simpson method (i.e., biplane method of disks) requiring area tracings of LV cavity in end-systole and end-diastole.

4.6. Blood Parameters

Blood was collected from the abdominal aorta at weeks 1, 3, and 15. Total blood count and hematocrit were measured from whole blood by a hematology analyzer (XE-2100, Sysmex Corporation, Kobe, Japan) [60] to characterize the severity of systemic inflammation and the compensatory increase in red blood cell synthesis associated with lung and heart damage due to RT.

4.7. Tissue Harvesting

At weeks 1, 3, and 15, the hearts of the animals of the respective subgroups were isolated under pentobarbital anesthesia (Euthasol, ip. 40 mg/kg, Produlab Pharma b.v., Raamsdonksveer, The Netherlands), and the blood was washed out in calcium-free Krebs-Henseleit solution. Then the hearts were weighed, left and right ventricles were separated and weighed, and the cross-section of the left ventricle at the ring of the papillae was cut and fixed in 4% buffered formalin for histological analysis. Other parts of the left ventricles were freshly frozen in liquid nitrogen and stored at −80 °C until further biochemical measurements. Body weight, tibia length, and weights of the lungs were also measured.

4.8. Hematoxylin-Eosin and Picrosirius Red and Fast Green Stainings

Five μm paraffin-embedded transverse cut sections of the formalin-fixed subvalvular areas of the left ventricles were stained with hematoxylin-eosin (HE) or picrosirius red and fast green (PSFG) as described previously [38,61]. Histological slides were scanned with a Pannoramic Midi II scanner (3D-Histech, Budapest, Hungary). On the digital HE images, cardiomyocyte cross-sectional areas were measured to verify the development of LVH at the cellular level. For the evaluation, the Biology Image Analysis Software (BIAS) was used [60]. BIAS (internal built, dated December 2019; https://single-cell-technologies.com/bias/, accessed on 29 November 2021) is developed by Single-Cell Technologies Ltd., Szeged, Hungary, and the first publicly available version is expected to be released in late 2021. Image pre-processing was followed by deep learning-based cytoplasm segmentation. User-selected objects were forwarded to the feature extraction module, configurable to extract properties from the selected cell components. Here, transverse transnuclear cardiomyocyte perimeters were measured in 100 (consecutive) cardiomyocytes selected on the basis of longitudinal orientation and mononucleation from a single cut-surface (digitalized histological slide) of the left ventricular tissue blocks. Cardiac fibrosis was assessed on PSFG slides with an in-house developed program [38,61]. Briefly, this program determines the proportion of red pixels of heart sections using two simple color filters. For each red–green–blue (RGB) pixel, the program calculates the color of the pixel in hue–saturation–luminance (HSL) color space. The first filter is used for detecting red portions of the image. The second filter excludes any white (empty) or light grey (residual dirt on the slide) pixels from further processing using a simple RGB threshold. In this way, the program groups each pixel into one of two sets: pixels considered red and pixels considered green but neither white, nor grey. Red pixels in the first set represent collagen content and fibrosis. Green pixels in the second set correspond to cardiac muscle. The mean values of 10 representative images were calculated and used for statistical evaluation in the case of each left ventricular slide. Medium-size vessels and their perivascular connective tissue sheet, the subepicardial and subendocardial areas were avoided as much as possible. Representative HE- and PSFG-stained slides were captured in Panoramic Viewer 1.15.4 (3D-Histech, Budapest, Hungary; https://old.3dhistech.com/pannoramic_viewer, accessed on 29 November 2021).

4.9. mRNA Expression Profiling by qRT-PCR

Quantitative RT-PCR was performed with gene-specific primers to monitor mRNA expression as described previously [59,60]. RNA was isolated using Qiagen RNeasy Fibrous Tissue Mini Kit (Qiagen, Hilden, Germany) from heart tissue. Then 100 μg of total RNA was reverse transcribed using iScript™ cDNA Synthesis Kit (BioRad Laboratories Inc., Hercules, CA, USA). Specific primers (*Agt*: angiotensinogen, #qRnoCED0051666; *Cma1*: chymase, #qRnoCED0005462; *Col1a1*: collagen type 1 alpha 1 chain, #qRnoCED0007857; *Ctgf*: connective tissue growth factor, #qRnoCED0001593; *Il1*: interleukin-1, #qRnoCID0002056; *Il6*: interleukin-6, #qRnoCID0053166; *Mmp2:* matrix metalloproteinase 2, #qRnoCID0002887; *Myh6*: α-myosin heavy chain, #qRnoCID0001766; *Myh7*: β-myosin heavy chain, #qRnoCED0001215; *Tgfb*: transforming growth factor-β, #qRnoCID0009191, *Tnf-α*: tumor necrosis factor-α, #qRnoCED0009117) and SsoAdvanced™ Universal SYBR® Green Supermix (BioRad Laboratories Inc., Hercules, CA, USA) were used according to the manufacturer's instructions. Ribosomal protein lateral stalk subunit P2 (*RpIp2*, forward primer sequence: *agcgccaaagacatcaagaa* and reverse primer sequence: *tcagctcactgatgaccttgtt*) was used as a housekeeping control gene for normalization.

4.10. Western Blot

To investigate gene expression changes at the protein level, a standard Western blot technique was used as described previously [59,60]. AT1R (41 kDa), AT2R (41 kDa), SMAD2/3 (52 and 60 kDa), TGF-βRII (85 kDa), STAT3 (79 and 86 kDa), pSTAT3 (79 and 86 kDa), AKT (60 kDa), pAKT (60 kDa), ERK1/2 (42 and 44 kDa), and pERK1/2 (42 and

44 kDa) with GAPDH (37 kDa) loading background were assessed at weeks 1, 3, and 15. Left ventricular samples (n =6–7 in each group, total n = 21 at week 1, total n = 20 at week 3, and total n = 20 at week 15) were homogenized with an ultrasonicator (UP100H, Hielscher, Germany) in Radio-Immunoprecipitation Assay (RIPA) buffer (50 mM Tris-HCl (pH 8.0), 150 mM NaCl, 0.5% sodium deoxycholate, 5 mM ethylenediamine tetra-acetic acid (EDTA), 0.1% sodium dodecyl sulfate, 1% NP-40; Cell Signaling Technology Inc., Danvers, MA, USA) supplemented with phenylmethanesulfonyl fluoride (PMSF; Sigma-Aldrich, St. Louis, MO, USA) and sodium fluoride (NaF; Sigma-Aldrich, Saint Louis, MO, USA). The crude homogenates were centrifuged at 15,000× g for 30 min at 4 °C. After quantifying the supernatants' protein concentrations using the BCA Protein Assay Kit (Pierce Thermo Fisher Scientific Inc., Waltham, MA, USA), 25 µg of reduced and denaturized protein was loaded. Then sodium dodecyl-sulfate polyacrylamide gel electrophoresis (SDS-PAGE, 50 V, 4 h) was performed (10% gel in case of AT1R, AT2R, SMAD2/3, TGF-βRII, STAT3, phospho-STAT3, AKT, phospho-AKT, ERK1/2, and phospho-ERK1/2) followed by the transfer of proteins onto a nitrocellulose membrane (10% methanol in case of AT1, AT2, SMAD2/3, TGF-βRII and 20% methanol in case of STAT, phospho-STAT, AKT, phospho-AKT, ERK1/2, phospho-ERK1/2, 35 V, 2 h). The efficacy of transfer was checked using Ponceau staining. The membranes were cut horizontally into parts corresponding to the molecular weights of AT1R, AT2R, SMAD2/3, TGF-βRII, STAT3, pSTAT3, AKT, pAKT, ERK1/2, pERK1/2, and GAPDH. Membranes were blocked for 1 h in 5% (w/v) bovine serum albumin (BSA, Sigma-Aldrich, Saint Louis, MO, USA) and were incubated with primary antibodies in the concentrations of 1:1000 against AT1R (#ab124734, Abcam PLC, Cambridge, UK), AT2R (#ab92445, Abcam PLC, Cambridge, UK), SMAD2/3 (#8685T, Cell Signaling Technology Inc., Danvers, MA, USA), TGF-β receptor II (#79424T, Cell Signaling Technology Inc., Danvers, MA, USA), STAT3 (#9139, Cell Signaling Technology Inc., Danvers, MA, USA), pSTAT3 (#9145, Cell Signaling Technology Inc., Danvers, MA, USA), AKT (#2920, Cell Signaling Technology Inc., Danvers, MA, USA), pAKT (#4060, Cell Signaling Technology Inc., Danvers, MA, USA), ERK1/2 (#4696, Cell Signaling Technology Inc., Danvers, MA, USA), pERK1/2 (#9101S, Cell Signaling Technology Inc., Danvers, MA, USA), or 1:5000 against GAPDH (#2118, Cell Signaling Technology Inc., Danvers, MA, USA) overnight at 4 °C in 5% BSA. Then the membranes were incubated with IRDye® 800CW Goat Anti-Rabbit and/or IRDye® 680RD Goat Anti-Mouse secondary antibody (LI-COR Biosciences, Lincoln, NE, USA, in the concentrations of 1:5000) for 1 h at room temperature in 5% BSA antibodies to detect proteins with similar molecular weight on the same membrane where it is applicable. Fluorescent signals were detected by Odyssey CLx machine (LI-COR Biosciences, Lincoln, NE, USA), and digital images were analyzed and evaluated by densitometry with Quantity One Software (Bio-Rad Laboratories Inc., Hercules, CA, USA).

4.11. Statistical Analysis

Statistical analysis was performed using Sigmaplot 12.0 for Windows (Systat Software Inc., San Jose, CA, USA). All values are presented as mean ± SEM. Specific sample numbers used for measurements are described in the corresponding figure legend. One-Way ANOVA was used to determine the statistical significance between all measured parameters within each time point. A Holm-Sidak test was used as a post-hoc test. $p < 0.05$ was accepted as a statistically significant difference.

5. Conclusions

In this study, we evaluated the effects of chronic administration of the selective AT1 receptor blocker losartan on cardiac remodeling, function, and molecular markers of inflammation, LVH, fibrosis, and heart failure in a rat model of RIHD. Our results suggest that the development of RIHD-associated LVH and fibrosis might be prevented or markedly slowed down by losartan if its administration starts early after RT. Losartan seems to ameliorate left ventricular fibrosis. The antiremodeling effects of losartan seem

to be associated with the repression of chymase and several elements of the canonical SMAD-dependent TGF-β signaling pathway in our rat model of RIHD. In contrast, the non-canonical SMAD-independent pathways, including the AKT and ERK1,2-mediated mechanisms, seem to be involved in the maintenance of compensatory hypertrophy in our late phase RIHD model. In order to clarify whether losartan and other ARBs may be protective against RIHD in humans, clinical trials enrolling a large number of patients are required for widening the indication of this otherwise routinely used drug of heart failure treatment.

Supplementary Materials: The following are available online at https://www.mdpi.com/article/10.3390/ijms222312963/s1.

Author Contributions: Conceptualization, Z.K., T.C. and M.S.; methodology, M.G.K., Z.Z.A.K., G.S., M.F., Z.V., K.F., B.K. and M.S.; software, F.K., A.K. and P.H.; validation, I.F., G.C., P.H. and Z.K.; formal analysis, M.G.K. and M.S.; investigation, M.G.K., Z.Z.A.K., G.S., M.F., Z.V., K.F., B.K. and M.S.; resources: G.C., I.F., T.C. and P.H., data curation: M.G.K., Z.Z.A.K., A.K. and M.S.; visualization: M.G.K. and M.S.; writing—original draft preparation, M.G.K., M.S. and Z.K.; writing—review and editing, M.G.K., T.C., M.S. and Z.K.; supervision, M.S.; project administration, M.G.K. and M.S.; funding acquisition, M.S. and T.C. All authors have read and agreed to the published version of the manuscript.

Funding: This research was funded by the projects NKFIH FK129094 (to M.S., funder: National Research, Development and Innovation Office), GINOP-2.3.2-15-2016-00040 (to T.C., funder: National Research, Development and Innovation Office), GINOP-2.3.2-15-2016-00034 (to TC, funder: National Research, Development and Innovation Office), EFOP-3.6.2-16-2017-00006 (LIVE LONGER) (to T.C., funder: National Research, Development and Innovation Office), and by the Ministry of Human Capacities (20391-3/2018/FEKUSTRAT) (to T.C., funder: Ministry of Human Capacities). M.G.K., Z.Z.A.K., and M.S. were supported by the New National Excellence Program of the Ministry of Human Capacities (ÚNKP-21-3-SZTE-97 to M.G.K., ÚNKP-21-3-SZTE-98 to Z.Z.A.K., and ÚNKP-20-5-SZTE-166 to M.S., funder: Ministry of Human Capacities). MS was supported by the János Bolyai Research Fellowship of the Hungarian Academy of Sciences. Z.Z.A.K. and M.G.K. were supported by the EFOP-3.6.3-VEKOP-16-2017-00009 project (funder: National Research, Development and Innovation Offic). The APC was funded by NKFIH FK129094 (funder: National Research, Development and Innovation Office).

Institutional Review Board Statement: The study was conducted according to the guidelines of the Declaration of Helsinki, and approved by the University of Szeged and the regional Animal Research Ethics Committee of Csongrád County (Csongrád county, Hungary; project license: XV./800/2019, date of approval: 30 May 2019). All institutional and national guidelines for the care and use of laboratory animals were followed.

Informed Consent Statement: Not applicable.

Data Availability Statement: The datasets used and/or analyzed during the current study are available from the corresponding authors on a reasonable request.

Acknowledgments: We thank Krisztián Daru for outstanding histological slide preparation and staining. We are grateful to our medical students Réka Losonczi, Klaudia Kupecz, Merse Kiss, and Dávid Volford to participate in the daily drug administration. We thank Bálint Cserni for creating the program for the picrosirius red and fast green image analysis.

Conflicts of Interest: Single-Cell Technologies Ltd., Szeged, Hungary, developed the Biology Image Analysis Software (BIAS). P.H. is the CEO, A.K. is a software architect, and F.K. is a software engineer at Single-Cell Technologies Ltd, Szeged, Hungary.

References

1. World Health Organization. Cardiovascular Diseases (CVDs). 2019. Available online: https://www.who.int/news-room/fact-sheets/detail/cardiovascular-diseases-(cvds) (accessed on 20 November 2021).
2. WHO. WHO Cancer. 2020. Available online: https://www.who.int/news-room/fact-sheets/detail/cancer (accessed on 20 November 2021).

3. Miller Mph, K.D.; Nogueira, L.; Mariotto, A.B.; Rowland, J.H.; Yabroff, K.R.; Alfano, C.M.; Jemal, A.; Kramer, J.L.; Siegel, R.L. Cancer treatment and survivorship statistics, 2019. *CA Cancer J. Clin.* **2019**, *69*, 363–385. [CrossRef]
4. Baskar, R.; Itahana, K. Radiation therapy and cancer control in developing countries: Can we save more lives? *Int. J. Med. Sci.* **2017**, *14*, 13–17. [CrossRef]
5. Menezes, K.M.; Wang, H.; Hada, M.; Saganti, P.B. Radiation Matters of the Heart: A Mini Review. *Front. Cardiovasc. Med.* **2018**, *5*, 83. [CrossRef]
6. Taylor, C.; Correa, C.; Duane, F.K.; Aznar, M.C.; Anderson, S.; Bergh, J.; Dodwell, D.; Ewertz, M.; Gray, R.; Jagsi, R.; et al. Estimating the Risks of Breast Cancer Radiotherapy: Evidence from Modern Radiation Doses to the Lungs and Heart and From Previous Randomized Trials. *J. Clin. Oncol.* **2017**, *35*, 1641–1649. [CrossRef]
7. van Nimwegen, F.A.; Schaapveld, M.; Cutter, D.J.; Janus, C.P.; Krol, A.D.; Hauptmann, M.; Kooijman, K.; Roesink, J.; van der Maazen, R.; Darby, S.C.; et al. Radiation Dose-Response Relationship for Risk of Coronary Heart Disease in Survivors of Hodgkin Lymphoma. *J. Clin. Oncol.* **2016**, *34*, 235–243. [CrossRef]
8. Sárközy, M.; Varga, Z.; Gáspár, R.; Szűcs, G.; Kovács, M.G.; Kovács, Z.Z.A.; Dux, L.; Kahán, Z.; Csont, T. Pathomechanisms and therapeutic opportunities in radiation-induced heart disease: From bench to bedside. *Clin. Res. Cardiol.* **2021**, *110*, 507–531. [CrossRef] [PubMed]
9. Zamorano, J.L.; Lancellotti, P.; Rodriguez Muñoz, D.; Aboyans, V.; Asteggiano, R.; Galderisi, M.; Habib, G.; Lenihan, D.J.; Lip, G.Y.H.; Lyon, A.R.; et al. 22016 ESC Position Paper on cancer treatments and cardiovascular toxicity developed under the auspices of the ESC Committee for Practice Guidelines: The Task Force for cancer treatments and cardiovascular toxicity of the European Society of Cardiology (ESC). *Eur. Heart J.* **2016**, *37*, 2768–2801. [CrossRef] [PubMed]
10. Rassaf, T.; Committee for Clinical Cardiovascular Medicine of the German Cardiac Society; Totzeck, M.; Backs, J.; Bokemeyer, C.; Hallek, M.; Hilfiker-Kleiner, D.; Hochhaus, A.; Lüftner, D.; Müller, O.J.; et al. Onco-Cardiology: Consensus Paper of the German Cardiac Society, the German Society for Pediatric Cardiology and Congenital Heart Defects and the German Society for Hematology and Medical Oncology. *Clin. Res. Cardiol.* **2020**, *109*, 1197–1222. [CrossRef]
11. Andratschke, N.; Maurer, J.; Molls, M.; Trott, K.-R. Late radiation-induced heart disease after radiotherapy. Clinical importance, radiobiological mechanisms and strategies of prevention. *Radiother. Oncol.* **2011**, *100*, 160–166. [CrossRef] [PubMed]
12. Taunk, N.; Haffty, B.G.; Kostis, J.B.; Goyal, S. Radiation-Induced Heart Disease: Pathologic Abnormalities and Putative Mechanisms. *Front. Oncol.* **2015**, *5*, 39. [CrossRef] [PubMed]
13. Tapio, S. Pathology and biology of radiation-induced cardiac disease. *J. Radiat. Res.* **2016**, *57*, 439–448. [CrossRef] [PubMed]
14. Forrester, S.J.; Booz, G.W.; Sigmund, C.D.; Coffman, T.M.; Kawai, T.; Rizzo, V.; Scalia, R.; Eguchi, S. Angiotensin II Signal Transduction: An Update on Mechanisms of Physiology and Pathophysiology. *Physiol. Rev.* **2018**, *98*, 1627–1738. [CrossRef]
15. Ocaranza, M.P.; Riquelme, J.A.; García, L.; Jalil, J.E.; Chiong, M.; Santos, R.A.S.; Lavandero, S. Counter-regulatory renin–angiotensin system in cardiovascular disease. *Nat. Rev. Cardiol.* **2020**, *17*, 116–129. [CrossRef] [PubMed]
16. Wu, R.; Zeng, Y. Does angiotensin II–aldosterone have a role in radiation-induced heart disease? *Med. Hypotheses* **2009**, *72*, 263–266. [CrossRef] [PubMed]
17. Cao, S.; Wu, R. Expression of Angiotensin II and Aldosterone in Radiation-induced Lung Injury. *Cancer Biol. Med.* **2012**, *9*, 254–260. [CrossRef]
18. Pinter, M.; Kwanten, W.J.; Jain, R.K. Renin–Angiotensin System Inhibitors to Mitigate Cancer Treatment–Related Adverse Events. *Clin. Cancer Res.* **2018**, *24*, 3803–3812. [CrossRef]
19. Gulati, G.; Heck, S.L.; Ree, A.H.; Hoffmann, P.; Schulz-Menger, J.; Fagerland, M.W.; Gravdehaug, B.; Von Knobelsdorff-Brenkenhoff, F.; Bratland, Å.; Storås, T.H.; et al. Prevention of cardiac dysfunction during adjuvant breast cancer therapy (PRADA): A 2 × 2 factorial, randomized, placebo-controlled, double-blind clinical trial of candesartan and metoprolol. *Eur. Heart J.* **2016**, *37*, 1671–1680. [CrossRef]
20. Sio, T.T.; Liang, J.J.; Chang, K.; Jayakrishnan, R.; Novotny, P.J.; Prasad, A.; Miller, R.C. Dosimetric Correlate of Cardiac-Specific Survival Among Patients Undergoing Coronary Artery Stenting After Thoracic Radiotherapy for Cancer. *Am. J. Clin. Oncol.* **2017**, *40*, 133–139. [CrossRef]
21. Ahamed, J.; Laurence, J. Role of Platelet-Derived Transforming Growth Factor-β1 and Reactive Oxygen Species in Radiation-Induced Organ Fibrosis. *Antioxid. Redox Signal.* **2017**, *27*, 977–988. [CrossRef]
22. Thum, T.; Galuppo, P.; Wolf, C.; Fiedler, J.; Kneitz, S.; van Laake, L.W.; Doevendans, P.A.; Mummery, C.L.; Borlak, J.; Haverich, A.; et al. MicroRNAs in the human heart: A clue to fetal gene reprogramming in heart failure. *Circulation* **2007**, *116*, 258–267. [CrossRef]
23. Boerma, M. Potential Targets for Intervention in Radiation-Induced Heart Disease. *Curr. Drug Targets* **2010**, *11*, 1405–1412. [CrossRef] [PubMed]
24. Froogh, G.; Pinto, J.T.; Le, Y.; Kandhi, S.; Aleligne, Y.; Huang, A.; Sun, D. Chymase-dependent production of angiotensin II: An old enzyme in old hearts. *Am. J. Physiol. Circ. Physiol.* **2017**, *312*, H223–H231. [CrossRef]
25. Liu, P.; Sun, M.; Sader, S. Matrix metalloproteinases in cardiovascular disease. *Can. J. Cardiol.* **2006**, *22*, 25B–30B. [CrossRef]
26. Saadat, S.; Noureddini, M.; Mahjoubin-Tehran, M.; Nazemi, S.; Shojaie, L.; Aschner, M.; Maleki, B.; Abbasi-Kolli, M.; Moghadam, H.R.; Alani, B.; et al. Pivotal Role of TGF-β/Smad Signaling in Cardiac Fibrosis: Non-coding RNAs as Effectual Players. *Front. Cardiovasc. Med.* **2021**, *7*, 256. [CrossRef] [PubMed]

27. Finnson, K.; Almadani, Y.; Philip, A. Non-canonical (non-SMAD2/3) TGF-β signaling in fibrosis: Mechanisms and targets. *Semin. Cell Dev. Biol.* **2020**, *101*, 115–122. [CrossRef]
28. Ye, S.; Luo, W.; Khan, Z.A.; Wu, G.; Xuan, L.; Shan, P.; Lin, K.; Chen, T.; Wang, J.; Hu, X.; et al. Celastrol Attenuates Angiotensin II–Induced Cardiac Remodeling by Targeting STAT3. *Circ. Res.* **2020**, *126*, 1007–1023. [CrossRef]
29. O'Donnell, L.; O'Neill, T.; Toner, M.; O'Briain, S.; Graham, I. Myocardial hypertrophy, fibrosis and infarction following exposure of the heart to radiation for Hodgkin's disease. *Postgrad. Med. J.* **1986**, *62*, 1055–1058. [CrossRef] [PubMed]
30. Monceau, V.; Llach, A.; Azria, D.; Bridier, A.; Petit, B.; Mazevet, M.; Strup-Perrot, C.; To, T.-H.-V.; Calmels, L.; Germaini, M.-M.; et al. Epac contributes to cardiac hypertrophy and amyloidosis induced by radiotherapy but not fibrosis. *Radiother. Oncol.* **2014**, *111*, 63–71. [CrossRef]
31. Saiki, H.; Moulay, G.; Guenzel, A.J.; Liu, W.; Decklever, T.D.; Classic, K.L.; Pham, L.; Chen, H.H.; Burnett, J.C.; Russell, S.J.; et al. Experimental cardiac radiation exposure induces ventricular diastolic dysfunction with preserved ejection fraction. *Am. J. Physiol. Circ. Physiol.* **2017**, *313*, H392–H407. [CrossRef]
32. Cuomo, J.R.; Sharma, G.K.; Conger, P.D.; Weintraub, N.L. Novel concepts in radiation-induced cardiovascular disease. *World J. Cardiol.* **2016**, *8*, 504–519. [CrossRef]
33. Wang, H.; Wei, J.; Zheng, Q.; Meng, L.; Xin, Y.; Yin, X.; Jiang, X. Radiation-induced heart disease: A review of classification, mechanism and prevention. *Int. J. Biol. Sci.* **2019**, *15*, 2128–2138. [CrossRef]
34. Hardy, D.; Liu, C.-C.; Cormier, J.N.; Xia, R.; Du, X.L. Cardiac toxicity in association with chemotherapy and radiation therapy in a large cohort of older patients with non-small-cell lung cancer. *Ann. Oncol.* **2010**, *21*, 1825–1833. [CrossRef] [PubMed]
35. van den Bogaard, V.A.B.; Ta, B.D.P.; van der Schaaf, A.; Bouma, A.B.; Middag, A.M.H.; Bantema-Joppe, E.J.; Van Dijk, L.V.; Van Dijk-Peters, F.B.J.; Marteijn, L.A.W.; de Bock, G.H.; et al. Validation and Modification of a Prediction Model for Acute Cardiac Events in Patients With Breast Cancer Treated With Radiotherapy Based on Three-Dimensional Dose Distributions to Cardiac Substructures. *J. Clin. Oncol.* **2017**, *35*, 1171–1178. [CrossRef]
36. Boerma, M.; Roberto, K.A.; Hauer-Jensen, M. Prevention and Treatment of Functional and Structural Radiation Injury in the Rat Heart by Pentoxifylline and Alpha-Tocopherol. *Int. J. Radiat. Oncol.* **2008**, *72*, 170–177. [CrossRef] [PubMed]
37. Kiscsatári, L.; Sárközy, M.; Kővári, B.P.; Varga, Z.; Gömöri, K.; Morvay, N.; Leprán, I.; Hegyesi, H.; Fábián, G.; Cserni, B.; et al. High-dose Radiation Induced Heart Damage in a Rat Model. *In Vivo* **2016**, *30*, 623–631.
38. Sárközy, M.; Gáspár, R.; Zvara, Á.; Kiscsatári, L.; Varga, Z.; Kővári, B.; Kovács, M.G.; Szűcs, G.; Fábián, G.; Diószegi, P.; et al. Selective Heart Irradiation Induces Cardiac Overexpression of the Pro-hypertrophic miR-212. *Front. Oncol.* **2019**, *9*, 598. [CrossRef]
39. Boerma, M.; Wang, J.; Kulkarni, A.; Roberto, K.A.; Qiu, X.; Kennedy, R.H.; Hauer-Jensen, M. Influence of Endothelin 1 Receptor Inhibition on Functional, Structural and Molecular Changes in the Rat Heart after Irradiation. *Radiat. Res.* **2008**, *170*, 275–283. [CrossRef]
40. Meléndez, G.C.; McLarty, J.L.; Levick, S.; Du, Y.; Janicki, J.S.; Brower, G. Interleukin 6 Mediates Myocardial Fibrosis, Concentric Hypertrophy, and Diastolic Dysfunction in Rats. *Hypertension* **2010**, *56*, 225–231. [CrossRef]
41. Schultz-Hector, S. Radiation-induced Heart Disease: Review of Experimental Data on Dose Reponse and Pathogenesis. *Int. J. Radiat. Biol.* **1992**, *61*, 149–160. [CrossRef]
42. Farhood, B.; Khodamoradi, E.; Hoseini-Ghahfarokhi, M.; Motevaseli, E.; Mahyari, H.M.; Musa, A.E.; Najafi, M. TGF-β in radiotherapy: Mechanisms of tumor resistance and normal tissues injury. *Pharmacol. Res.* **2020**, *155*, 104745. [CrossRef]
43. Lu, Z.; Xu, S. ERK1/2 MAP kinases in cell survival and apoptosis. *IUBMB Life* **2006**, *58*, 621–631. [CrossRef]
44. Miyazaki, M.; Takai, S. Tissue Angiotensin II Generating System by Angiotensin-Converting Enzyme and Chymase. *J. Pharmacol. Sci.* **2006**, *100*, 391–397. [CrossRef]
45. Company, C.; Piqueras, L.; Abu Nabah, Y.N.; Escudero, P.; Blanes, J.I.; Jose, P.J.; Morcillo, E.J.; Sanz, M.-J. Contributions of ACE and mast cell chymase to endogenous angiotensin II generation and leucocyte recruitment in vivo. *Cardiovasc. Res.* **2011**, *92*, 48–56. [CrossRef]
46. Boerma, M.; Zurcher, C.; Esveldt, I.; Schutte-Bart, C.; Wondergem, J. Histopathology of ventricles, coronary arteries and mast cell accumulation in transverse and longitudinal sections of the rat heart after irradiation. *Oncol. Rep.* **2004**, *12*, 213–219. [CrossRef]
47. Yarom, R.; Harper, I.S.; Wynchank, S.; Van Schalkwyk, D.; Madhoo, J.; Williams, K.; Salie, R.; Genade, S.; Lochner, A. Effect of Captopril on Changes in Rats' Hearts Induced by Long-Term Irradiation. *Radiat. Res.* **1993**, *133*, 187–197. [CrossRef]
48. Schultz, J.E.J.; Witt, S.A.; Glascock, B.J.; Nieman, M.L.; Reiser, P.J.; Nix, S.L.; Kimball, T.R.; Doetschman, T. TGF-β1 mediates the hypertrophic cardiomyocyte growth induced by angiotensin II. *J. Clin. Investig.* **2002**, *109*, 787–796. [CrossRef]
49. Wassmann, S.; Stumpf, M.; Strehlow, K.; Schmid, A.; Schieffer, B.; Böhm, M.; Nickenig, G. Interleukin-6 Induces Oxidative Stress and Endothelial Dysfunction by Overexpression of the Angiotensin II Type 1 Receptor. *Circ. Res.* **2004**, *94*, 534–541. [CrossRef]
50. Miguel-Carrasco, J.L.; Beaumont, J.; José, G.S.; Moreno, M.; López, B.; Gonzalez, A.; Zalba, G.; Díez, J.; Fortuño, A.; Ravassa, S. Mechanisms underlying the cardiac antifibrotic effects of losartan metabolites. *Sci. Rep.* **2017**, *7*, 1–9. [CrossRef] [PubMed]
51. Wu, M.; Peng, Z.; Zu, C.; Ma, J.; Lu, S.; Zhong, J.; Zhang, S. Losartan Attenuates Myocardial Endothelial-To-Mesenchymal Transition in Spontaneous Hypertensive Rats via Inhibiting TGF-β/Smad Signaling. *PLoS ONE* **2016**, *11*, e0155730. [CrossRef] [PubMed]
52. Zhang, W.; Elimban, V.; Xu, Y.J.; Zhang, M.; Nijjar, M.S.; Dhalla, N.S. Alterations of Cardiac ERK1/2 Expression and Activity Due to Volume Overload Were Attenuated by the Blockade of RAS. *J. Cardiovasc. Pharmacol. Ther.* **2010**, *15*, 84–92. [CrossRef] [PubMed]

53. Yang, W.; Zhang, J.; Wang, H.; Gao, P.; Singh, M.; Shen, K.; Fang, N. Angiotensin II downregulates catalase expression and activity in vascular adventitial fibroblasts through an AT1R/ERK1/2-dependent pathway. *Mol. Cell. Biochem.* **2011**, *358*, 21–29. [CrossRef]
54. Xiong, W.; Meisinger, T.; Knispel, R.; Worth, J.M.; Baxter, B.T. MMP-2 regulates Erk1/2 phosphorylation and aortic dilatation in Marfan syndrome. *Circ. Res.* **2012**, *110*, e92–e101. [CrossRef]
55. Asano, K.; Dutcher, D.L.; Port, J.D.; Minobe, W.A.; Tremmel, K.D.; Roden, R.L.; Bohlmeyer, T.J.; Bush, E.W.; Jenkin, M.J.; Abraham, W.T.; et al. Selective Downregulation of the Angiotensin II AT 1 -Receptor Subtype in Failing Human Ventricular Myocardium. *Circulation* **1997**, *95*, 1193–1200. [CrossRef] [PubMed]
56. Hermans, M.A.W.; Van Lennep, J.E.R.; Van Daele, P.L.A.; Bot, I. Mast Cells in Cardiovascular Disease: From Bench to Bedside. *Int. J. Mol. Sci.* **2019**, *20*, 3395. [CrossRef] [PubMed]
57. Wang, T.; Gao, W.; Xiao, K.; Liu, Q.; Jia, R. Interaction between interleukin-6 and angiotensin II receptor 1 in the hypothalamic paraventricular nucleus contributes to progression of heart failure. *Mol. Med. Rep.* **2017**, *15*, 4259–4265. [CrossRef] [PubMed]
58. Chen, H.; Louie, A.; Higginson, D.; Palma, D.; Colaco, R.; Sahgal, A. Stereotactic Radiosurgery and Stereotactic Body Radiotherapy in the Management of Oligometastatic Disease. *Clin. Oncol.* **2020**, *32*, 713–727. [CrossRef]
59. Sárközy, M.; Márványkövi, F.M.; Szűcs, G.; Kovács, Z.Z.A.; Szabó, M.R.; Gáspár, R.; Siska, A.; Kővári, B.; Cserni, G.; Földesi, I.; et al. Ischemic preconditioning protects the heart against ischemia-reperfusion injury in chronic kidney disease in both males and females. *Biol. Sex Differ.* **2021**, *12*, 1–20. [CrossRef]
60. Kovács, Z.Z.A.; Szűcs, G.; Freiwan, M.; Kovács, M.G.; Márványkövi, F.M.; Dinh, H.; Siska, A.; Farkas, K.; Kovács, F.; Kriston, A.; et al. Comparison of the antiremodeling effects of losartan and mirabegron in a rat model of uremic cardiomyopathy. *Sci. Rep.* **2021**, *11*, 1–18. [CrossRef]
61. Sárközy, M.; Gáspár, R.; Zvara, Á.; Siska, A.; Kővári, B.P.; Szűcs, G.; Márványkövi, F.; Kovács, M.G.; Diószegi, P.; Bodai, L.; et al. Chronic kidney disease induces left ventricular overexpression of the pro-hypertrophic microRNA-212. *Sci. Rep.* **2019**, *9*, 1–16. [CrossRef]

II.

frontiers in Oncology

ORIGINAL RESEARCH
published: 16 July 2019
doi: 10.3389/fonc.2019.00598

Selective Heart Irradiation Induces Cardiac Overexpression of the Pro-hypertrophic miR-212

Márta Sárközy[1], Renáta Gáspár[1], Ágnes Zvara[2], Laura Kiscsatári[3], Zoltán Varga[3], Bence Kővári[4], Mónika G. Kovács[1], Gergő Szűcs[1], Gabriella Fábián[3], Petra Diószegi[1], Gábor Cserni[4], László G. Puskás[2], Thomas Thum[5], Zsuzsanna Kahán[3], Tamás Csont[1] and Sándor Bátkai[5]*

[1] Metabolic Diseases and Cell Signaling Group, Department of Biochemistry, Interdisciplinary Centre of Excellence, University of Szeged, Szeged, Hungary, [2] Laboratory for Functional Genomics, Biological Research Center of the Hungarian Academy of Sciences, Institute of Genetics, Szeged, Hungary, [3] Department of Oncotherapy, Faculty of Medicine, University of Szeged, Szeged, Hungary, [4] Department of Pathology, University of Szeged, Szeged, Hungary, [5] Institute of Molecular and Translational Therapeutic Strategies (IMTTS), Hanover Medical School, Hanover, Germany

OPEN ACCESS

Edited by:
Timothy James Kinsella, Warren Alpert Medical School of Brown University, United States

Reviewed by:
Michael Wayne Epperly, University of Pittsburgh, United States
Heng-Hong Li, Georgetown University, United States

***Correspondence:**
Márta Sárközy
sarkozy.marta@med.u-szeged.hu

Specialty section:
This article was submitted to Radiation Oncology, a section of the journal Frontiers in Oncology

Received: *30 January 2019*
Accepted: *17 June 2019*
Published: *16 July 2019*

Citation:
Sárközy M, Gáspár R, Zvara Á, Kiscsatári L, Varga Z, Kővári B, Kovács MG, Szűcs G, Fábián G, Diószegi P, Cserni G, Puskás LG, Thum T, Kahán Z, Csont T and Bátkai S (2019) Selective Heart Irradiation Induces Cardiac Overexpression of the Pro-hypertrophic miR-212. Front. Oncol. 9:598. doi: 10.3389/fonc.2019.00598

Background: A deleterious, late-onset side effect of thoracic radiotherapy is the development of radiation-induced heart disease (RIHD). It covers a spectrum of cardiac pathology including also heart failure with preserved ejection fraction (HFpEF) characterized by left ventricular hypertrophy (LVH) and diastolic dysfunction. MicroRNA-212 (miR-212) is a crucial regulator of pathologic LVH via FOXO3-mediated pathways in pressure-overload-induced heart failure. We aimed to investigate whether miR-212 and its selected hypertrophy-associated targets play a role in the development of RIHD.

Methods: RIHD was induced by selective heart irradiation (50 Gy) in a clinically relevant rat model. One, three, and nineteen weeks after selective heart irradiation, transthoracic echocardiography was performed to monitor cardiac morphology and function. Cardiomyocyte hypertrophy and fibrosis were assessed by histology at week 19. qRT-PCR was performed to measure the gene expression changes of miR-212 and forkhead box O3 (FOXO3) in all follow-up time points. The cardiac transcript level of other selected hypertrophy-associated targets of miR-212 including extracellular signal-regulated kinase 2 (ERK2), myocyte enhancer factor 2a (MEF2a), AMP-activated protein kinase, (AMPK), heat shock protein 40 (HSP40), sirtuin 1, (SIRT1), calcineurin A-alpha and phosphatase and tensin homolog (PTEN) were also measured at week 19. Cardiac expression of FOXO3 and phospho-FOXO3 were investigated at the protein level by Western blot at week 19.

Results: In RIHD, diastolic dysfunction was present at every time point. Septal hypertrophy developed at week 3 and a marked LVH with interstitial fibrosis developed at week 19 in the irradiated hearts. In RIHD, cardiac miR-212 was overexpressed at week 3 and 19, and FOXO3 was repressed at the mRNA level only at week 19. In contrast, the total FOXO3 protein level failed to decrease in response to heart irradiation at week 19. Other selected hypertrophy-associated target genes failed to change at the mRNA level in RIHD at week 19.

Conclusions: LVH in RIHD was associated with cardiac overexpression of miR-212. However, miR-212 seems to play a role in the development of LVH via FOXO3-independent mechanisms in RIHD. As a central regulator of pathologic remodeling, miR-212 might become a novel target for RIHD-induced LVH and heart failure.

Keywords: thoracic irradiation, left ventricular hypertrophy, heart failure with preserved ejection fraction (HFpEF), miRNA-212, FOXO3

INTRODUCTION

Radiotherapy has an important role, among other therapeutic modalities, in the treatment of thoracic tumors including breast, lung, esophageal and childhood cancers or Hodgkin's lymphoma. About half of cancer patients are treated with radiotherapy (1). Although the application of modern radiotherapy planning and delivery techniques significantly improves the radiation protection of the heart, in many cases, the whole heart, or part of it, still receives a dose sufficient enough to cause radiation-induced heart disease (RIHD) with chronic, and often severe consequences (1). RIHD develops many years or decades after radiotherapy in a dose-dependent manner (2, 3). Premature coronary heart disease, electrical conduct defects or valve abnormalities are often associated with RIHD (4–6). In the early phase, RIHD often presents as heart failure with preserved ejection fraction (HFpEF), characterized by LVH and diastolic dysfunction (1, 7, 8). Radiotherapy significantly improves cancer patient survival; however, in the long-term, patients are at risk of RIHD and subsequent heart failure which becomes a major health issue affecting outcome, quality of life and health care costs (1). Unfortunately, therapeutic options for RIHD are currently insufficient.

Radiation deteriorates the heart structure and function by inducing changes to the vasculature, i.e., coronary arteries and microvessels, and directly acting on the myocardium (9). The focus of the studies so far has been on the vascular effects, which indirectly influence the myocardium (3, 6, 10, 11). Recently, more data has become available on the radiation-induced direct effect on the myocardial structure. Interstitial inflammation and progressive fibrosis are well-known pathological effects of RIHD (12). They have been shown to be mediated by oxidative stress, the activation of pathologic NO-cGMP-PKG signaling, cytokine and growth factor cascades such as IL-4, IL-13, Rho/ROCK pathway and transforming growth factor beta (TGF-β) (1, 7, 9, 13, 14). Histopathological examination of cardiac lesions of RIHD shows hypertrophic cardiomyocytes, inflammatory cells, fibroblasts, and excessive deposition of collagens (1, 7, 14). Radiation-induced hypertrophy and fibrosis of the myocardium ultimately leads to a decrease in elasticity, ductility, and the development of diastolic heart failure. Only a few studies exist so far on the mechanisms of radiation-induced diffuse myocardial injury. The initial phase of RIHD includes reactive cardiac hypertrophy with enlarged cardiomyocytes (1, 7, 15). Very little is known about the mechanisms of cardiac hypertrophy and the pathological remodeling in RIHD. We have previously developed a clinically relevant rat model of RIHD, characterized by LVH and simultaneous interstitial fibrosis (16). Our present study is based on this RIHD model.

Endogenous microRNAs (miRs, 22 bp) are non-coding RNA species that are post-transcriptional regulators targeting specific mRNAs, resulting in an increase of mRNA degradation via complementary binding and the suppression of protein synthesis, thus influencing cellular function (17). miRs have been described as "master switches" in cardiovascular biology, and the dysregulation of specific miRs are key pathological factors in many cardiovascular diseases (18–21). The miR-212/132 cluster is considered to be a central regulator of the development of pressure-overload-induced LVH and heart failure via the repression of the anti-hypertrophic transcription factor FOXO3 in mice with transverse aortic constriction (TAC) (22). Moreover, the overexpression of miR-212 separate from miR-132, was reported to play a role in the development of LVH and heart failure via fetal gene reprogramming in human hearts (23). Furthermore, the pro-hypertrophic potential of miR-212 was also confirmed in primary neonatal rat cardiomyocytes (24). Beyond FOXO3, other predicted or validated LVH-associated direct targets of miR-212 have been identified. They include e.g., the extracellular signal-regulated kinase 2 (ERK2) (25), myocyte enhancer factor 2a (MEF2a) (26); AMP-activated protein kinase (AMPK) (27); heat shock protein 40 (HSP40) (28); sirtuin 1 (SIRT1) (29); calcineurin A-alpha (30); and phosphatase and tensin homolog (PTEN) (31).

So far there is no literature available on cardiac miR-212 and its targets in the development of RIHD. Therefore, we aimed to investigate the potential role of miR-212 and its selected hypertrophy-associated targets in the development of LVH during the early phases of RIHD.

Abbreviations: AKT, protein kinase B; AMPK, AMP-activated protein kinase; cGMP, cyclic guanosine monophosphate; ERK2, extracellular signal-regulated kinase 2; FOXO3, forkhead box O3; HFpEF, heart failure with preserved ejection fraction; Hsp, heat shock protein; IL, interleukin; LVH, left ventricular hypertrophy; Mef, myocyte enhancer factor; miR, microRNA; NO, nitric oxide; PKG, cGMP-dependent protein kinase; PTEN, phosphatase and tensin homolog; RIHD, radiation-induced heart disease; ROCK, Rho-associated kinase; TAC, transverse aortic constriction; TGF-β, transforming growth factor beta.

MATERIALS AND METHODS

The datasets generated for this study are available on request from the corresponding author. This study was carried out in accordance with the recommendations of the National Institutes of Health Guide for the Care and Use of Laboratory Animals (NIH Publication No. 85-23, Revised 1996). The protocol was

approved by the Animal Research Ethics Committee of Csongrád County (XV.1181/2013) and the University of Szeged. All institutional and national guidelines for the care and use of laboratory animals were followed.

Animals

A total of 48 male Sprague-Dawley rats (200–220 g, 6–7 weeks old) were used ($n = 8$ in each group) in three separate experiments. After 1 week of acclimatization in a temperature-controlled room (22 ± 2°C; relative humidity 55 ± 10%), the animals were randomly assigned to different groups. A total of 24 animals received selective heart irradiation to induce RIHD, and a total of 24 animals served as controls. The animals were housed in pairs in individually ventilated cages (Sealsafe IVC system, Italy) in a temperature-controlled room with a 12 h:12 h light/dark cycle. Standard rat chow supplemented with 5% fat (Innovo Kft., Gödöllő, Hungary) and tap water were supplied *ad libitum* (16).

Experimental Setup

Animals were divided into three control and three irradiated groups in separate experiments ($n = 8$ in each group) (**Figure 1**). In the irradiated groups, animals received a single dose of 50 Gy delivered to the whole heart to induce RIHD. Groups were followed-up for 1, 3, and 19 weeks, respectively. Cardiac morphology and function were assessed by transthoracic echocardiography in all time points. The development of LVH and fibrosis in chronic RIHD was verified by the measurement of myocardial fiber diameters as well as picrosirius red staining for collagen at week 19. Total RNA was isolated from the hearts, and the myocardial expression of miR-212 and its direct target FOXO3 were measured by qRT-PCR in every time point. Myocardial expression of selected mRNA targets beyond FOXO3 was also measured by qRT-PCR at week 19. Moreover, cardiac expression of total-FOXO3, phospho-FOXO3, total-AKT, and phospho-AKT were measured using Western blot technique at week 19.

Heart Irradiation

Heart irradiation with a single dose of 50 Gy was carried out as described previously (16). Briefly, the planning of the irradiation was based on a 3D model (**Figure 1A**), and the dose was delivered to the geometric center of the heart. For better coverage of the heart and lung protection, a 6 MeV electron radiation was given with a circle-shaped aperture with a 2 cm diameter (**Figure 1B**). The radiation dose was delivered with a Primus linear accelerator (Siemens Healthcare GmbH, Erlangen, Germany) at a dose intensity of 5 Gy/min if the appropriate position of the animal was proven using a built-in electronic portal imaging device (**Figure 1C**). Before the irradiation, rats were anesthetized with sodium pentobarbital (Euthasol, ip. 40 mg/kg, Produlab Pharma b.v., Raamsdonksveer, The Netherlands), then fixed in the supine position to a flat surface couch.

Transthoracic Echocardiography

Cardiac morphology and function were assessed by transthoracic echocardiography at week 1, 3, and 19 to monitor the development of RIHD (**Figure 1D**). Rats were anesthetized with 2% isoflurane (Forane, AESICA, Queenborough Limited Kent, UK). Then, the chest was shaved, and the rat was placed in a supine position onto a heating pad. Two-dimensional, M-mode, Doppler, and tissue Doppler echocardiographic examinations were performed in accordance with the criteria of the American Society of Echocardiography with a Vivid 7 Dimension ultrasound system (General Electric Medical Systems) using a phased array 5.5–12 MHz transducer (10S probe) as described previously (16, 32, 33). Data of three consecutive heart cycles were analyzed (EchoPac Dimension software; General Electric Medical Systems) by an experienced investigator in a blinded manner. The mean values of three measurements were calculated and used for statistical evaluation.

Ex vivo Cardiac Perfusions and Tissue Harvesting

The hearts were weighed after 5 min of *ex vivo* heart perfusion (34–36). Apical and basal parts of the heart were freshly frozen and used for biochemical measurements in every follow-up time point (**Figure 1D**). A cross-section of the whole heart at the ring of the papillae was cut and fixed in 4% buffered formalin for histological analysis at week 19 (**Figure 1D**). Following the removal of the heart, the presence of pleural fluid was checked and collected from the chest. Body and lung weights were also measured in every follow-up time point.

Hematoxylin-Eosin Staining

Five-micrometer paraffin-embedded transverse cut sections of the formalin-fixed subvalvular area of the ventricles were stained with hematoxylin-eosin, in the samples collected at week 19. On these slides, myocardial fiber diameters were measured to verify the development of LVH as described previously (37, 38). Transverse transnuclear widths (cardiomyocyte diameter) were measured of 100 longitudinally oriented, mono-nucleated cardiomyocytes on left ventricle sections cut on the same plane (37, 38).

Picrosirius Red Staining and Image Analysis

Five-micrometer paraffin-embedded transverse cut sections of the formalin-fixed subvalvular area of the ventricles were stained with picrosirius red staining in the samples collected at week 19, to assess cardiac fibrosis as described previously [**Figure 1D**; (16, 38)]. Histological slides were scanned with a Pannoramic P250 scanner (3D-Histech, Budapest, Hungary) and digital images at the magnification of ×40 and ×100 were captured. Medium-size vessels and their perivascular connective tissue sheet, the subepicardial and subendocardial areas were avoided as best as possible. The picrosirius red dyed images were analyzed with an in-house developed program as described previously (16, 38). This program determines the proportion of red pixels of heart sections using two simple color filters. For each Red-Green-Blue (RGB) pixel, the program calculates the color of the pixel in Hue-Saturation-Luminance (HSL) color space. The first filter is used for detecting red portions of the image. The second filter excludes any white (empty) or light gray (residual dirt on the slide) pixel from further processing using a simple RGB threshold. In this

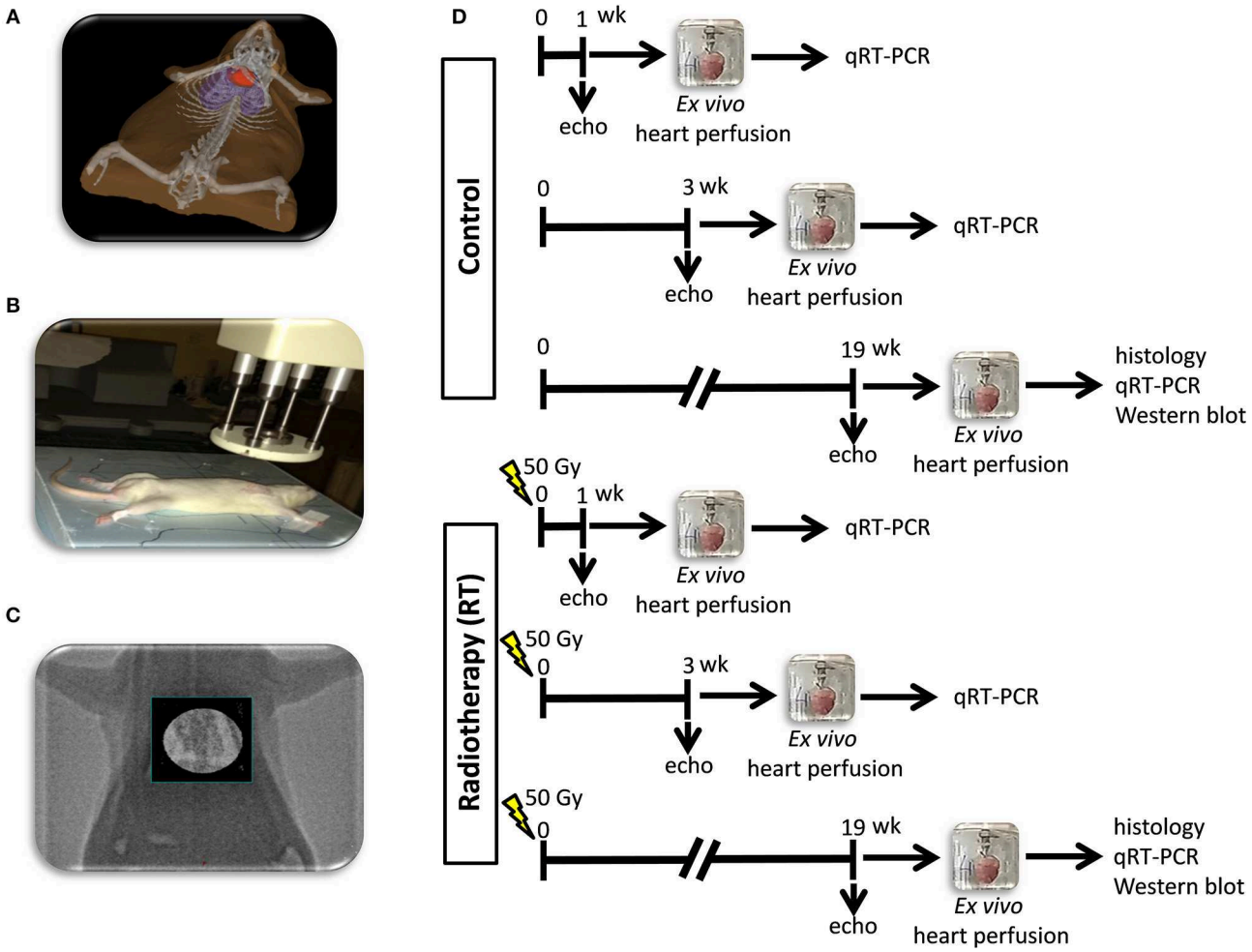

FIGURE 1 | Experimental protocol figure. **(A)** 3D visualization of the rat heart based on CT scans, **(B)** positioning of the rat for delivering the radiation dose with a Primus linear accelerator under sodium pentobarbital anesthesia, **(C)** appropriate position of the animal proven by portal imaging, **(D)** experimental protocol.

way, the program groups each pixel into one of two sets: pixels considered red and pixels considered green but neither red, nor white, nor gray. Red pixels in the first set correspond to connective tissue and fibrosis. Green pixels in the second set correspond to cardiac muscle. Dividing the number of elements in the first set by the number of elements in both sets gives the proportion of the connective tissue compartment of the heart area examined.

MicroRNA Expression Profiling by qRT-PCR

Quantitative RT-PCR was performed with miR-specific primers to monitor miR expression as described earlier [**Figure 1D**; (22, 38)]. In the case of miR-212, RNA was isolated using Trizol reagent (Invitrogen, #15596-018) from heart tissue. For quantitative detection of miR-212, TaqMan MicroRNA Reverse Transcription Kit (Applied Biosystems, #4366597), TaqMan miR-212, and snoRNA (U64702) Assays (Applied Biosystems, #A25576 and #4427975), and Absolute Blue qPCR Mix (Abgene, #AB-4136/B) were used according to the manufacturer's instructions. SnoRNA was used as a control for normalization.

mRNA Expression Profiling by qRT-PCR

Target mRNAs of miR-212 associated with cardiac hypertrophy and heart failure were selected in the TargetScan database. Quantitative RT-PCR was performed with gene-specific primers to monitor mRNA expression as described previously [**Figure 1D**; **Table 1**; (38, 39)]. RNA was isolated using Qiagen RNeasy Fibrous Tissue Mini Kit (Qiagen, #74704) from heart tissue. Briefly, 3 μg of total RNA was reverse transcribed using High-Capacity cDNA Reverse Transcription Kit (Applied Biosystems, #4368814), specific primers and FastStart Essential DNA Green Master (Roche, #06402712001) were used according to the manufacturer's instructions. Peptidyl prolyl isomerase A (Ppia), hypoxanthine phosphoribosyltransferase 1 (Hprt1), ribosomal protein lateral stalk subunit P2 (Rplp2), and glyceraldehyde-3-phosphate dehydrogenase (Gapdh) were used as controls for normalization (**Table 1**).

TABLE 1 | Primer sequences.

Gene name	Gene symbol	Forward primer sequence	Reverse primer sequence
Peptidylprolyl isomerase A (cyclophilin A)	*Ppia*	tgctggaccaaacacaaatg	caccttcccaaagaccacat
Hypoxanthine phosphoribosyltransferase 1	*Hprt1*	gaccggttctgtcatgtcg	acctggttcatcatcactaatcac
Ribosomal protein lateral stalk subunit P2	*Rplp2*	agcgccaaagacatcaagaa	tcagctcactgatgaccttgtt
Glyceraldehyde-3-phosphate dehydrogenase (GAPDH)	*Gapdh*	gaagggctcatgaccacagt	ggatgcagggatgatgttct
Natriuretic peptide A (ANP)	*Nppa*	cacagatctgatggatttcaaga	cctcatcttctaccggcatc
Natriuretic peptide B (BNP)	*Nppb*	gtcagtcgcttgggctgt	ccagagctggggaaagaag
Myosin heavy polypeptide 6, cardiac muscle, alpha (α-MHC)	*Myh6*	cgaaactgaaaacggcaag	catagcgctccttgagattgt
Myosin heavy polypeptide 7, cardiac muscle, beta (β-MHC)	*Myh7*	atccctggatcaggacaaga	agcttcaggtcaccctcca
Protein phosphatase 3 catalytic subunit alpha	*Ppp3ca*	tgaggctgaaaaagcaatacg	aaaccctttgcctcttcaaaa
Protein phosphatase 3 catalytic subunit beta	*Ppp3cb*	tcagaagaagatggatttgacg	tgctcggatcttgttcctg
Nuclear factor of activated T-cells, cytoplasmic, calcineurin-dependent 4	*Nfatc4*	gggggctgtcaaggctgctc	gcgcccgatgtctgtctcacc
Muscle atrophy F-box protein (atrogin 1)	*Fbx32*	ccatcaggagaagtggatctatgtt	gttcatgaagttcttttgggcgatgc
Myocyte-enriched calcineurin-interacting protein 1 (MCIP1.4)	*Rcan1*	agctccctgattgcctgtgt	tttggccctggtctcacttt
Forkhead box O3	*Foxo3*	gctaagcaggcctcatctca	ttcggtcagtttgagggtct
Mitogen activated protein kinase 1 (ERK2)	*Mapk1*	tctgcaccgtgacctcaa	gcaaggccaaagtcacaga
Myocyte enhancer factor 2a	*Mef2a*	gcacacagagcaccttgtaga	ttaggagacaagtagtccaaggaag
Protein kinase AMP-activated catalytic subunit alpha 2 (AMPK)	*Prkaa2*	gacaatcggagctatcttctagactt	aggtgttgaagaaccagacctc
DnaJ heat shock protein family (Hsp40) member A2	*Dnaja2*	aggtgtgcgcattatgataaga	cggtctttttcattgatgacct
Sirtuin 1, transcript variant X1 (predicted)	*Sirt1*	ttcgtggagatatttttaatcaggt	ctggtaagttttcaccaaagaagac
Phosphatase and tensin homolog	*Pten*	catgagcgagttggtcaaga	ccatgctgtgctggttca
Collagen type III alpha 1	*Col3a1*	gaggaatgggtggctatcct	ggtatccaggagaaccaggag
Collagen type I alpha 1	*Col1a1*	gggtctagacatgttcagctttg	ggcagtggcccctaagag

Matrix Metalloprotease 2 (MMP-2) Zymography

Cardiac MMP-2 activity was measured at week 19 from homogenized samples, to estimate the collagen breakdown in the cardiac extracellular matrix as we described previously (40, 41). Briefly, polyacrylamide gels were copolymerized with gelatin, and a 40 μg protein was separated by electrophoresis (150 V, 1.5 h) in each lane. Following electrophoresis, gels were washed with 2.5% Triton X-100 and incubated for 20 h at 37°C in incubation buffer. Gels were then stained with 0.05% Coomassie Brilliant Blue in a mixture of methanol/acetic acid/water and de-stained in aqueous 4% methanol/8% acetic acid. Zymograms were digitally scanned, and band intensities were quantified using Quantity One software (Bio-Rad, Hercules, CA) (41).

Western Blot

To investigate gene expression changes at protein quantity and activity level, standard Western blot technique was used in case of phospho-AKT, AKT, phospho-FOXO3, and FOXO3 with GAPDH loading background at week 19 [**Figure 1D**; (38, 42, 43)]. Heart tissue samples (n = 7–8) were homogenized with an ultrasonicator (UP100H Hielscher, Teltow, Germany) in RIPA (Radioimmunoassay) buffer (50 mM Tris–HCl (pH 8.0), 150 mM NaCl, 0.5% sodium deoxycholate, 5 mM EDTA, 0.1% SDS, 1% NP-40 (Cell Signaling, Carlsbad, CA, USA) supplemented with protease inhibitor cocktail and phosphatase inhibitors PMSF and NaF (Sigma, Saint Louis, MO, USA). The crude homogenates were centrifuged at 15,000 × g for 30 min at4°C. After quantification of protein concentrations of the supernatants, using the BCA Protein Assay Kit (Pierce, Rockford, IL, USA), 25 μg reduced and denaturated protein was loaded and SDS-PAGE (10% gel, 90 V, 2 h) was performed followed by the transfer of proteins onto a nitrocellulose membrane (20% methanol, 35 V, 2 h). The efficacy of the transfer was checked using Ponceau staining. The membranes were cut horizontally into three parts corresponding to the molecular weights of AKT, FOXO3, and GAPDH. Then the membranes were blocked for 1 h in 5% (w/v) BSA at room temperature and then incubated with primary antibodies (Cell Signaling, Beverly, MA, USA; overnight, 4°C, 5% BSA) in the concentrations of 1:1,000 against AKT (#9272), phosho-AKT (Ser473, #4060), phospho-FOXO3 (Ser253; #13129), 1:500 against FOXO3 (#2497) or 1:5,000 against GAPDH (#2118 overnight, 4°C, 1% BSA). Then the membranes were incubated with horseradish peroxidase (HRP)-conjugated goat anti-rabbit secondary antibody 1:2,000 (1:1,000 for FOXO3, 1:5,000 for GAPDH) (Dako Corporation, Santa Barbara, CA, USA; 45 min, room temperature, 1% BSA). After assessment of phosphorylated proteins, the membranes were stripped and reassessed for the total amount of proteins. An enhanced chemiluminescence kit

TABLE 2 | Characteristics of the RIHD models at week 1, 3, and 19, respectively.

Parameter (unit)	Week 1			Week 3			Week 19		
	Control	RT	*p*-value	Control	RT	*p*-value	Control	RT	*p*-value
Body weight at the endpoint (g)	270 ± 9	254 ± 8	0.205	394 ± 11$^{\#}$	366 ± 10$^{\#}$	0.091	597 ± 24$^{\#}$	425 ± 43$^{\#*}$	0.004
Heart weight (g)	1.21 ± 0.07	1.13 ± 0.05	0.340	1.33 ± 0.05	1.45 ± 0.09$^{\#}$	0.286	1.74 ± 0.08$^{\#}$	1.34 ± 0.06$^{\#*}$	0.002
Lung weight (g)	1.35 ± 0.06	1.64 ± 0.07*	0.006	2.01 ± 0.09$^{\#}$	2.72 ± 0.25$^{\#*}$	0.014	2.29 ± 0.17$^{\#}$	2.26 ± 0.18$^{\#}$	0.883
Heart weight/body weight ratio*1,000	4.45 ± 0.13	4.44 ± 0.10	0.918	3.38 ± 0.10$^{\#}$	3.99 ± 0.32$^{\#}$	0.100	2.92 ± 0.09$^{\#}$	3.36 ± 0.35$^{\#}$	0.239

*Values are mean ± SEM, n = 8, *p < 0.05 vs. control, unpaired t-test within the same time points. p-values refer to the unpaired t-test at each time point. #p < 0.05 vs. week 1 within the same group (control or RT), One-Way ANOVA, Bonferroni post-hoc test. RT, radiotherapy.*

(Cell Signaling, Carlsbad, CA, USA) was used to develop the membranes. The chemiluminescence signals were analyzed and evaluated by Quantity One Software. Signals of GAPDH and FOXO3, as well as AKT, develop at different time points. Therefore, the expositions times are different for GAPDH, FOXO3, and AKT. For signal evaluation of Western blots, we always used the non-oversaturated films for correct signal detection (**Supplementary Figures**).

Statistical Analysis

Statistical analysis was performed using Sigmaplot 12.0 for Windows (Systat Software Inc.). All values are presented as mean ± SEM except the gene expression data measured by qRT-PCR. Data showed normal distribution unless otherwise indicated. Data measured at different follow-up time points in separate experiments including body weight, heart weight, heart weight to body weight ratio, lung weight and echocardiographic parameters were compared using One-Way ANOVA between the groups. A Bonferroni test was used as a *post-hoc* test. A two sample *t*-test (in case of the normal distribution of the data) or Mann Whitney *U*-test (in case of the non-normal distribution of the data) was used to determine the effect of RIHD on all measured parameters within each time point. $P < 0.05$ was accepted as a statistically significant difference. In the case of target genes, the analysis of relative gene expression data was performed using the $2^{-\Delta\Delta Ct}$ method. Gene expression ratios with a $p < 0.05$ and fold change of <-2.00 or fold change of >2.00 were considered as repression or overexpression respectively in gene activity.

RESULTS

Characteristics of the RIHD Models

At week 1, there was no difference in the body weight between the control and irradiated groups (**Table 2**). At week 3, the irradiated animals presented a trend toward a lower body weight as compared to the time-matched controls (**Table 2**). At week 19, the irradiated rats showed significantly lower body weight as compared to the time-matched controls (**Table 2**). At autopsy at week 1 and 3, there was no pleural fluid in the irradiated animals. At week 19, the presence of extensive pleural fluids was found in almost all animals in the irradiated group (data not shown). At the macroscopic level, no major heart pathologies (including the large vessels, the valves, the coronary arteries, etc.) were observed in the irradiated groups at any follow-up time point. At week 1 and 3, lung weights were significantly increased in the irradiated groups as compared to the time-matched controls (**Table 2**). A higher lung weight might suggest the presence of acute inflammation and lung edema due to the acute deteriorating effects of ionizing radiation. At week 19, no difference was found in lung weights between the groups (**Table 2**). At week 1 and 3, there was no difference in heart weights between the irradiated groups and their time-matched controls (**Table 2**). However, the heart to body weight ratio showed a trend toward an increase in the irradiated group at week 3 (**Table 2**). The increased heart to body weight ratio might suggest the development of starting cardiac hypertrophy. At week

TABLE 3 | Effects of radiotherapy on various *in vivo* left ventricular morphological and functional parameters measured by transthoracic echocardiography at week 1, 3, and 19, respectively.

Parameter (unit)	View/Mode	Week 1			Week 3			Week 19		
		Control	RT	*p*-value	Control	RT	*p*-value	Control	RT	*p*-value
Posterior wall thickness-systolic (mm)	Long axis/MM	2.78 ± 0.12	2.95 ± 0.11	0.307	2.94 ± 0.11	3.16 ± 0.12	0.214	3.19 ± 0.16$^{\#}$	3.37 ± 0.24$^{\#}$	0.526
Posterior wall thickness-diastolic (mm)	Long axis/MM	1.85 ± 0.07	1.76 ± 0.07	0.357	2.01 ± 0.12	1.80 ± 0.13	0.122	2.00 ± 0.11	2.44 ± 0.14$^{\#*}$	0.026
Septal wall thickness-systolic (mm)	Long axis/MM	2.91 ± 0.13	3.06 ± 0.08	0.349	3.13 ± 0.08	3.54 ± 0.13*	0.017	3.27 ± 0.13$^{\#}$	3.71 ± 0.29$^{\#}$	0.186
Septal wall thickness-diastolic (mm)	Long axis/MM	1.64 ± 0.07	1.79 ± 0.10	0.233	1.65 ± 0.05	1.85 ± 0.04*	0.009	1.87 ± 0.12$^{\#}$	2.69 ± 0.34$^{\#*}$	0.037
Left ventricular end diastolic diameter (mm)	Long axis/MM	7.73 ± 0.10	7.31 ± 0.15*	0.035	7.99 ± 0.13	7.63 ± 0.25	0.207	8.55 ± 0.14$^{\#}$	6.04 ± 0.52$^{\#*}$	0.000
Left ventricular end systolic diameter (mm)	Long axis/MM	4.45 ± 0.20	3.76 ± 0.23*	0.048	4.37 ± 0.16	3.50 ± 0.26*	0.011	4.13 ± 0.23	2.59 ± 0.55$^{\#*}$	0.021
Fractional shortening (%)	Long axis/MM	43 ± 3	48 ± 3	0.152	45 ± 2	54 ± 3*	0.020	46 ± 1	63 ± 6$^{\#*}$	0.013
Left ventricular end-diastolic volume (µl)	Four chamber/2D	135 ± 15	94 ± 6*	0.023	120 ± 9	114 ± 8	0.646	262 ± 27$^{\#}$	91 ± 13*	0.000
Left ventricular end-systolic volume (µl)	Four chamber/2D	54 ± 6	33 ± 3*	0.008	38 ± 3$^{\#}$	37 ± 3	0.871	100 ± 17$^{\#}$	36. ± 5.*	0.003
Stroke volume (µl)	Four chamber/2D	82 ± 9	61 ± 5	0.064	82 ± 6	77 ± 6	0.676	162 ± 14$^{\#}$	56 ± 9*	0.000
Heart rate (beats/min)	Four chamber/2D	349 ± 10	373 ± 6	0.052	338 ± 14	352 ± 14	0.488	291 ± 7$^{\#}$	279 ± 7$^{\#}$	0.278
E/e'-wave (m/s)	4 chamber/PWD	13 ± 1	23 ± 1*	0.002	15 ± 1	30 ± 3*	0.000	17 ± 1	25 ± 2	0.004
e'-wave (m/s)	4 chamber/TD	0.079 ± 0.005	0.042 ± 0.002*	0.009	0.071 ± 0.007	0.038 ± 0.003*	0.006	0.055 ± 0.004$^{\#}$	0.042 ± 0.005*	0.009
Maximal LV outflow tract velocity (m/s)	4 chamber/PWD	3.81 ± 0.38	4.38 ± 0.71	0.496	2.57 ± 0.36	2.10 ± 0.33$^{\#}$	0.363	4.11 ± 0.63	2.04 ± 0.54$^{\#*}$	0.030
Mean LV outflow tract velocity (m/s)	4 chamber/PWD	2.60 ± 0.30	2.98 ± 0.49	0.518	1.62 ± 0.23	1.53 ± 0.26$^{\#}$	0.548	2.50 ± 0.41	1.28 ± 0.36$^{\#*}$	0.046

Transthoracic echocardiographic measurements were performed 1, 3, and 19 weeks after the selective heart irradiation in separated experiments. Values are mean ± SEM, n = 8, $^{*}p < 0.05$ vs. control, unpaired t-test within the same time point. p-values refer to the unpaired t-test at each time point. $^{\#}p < 0.05$ vs. week 1 within the same group (control or RT), One-Way ANOVA, Bonferroni post-hoc test. 2D, two-dimensional, E-wave, early ventricular filling velocity; LV, left ventricular, MM, M (motion) Mode; PW, pulse wave; RT, radiotherapy; TD, tissue Doppler.

19, the tibia length (4.23 ± 0.05 vs. 4.46 ± 0.04 cm, $p = 0.003$) and the heart weight was significantly lower in the irradiated group than in the control group pointing out the growth retardation in these animals (**Table 2**). At week 19, no sign of radiation-induced pneumonitis or lung fibrosis was visible, confirming the appropriateness of our models for the study of the acute and chronic effects of selective heart irradiation. At week 19, all of the morphometric parameters (body weight, heart weight, heart weight to body weight ratio, and lung weight) were significantly higher in both the control and irradiated groups as compared to week 1 parameters within the same group, due to the growth of the animals (**Table 2**).

HFpEF Developed in RIHD at Week 19

Transthoracic echocardiography was performed at week 1, 3, and 19 in separate experiments to investigate whether the development of acute and chronic RIHD leads to an alteration in myocardial morphology and function (**Table 3**; **Figures 1A**, **2**).

At week 1, the left ventricular wall thicknesses were not different between the irradiated and time-matched control groups (**Table 3**). In contrast, the left ventricular end-systolic and end-diastolic diameters, as well as the volumes, were significantly decreased in the irradiated animals, proving an acute dysfunction in the contraction and relaxation as well (**Table 3**). Stroke volume showed a statistically non-significant trend toward a decrease in the irradiated animals as compared to the time-matched controls (**Table 3**). There was a trend toward an increase in heart rate in the irradiated animals, likely a compensatory mechanism, to maintain cardiac output (**Table 3**). The ratio of the early flow velocity E and the septal mitral annulus velocity e′ significantly increased, and e′ significantly decreased in irradiated rats indicating the presence of concomitant diastolic dysfunction (**Table 3**).

At week 3, septal wall-thicknesses both in diastole and systole were significantly increased in the irradiated rats indicating the development of LVH (**Table 3**). The left ventricular end-systolic diameter was significantly decreased, and fractional shortening was significantly increased in the irradiated animals in this early phase of hypertrophy (**Table 3**). Diastolic dysfunction was also present in the irradiated group characterized by significantly increased E/e′ and significantly decreased e′ (**Table 3**).

At week 19, left ventricular wall thicknesses including anterior and inferior walls both in systole and diastole, as well as septal and posterior walls in diastole, significantly increased in irradiated rats pointing to the presence of a marked concentric LVH (**Table 3**; **Figures 2A–C**). In addition, both left ventricular end-systolic and end-diastolic diameters significantly decreased in irradiated animals as compared to the controls (**Figure 2D**). Indeed, left ventricular end-systolic, as well as end-diastolic volumes also decreased in irradiated rats (**Table 3**). In contrast, ejection fraction remained unchanged in irradiated rats showing a characteristic picture of HFpEF (**Figure 2E**). There was no difference in heart rate between the two groups at this stage (**Table 3**). Stroke volume and cardiac output were significantly reduced in irradiated rats as compared to controls (**Table 3**; **Figure 2F**). More importantly, e′ was significantly decreased and

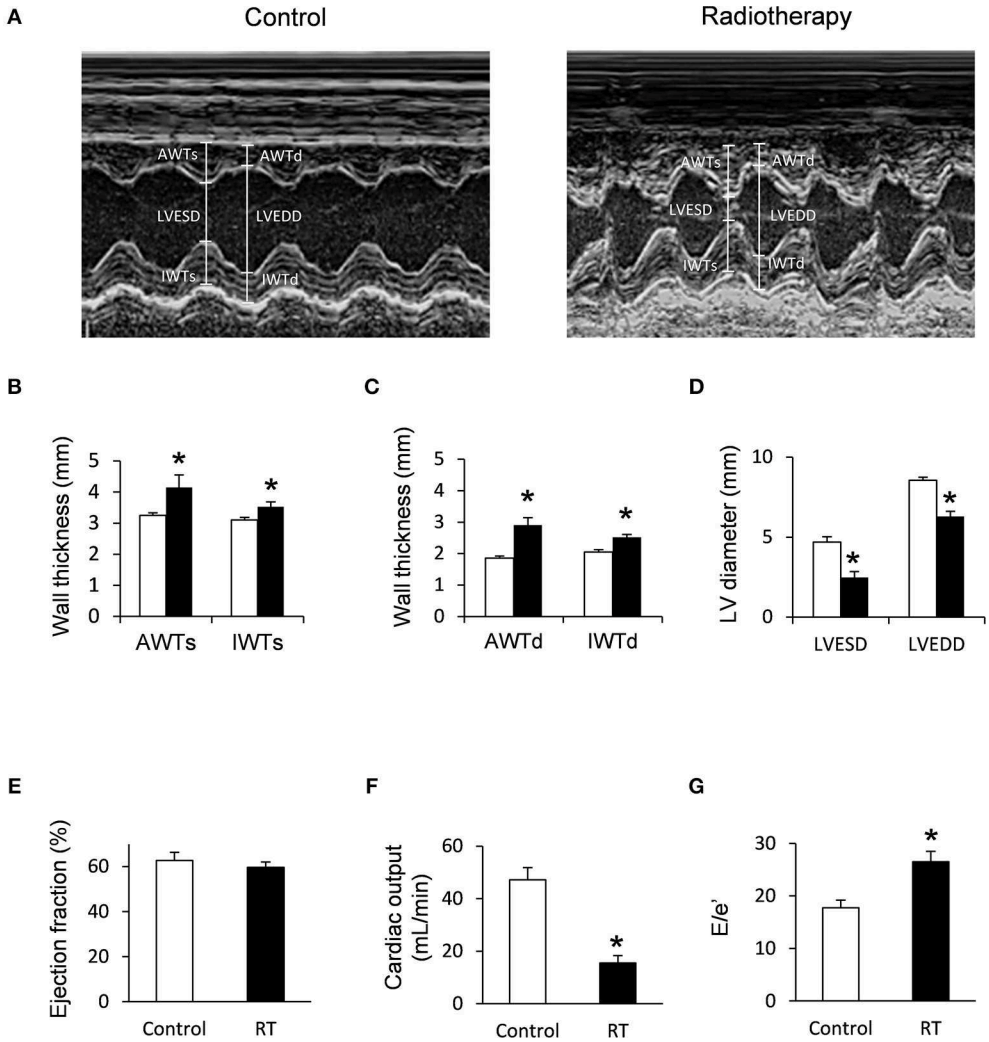

FIGURE 2 | Echocardiographic results at week 19. **(A)** Representative M-mode images, **(B)** anterior and inferior wall thicknesses in systole (AWTs and IWTs), **(C)** anterior and inferior wall thicknesses in diastole (AWTd and IWTd), **(D)** left ventricular end systolic diameter (LVESD) and left ventricular end diastolic diameter (LVEDD), **(E)** ejection fraction, **(F)** cardiac output, and **(G)** E/e' ratio. White bars represent control group and black bars represent the irradiated group. RT means radiotherapy. Values are means ± SEM, $n = 8$, $^*p < 0.05$.

E/e′ was significantly increased indicating diastolic dysfunction (**Table 3**; **Figure 2G**).

Septal and posterior wall thicknesses were significantly increased both in the control and irradiated group at week 19 as compared to data measured at week 1 in the same group, due to the growth of the animals (**Table 3**). Interestingly, left ventricular end-diastolic and end-systolic diameters were significantly decreased in the RIHD group at week 19 as compared to week 1 values, indicating the presence of marked concentric hypertrophy (**Table 3**). In the control group, left ventricular end-diastolic diameter was significantly increased at week 19 as compared to week 1 values, due to the normal growth of the animals (**Table 3**). Heart rate was significantly decreased in both the control and irradiated groups at week 19 as compared to week 1 values which might be caused by the aging of the animals (**Table 3**).

Cardiomyocyte Hypertrophy and Interstitial Fibrosis in RIHD at Week 19

To verify the development of severe LVH seen on echocardiographic images at week 19, cardiomyocyte diameters were measured histologically (**Figures 3A,B**). Cross-sectional cardiomyocyte diameters significantly increased in RIHD proving the presence of LVH at the cellular level at week 19 (**Figure 3B**).

Collagen deposition was assessed to investigate the development of fibrosis in response to selective heart irradiation at week 19 (**Figures 3C,D**). Significant interstitial fibrosis was found with slight but consistent collagen depositions in all studied segments of the irradiated hearts (**Figures 3C,D**). MMP2 activity also showed a decreasing trend at week 19 (**Figure 3E**), suggesting that the balance between collagen breakdown and deposition might be shifted toward deposition.

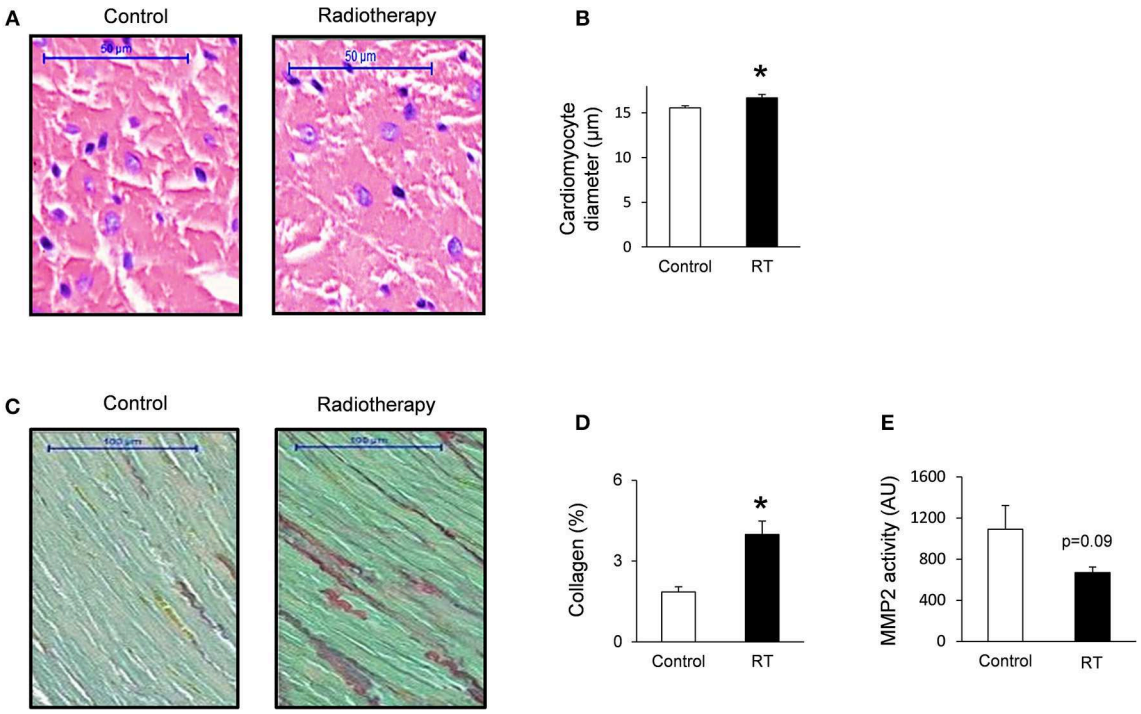

FIGURE 3 | Histology and zymography results at week 19. **(A)** Hematoxylin-eosin stained slides, **(B)** cardiomyocyte diameter, **(C)** picrosirius red and fast green stained slides, **(D)** cardiac collagen content, and **(E)** MMP2 activity. White bars represent control group and black bars represent the irradiated group. RT means radiotherapy. Values are means ± SEM, $n = 8$, $^*p < 0.05$.

Molecular Markers of Cardiac Hypertrophy and Fibrosis

The expression of cardiac hypertrophy (alpha-MHC and beta-MHC), fibrosis (collagen type I alpha 1 - *Col1a1* - and collagen type III alpha 1- *Col3a1* -) and heart failure (A-type natriuretic peptide [ANP] and B-type natriuretic peptide [BNP]) markers were measured by qRT-PCR at week 1, 3, and 19 (**Tables 4**, **5**). At week 1 and 3, the cardiac expression of these markers showed no difference among the irradiated and time-matched control groups (**Table 4**).

At week 19, the beta-MHC to alpha-MHC ratio showed a 2.7-fold increase among cardiac hypertrophy markers. The cardiac expression of alpha-MHC significantly decreased in RIHD as compared to the controls (**Table 5**). However, the cardiac beta-MHC mRNA level did not change in RIHD as compared to controls. The cardiac expression of pro-hypertrophic protein phosphatase 3, catalytic subunit alpha and beta (i.e., calcineurin A-alpha and calcineurin A-beta), myocyte enhancer factor 2D (*Mef2d*), and myocyte enhancer factor 2C (*Mef2c*) did not change in response to selective heart irradiation as compared to the controls (**Table 5**). The anti-hypertrophic atrogin-1 and the pro-hypertrophic calcineurin pathway element myocyte-enriched calcineurin-interacting protein 1.4 (MCIP 1.4) did not change significantly in RIHD as compared to the controls (**Table 5**). Among fibrosis and remodeling markers, the more elastic *Col3a1* showed significant down-regulation in RIHD; however, the more rigid *Col1a1* failed to change in RIHD (**Table 5**). Consistently, the ratio of *Col1a1* to *Col3a1* increased, which is a characteristic change in left ventricular fibrosis and remodeling (44–46). Moreover, the mRNA levels of the heart failure markers, ANP and BNP, significantly increased in RIHD as compared to the controls (**Table 5**).

Cardiac Overexpression of miR-212 at Week 3 and 19

At week 1, there was no change in the cardiac expression of miR-212 between the irradiated and control groups (**Table 5**). Both at week 3 and 19, miR-212 was significantly overexpressed in the irradiated hearts as compared to the controls (**Table 4**; **Figure 4A**).

Repression of the Anti-hypertrophic FOXO3 at the mRNA Level in RIHD Only at Week 19

Both at week 1 and 3, there was no change in the cardiac expression of the anti-hypertrophic miR-212 target molecule FOXO3 between the irradiated and time-matched control groups (**Table 4**). In contrast, cardiac expression of FOXO3 was significantly decreased at the mRNA level in irradiated hearts as compared to controls at week 19 (**Table 5**; **Figure 4E**).

TABLE 4 | Cardiac gene expression changes 1 and 3 weeks after the selective heart irradiation (qRT-PCR results).

Gene name	Gene symbol	Week 1				Week 3			
		Log_2 change	SD log_2 change	*p*-value	Fold change	Log_2 change	SD log_2 change	*p*-value	Fold change
miR-212	*miR-212*	−0.38	0.63	0.183	−1.30	1.11	0.38	0.000	2.15*
Forkhead box O3	*Foxo3*	−0.02	0.41	0.916	−1.01	−0.19	0.29	0.170	−1.14
Myosin, Heavy Polypeptide 6, Cardiac Muscle, Alpha (α-MHC)	*Myh6*	−0.45	0.29	0.009	−1.37	−0.38	0.61	0.193	−1.30
Myosin, Heavy Polypeptide 7, Cardiac Muscle, Beta (β-MHC)	*Myh7*	−0.13	0.23	0.237	−1.09	−0.12	0.59	0.666	−1.08
Collagen, type III, alpha 1	*Col3a1*	−0.52	0.61	0,079	−1.44	1.11	0.97	0.027	1.24
Collagen, type I, alpha 1	*Col1a1*	−0.43	0.46	0.171	−1.37	0.39	0.59	0.171	1.31
Natriuretic peptide A (ANP)	*Nppa*	0.76	1.26	0.198	1.71	0.56	0.97	0.231	1.47
Natriuretic peptide B (BNP)	*Nppb*	−0.09	0.75	0.789	−1.08	0.55	0.76	0.132	1.46

Gene expression ratios at week 1 and 3, respectively, (radiotherapy vs. control). Fold change of < −2.00 or >2.00 (repression or overexpression respectively) and a $p < 0.05$ were considered as a significant change. n = 6, unpaired t-test or Mann-Whitney U-test.*

TABLE 5 | Cardiac gene expression changes 19 weeks after the selective heart irradiation (qRT-PCR results).

	Gene name	Gene symbol	Log_2 change	SD log_2 change	*p*-value	Fold change
miR-212 targets	Forkhead box O3	*Foxo3*	−1.01	1.11	0.000	−2.01*
	Mitogen activated protein kinase 1 (ERK2)	*Mapk1*	−0.47	0.34	0.000	−1.39
	Myocyte enhancer factor 2a	*Mef2a*	−0.10	0.52	0.051	1.10
	Protein kinase AMP-activated catalytic subunit alpha 2 (AMPK)	*Prkaa2*	−0.49	0.46	0.000	−1.41
	DnaJ heat shock protein family (Hsp40) member A2	*Dnaja2*	−0.41	0.43	0.000	−1.33
	Sirtuin 1. transcript variant X1	*Sirt1*	−0.34	0.38	0.000	−1.26
	Protein phosphatase 3 catalytic subunit alpha (Calcineurin A-alpha)	*Ppp3ca*	−0.45	0.61	0.000	−1.37
	Phosphatase and tensin homolog (PTEN)	*Pten*	−0.04	0.27	0.408	−1.03
Other Genes	Myosin heavy polypeptide 6, cardiac muscle, alpha (α-MHC)	*Myh6*	−2.04	1.08	0.007	−4.11*
	Myosin heavy polypeptide 7 cardiac muscle, beta (β-MHC)	*Myh7*	−0.62	0.33	0.003	−1.53
	Collagen type III alpha 1	*Col3a1*	−1.45	0.87	0.000	−2.73*
	Collagen type I alpha 1	*Col1a1*	0.14	0.72	0.253	1.10
	Protein phosphatase 3 catalytic subunit beta (Calcineurin A-beta)	*Ppp3cb*	−0.44	0.24	0.000	−1.36
	Muscle atrophy F-box protein (Atrogin-1)	*Fbxo32*	−0.17	0.25	0.159	−1.12
	Myocyte-enriched calcineurin-interacting protein 1 (MCIP1.4)	*Rcan1*	−0.18	0.51	0.455	−1.13
	Natriuretic peptide A (ANP)	*Nppa*	3.88	1.80	0.000	14.77*
	Natriuretic peptide B (BNP)	*Nppb*	1.50	0.53	0.000	2.83*

Gene expression ratios at week 19 (radiotherapy vs. control). Fold change of <−2.00 or >2.00 (repression or overexpression. respectively) and a $p < 0.05$ were considered as a significant change. n = 6, unpaired t-test or Mann-Whitney U-test.*

Phospho-FOXO3/Total FOXO3 Ratio in RIHD at Week 19

The expression of the anti-hypertrophic miR-212 target molecule FOXO3 was also investigated at the protein level using a Western blot technique at week 19. Total FOXO3 protein levels failed to decrease in the irradiated hearts as compared to the controls (**Figure 4F**). The cardiac phospho-FOXO3 level and the phospho-FOXO3/total FOXO3 ratio showed a statistically non-significant trend toward an increase in RIHD as compared to the control group (**Figures 4G,H**). An increased phospho-FOXO3/total FOXO3 ratio is considered to be a characteristic shift in pressure-overload-induced cardiac hypertrophy forms (47). In our RIHD model, the statistically non-significant trend toward an increase in the phospho-FOXO3/total FOXO3 ratio seems to be independent of the effect of miR-212 in RIHD (**Figure 5**).

Decreased Cardiac phospho-AKT Level in RIHD at Week 19

Moreover, we investigated the cardiac amount of both total AKT and phospho-AKT proteins using Western blot. Phospho-AKT is a positive regulator of the FOXO3 protein phosphorylation, leading to a pro-hypertrophic shift in the phospho-FOXO3/FOXO3 ratio in pressure-overload-induced LVH models [**Figure 5**; (48)]. In our RIHD model, the cardiac amount of total AKT did not differ between the two groups

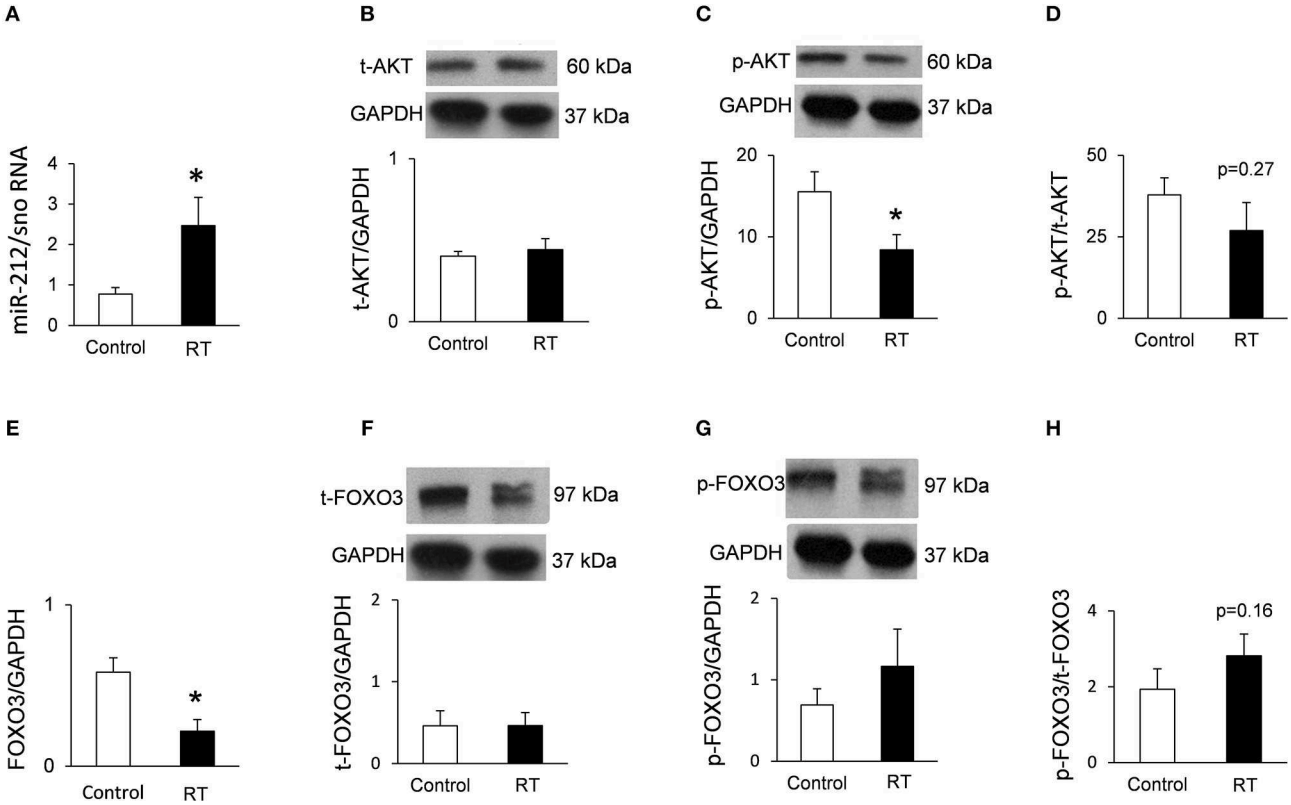

FIGURE 4 | qRT-PCR and Western blot results at week 19. **(A)** Cardiac miR-212 expression, **(B)** cardiac total AKT expression, **(C)** cardiac phospho-AKT expression, **(D)** cardiac phospho-AKT/total AKT ratio, **(E)** cardiac FOXO3 mRNA expression, **(F)** cardiac total FOXO3 expression, **(G)** cardiac phospho-FOXO3 expression, and **(H)** cardiac phospho-FOXO3/total FOXO3 ratio. White bars represent control group and black bars represent the irradiated group. RT means radiotherapy. Values are means ± SEM, $n = 7–8$, $^*p < 0.05$. In case of Western blot results, only the representative blot image was shown, and the mean was calculated.

(**Figure 4B**). However, the amount of phospho-AKT was significantly decreased in the irradiated hearts as compared to the controls (**Figure 4C**). The phospho-AKT/total AKT ratio showed a statistically non-significant trend toward a decrease in cardiac RIHD samples (**Figure 4D**). Hence, AKT does not seem to play a crucial role in the regulation of FOXO3 in RIHD (**Figure 5**).

Hypertrophy Associated mRNA Targets Beyond FOXO3 in RIHD at Week 19

Several predictive miR-212 targets associated with hypertrophy have been identified beyond FOXO3. Among those, we have also investigated the cardiac expression of the extracellular signal-regulated kinase 2 (ERK2), the myocyte enhancer factor 2a (*Mef2a*); the protein kinase AMP-activated catalytic subunit alpha 2 (AMPK); DnaJ heat shock protein family member A2 (*Hsp40*); sirtuin 1, transcript variant X1 (*Sirt1*); protein phosphatase 3 catalytic subunit alpha (calcineurin A-alpha); phosphatase and tensin homolog (PTEN) (**Table 5**). These target mRNAs failed to show significant down-regulation in response to selective heart irradiation as compared to the control hearts (**Table 5**).

DISCUSSION

We have previously described the rat model of RIHD in the chronic phase (16). In our present study, we have characterized the rat model of RIHD in the acute phase, 1 and 3 weeks after selective heart irradiation. We also confirm the presence of diastolic dysfunction in this model in every investigated phase (49). In our present study, mild septal hypertrophy was found 3 weeks after the selective heart irradiation. Marked cardiac morphological and functional changes were confirmed 19 weeks after the selective heart irradiation, in the form of concentric LVH and diastolic dysfunction, which are the hallmarks of HFpEF. These morphological and functional changes were similar to those reported in other studies (1, 7).

Two major components are thought to be responsible for the development of RIHD in humans. One is the progressive atherosclerosis of the coronary arteries due to endothelial damage (5, 6). The other is diffuse injury and inflammation of the myocardium caused by the loss of capillaries and cardiomyocytes (9). These mechanisms could lead to compensatory cardiomyocyte hypertrophy and interstitial fibrosis in the early stages of RIHD (5, 6). The injury of coronary arteries is difficult to test in wild-type rodent

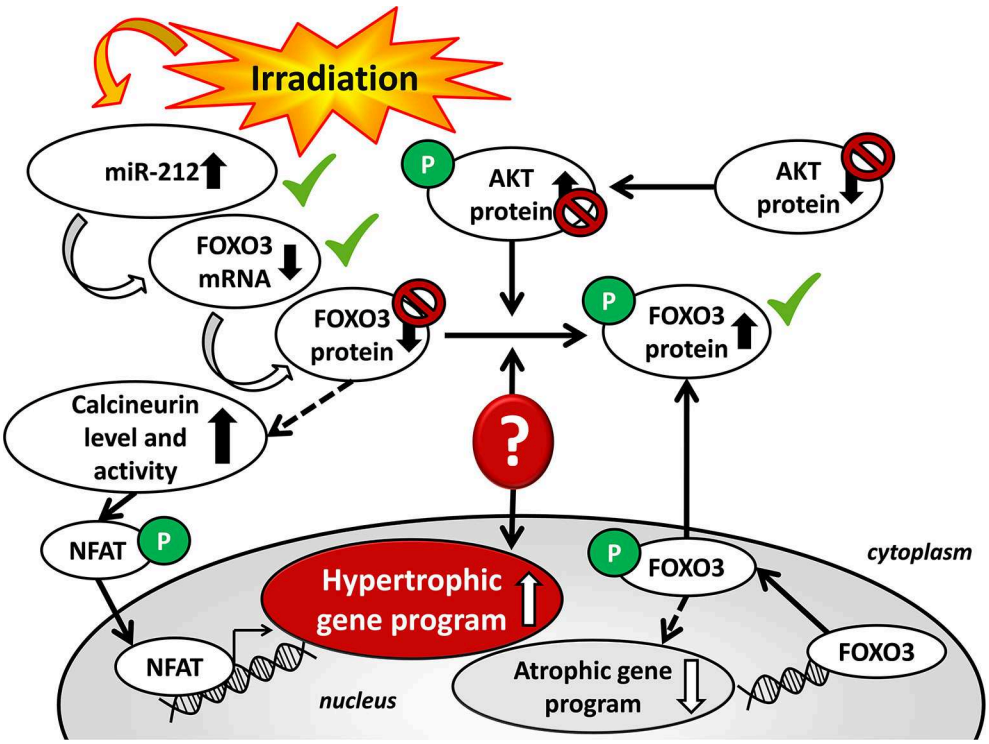

FIGURE 5 | Putative mechanisms in the development of left ventricular hypertrophy in RIHD.

models due to different serum lipid profiles (i.e., higher HDL-cholesterol and lower LDL-cholesterol levels as compared to humans) which naturally protect them from the development of atherosclerosis (50). In our present study, the lack of atherosclerosis makes it possible to study the direct effects and mechanisms of diffuse myocardial injury and chronic inflammation components. Available studies are mainly focused on macro- and microvascular contributions in RIHD (3, 6, 10, 11). So far only a few studies investigated the molecular mechanisms of radiation-induced diffuse myocardial injury and compensatory hypertrophy (1, 7, 15).

In our present study, picrosirius red staining indicates an increased interstitial accumulation of collagens in the RIHD hearts. Generally, the increased collagen deposition could be explained by either the stimulation of production or the reduced turnover of the mRNAs and/or proteins of different collagen types. In our RIHD model, we could not demonstrate increased expressions of collagens at the mRNA level at week 19, only a decrease in *Col3a1* and no change in *Col1a1* expression. Likely, the excessive stimulation of collagen expression happens at the mRNA level at earlier time points, and only the result of an earlier stimulation was visible at the protein level in our study. However, we observed a trend toward reduced MMP-2 activity in RIHD hearts at week 19, which might indicate a reduced turnover of collagens at the protein level. There was no change in the cardiac gene expression of *Col1a1* and *Col3a1* in the early phases of RIHD. Therefore, the 1- and 3-week follow-up times seem to be too early to detect significant stimulation of collagen gene expression at the mRNA level in RIHD. The key mediator of radiation-induced cardiac fibrosis is thought to be a transforming growth factor beta (TGF-β1) (15, 51). In our previous experiments, increased plasma levels of TGF-β1 and growth differentiation factor 15 (GDF-15) were shown 12 weeks after the selective heart irradiation with 50 Gy (16). Another possible explanation is that our RIHD model in week 19 is not in the phase of severe fibrotic remodeling, which ultimately leads to systolic heart failure with reduced ejection fraction (HFrEF). According to our experimental data, the heart at 19 weeks following irradiation is best characterized by hypertrophy, mild interstitial fibrosis, and diastolic dysfunction, demonstrating characteristic HFpEF. Another study demonstrated that the degeneration of cardiomyocytes extended until 100 days after the irradiation (15). In our chronic RIHD model, the mild interstitial fibrosis might be developed as a reaction to diffuse cardiomyocyte cell death (52). This replacement fibrosis is thought to be essential in the adaptation to the loss of cardiac parenchyma and the preservation of the heart structure in different heart failure models (52). Thus, more severe fibrosis might be detectable at a later stage (>19 weeks), followed by dilatation of the heart, thinner walls and end-stage heart failure with reduced ejection fraction in RIHD (15). A study with a 16-month follow-up time reported that interstitial collagen deposition had a progressive nature (15).

It is also interesting to note that the gene expression of type III collagen fibers was significantly repressed, and the expression

of type I collagen fibers were not changed in response to selective heart irradiation in our present study at week 19. Collagen type III is of the thinner and more elastic fiber type, whereas collagen type I is of the thicker and more rigid fiber type (44). The increased ratio of *Col1a1* to *Col3a1* at the protein level could be a factor in the stiffness and resistance to stretch in both in HFpEF and HFrEF in different heart failure and hypertrophy forms (44–46).

Unfortunately, therapeutic options for RIHD are currently insufficient. Since interstitial fibrosis is a final major endpoint of RIHD, our chronic model seems to be an adequate one, in a series of future investigations with different anti-fibrotic agents to prevent fibrosis in an early phase. Interestingly, a recent study showed cardioprotective effects of an endogenously released small peptide N-acetyl-Ser-Asp-Lys-Pro (Ac-SDKP) in a rat model of RIHD. In this experimental study, Ac-SDKP was reported to inhibit inflammation, fibrosis, and reduce macrophage activation (53).

A number of studies demonstrated that miRs are critical contributors to cardiovascular biology and disease development (18–21, 54). So far, only two studies have been published, describing that miR-1, as well as miR-15b, were repressed and miR-21 was overexpressed in RIHD (55, 56). It has been demonstrated that hypertrophic stimuli upregulated cardiac expression of miR-212, which is necessary and sufficient to drive the hypertrophic growth of cardiomyocytes (22). MiR-212 was shown to be a key regulator of the development of LVH and heart failure via the repression of the anti-hypertrophic transcription factor FOXO3 and overactivation of the calcineurin/NFAT signaling during heart failure development (22). In our present study, LVH was accompanied by the overexpression of miR-212 3 and 19 weeks after the selective heart irradiation. Interestingly, the repression of FOXO3 at the mRNA level was present in cardiac tissue samples in RIHD only at week 19 (**Figure 5**). In contrast, the FOXO3 protein level failed to decrease, and the phospho-FOXO3/total FOXO3 ratio showed a non-significant trend toward an increase in RIHD at week 19 (**Figure 5**). Although, the increased phospho-FOXO3/total FOXO3 ratio is a characteristic shift in cardiac hypertrophy forms (47); it seems to be independent of the effect of miR-212 in chronic RIHD. FOXO transcription factors are also regulated by the protein kinase AKT [**Figure 5**; (48, 57)]. Therefore, we also measured the protein levels of both total and phospho-AKT at week 19. The total-AKT level and the phospho-AKT/total AKT ratio failed to change significantly in the irradiated hearts as compared to the controls. It has also been demonstrated in other LVH models that the repression of the FOXO3 level could indirectly lead to the overactivity of the hypertrophic calcineurin/NFAT pathway (57). In our present study, cardiac mRNA levels of calcineurin A-alpha and calcineurin A-beta showed a statistically non-significant decrease in the irradiated hearts as compared to the controls. These results suggest that the AKT/FOXO3 mediated pathways might not play a crucial role in the development of LVH in chronic RIHD. Nonetheless, the FOXO3 protein level and its phosphorylation are also regulated by various molecules beyond miR-212.

In our chronic RIHD model, we also investigated the expression of selected regulatory genes that are predicted targets of miR-212 and are associated with cardiac hypertrophy in other LVH forms. Target mRNAs were Mef2a, AMPK, Hsp40, sirtuin 1, calcineurin A-alpha, PTEN, and ERK2. These target mRNAs failed to show a significant change in RIHD as compared to the control hearts. Therefore, we did not further investigate their cardiac expression at the protein level.

The development of the LVH and HFpEF in RIHD seems to be unique and very different from other forms of cardiac hypertrophies, such as the commonly studied pressure-overload-induced compensatory hypertrophy and subsequent heart failure. In RIHD, compensatory hypertrophy, cell survival, and recovery mechanisms could be activated simultaneously in a distinct manner. These individual pathways may converge in the same direction toward key down-stream regulators (e.g., FOXO3) and the ensuing opposite effects may extinct each other at the protein level.

In this study, the focus was on the miR-212 with its selected hypertrophy-associated target mRNA molecules, the relative role of other miRNAs or other miR-212 targets were not assessed in the development of cardiac hypertrophy in RIHD.

In summary, this is the first study to report that LVH and HFpEF are accompanied by characteristic overexpression of miR-212 in the heart, both in the early and later phases of RIHD. Our results suggest that miR-212 might play a significant role in the development of RIHD via FOXO3/AKT independent mechanisms, and the molecular mechanism of the development of RIHD is distinct from other forms of hypertrophy and pathological remodeling.

LIMITATIONS

Our results regarding altered cardiac gene expression due to RIHD are based on selected miRNAs and mRNA target molecules, however, measurement of the full rat transcriptome should be performed in the future. Our study is descriptive; therefore, future studies providing more in-depth mechanistic insights should be carried out. Moreover, therapeutic intervention was out of the scope of our present exploratory study.

AUTHOR CONTRIBUTIONS

MS coordinated the study, performed transthoracic echocardiography and qRT-PCR for miR-212, evaluated experimental data, drafted, proofread, and edited the manuscript. RG and PD performed Western blot experiments. ÁZ performed qRT-PCR for mRNA targets. MS, LK, and GF treated the animals, isolated organs, and prepared samples. ZV and ZK planned and performed irradiation. BK and GC performed HE and picrosirius red staining and analyzed images. MK measured cardiomyocyte diameters. GS performed MMP2 zymography. TT, ZK, and TC consulted, proofread, and edited the manuscript. MS and SB

developed the study concept, edited, and revised the manuscript. All authors read and approved the final manuscript.

FUNDING

The work and publication were supported by the projects GINOP-2.3.2-15-2016-00040, NKFIH K115990, and FK129094, EFOP-3.6.2-16-2017-00006 (LIVE LONGER) and by the Ministry of Human Capacities (20391-3/2018/FEKUSTRAT). MS and MK were supported by the New National Excellence Program of the Ministry of Human Capacities (UNKP-17-4-I-SZTE-43, UNKP-17-2-I-SZTE-30, UNKP-18-4-SZTE-63, and UNKP-18-3-II-SZTE-15). MS is supported by the János Bolyai Research Fellowship of the Hungarian Academy of Sciences. MK was supported by the EFOP 3.6.3-VEKOP-16-2017-00009. The study was also partly funded by the EU funded ERANET program EXPERT (to TT), and the Deutsche Forschungsgemeinschaft KFO311 (to TT).

ACKNOWLEDGMENTS

We especially thank Bálint Cserni for writing the program for image analysis and Morgane Batkai language editor for proofreading the manuscript.

SUPPLEMENTARY MATERIAL

The Supplementary Material for this article can be found online at: https://www.frontiersin.org/articles/10.3389/fonc.2019.00598/full#supplementary-material

REFERENCES

1. Monceau V, Llach A, Azria D, Bridier A, Petit B, Mazevet M, et al. Epac contributes to cardiac hypertrophy and amyloidosis induced by radiotherapy but not fibrosis. *Radiother Oncol*. (2014) 111:63–71. doi: 10.1016/j.radonc.2014.01.025
2. Stewart FA, Seemann I, Hoving S, Russell NS. Understanding radiation-induced cardiovascular damage and strategies for intervention. *Clin Oncol*. (2013) 25:617–24. doi: 10.1016/j.clon.2013.06.012
3. Schultz-Hector S, Trott KR. Radiation-induced cardiovascular diseases: is the epidemiologic evidence compatible with the radiobiologic data? *Int J Radiat Oncol Biol Phys*. (2007) 67:10–8. doi: 10.1016/j.ijrobp.2006.08.071
4. Sridharan V, Sharma SK, Moros EG, Corry PM, Tripathi P, Lieblong BJ, et al. Effects of radiation on the epidermal growth factor receptor pathway in the heart. *Int J Radiat Biol*. (2013) 89:539–47. doi: 10.3109/09553002.2013.782110
5. Andratschke N, Maurer J, Molls M, Trott KR. Late radiation-induced heart disease after radiotherapy. Clinical importance, radiobiological mechanisms and strategies of prevention. *Radiother Oncol*. (2011) 100:160–6. doi: 10.1016/j.radonc.2010.08.010
6. Adams MJ, Hardenbergh PH, Constine LS, Lipshultz SE. Radiation-associated cardiovascular disease. *Crit Rev Oncol Hematol*. (2003) 45:55–75. doi: 10.1016/S1040-8428(01)00227-X
7. Saiki H, Moulay G, Guenzel AJ, Liu W, Decklever TD, Classic KL, et al. Experimental cardiac radiation exposure induces ventricular diastolic dysfunction with preserved ejection fraction. *Am J Physiol Heart Circ Physiol*. (2017) 313:H392–H407. doi: 10.1152/ajpheart.00124.2017
8. O'Donnell L, O'Neill T, Toner M, O'Briain S, Graham I. Myocardial hypertrophy, fibrosis and infarction following exposure of the heart to radiation for Hodgkin's disease. *Postgrad Med J*. (1986) 62:1055–8. doi: 10.1136/pgmj.62.733.1055
9. Taunk NK, Haffty BG, Kostis JB, Goyal S. Radiation-induced heart disease: pathologic abnormalities and putative mechanisms. *Front Oncol*. (2015) 5:39. doi: 10.3389/fonc.2015.00039
10. Gabriels K, Hoving S, Seemann I, Visser NL, Gijbels MJ, Pol JF, et al. Local heart irradiation of ApoE$^{-/-}$ mice induces microvascular and endocardial damage and accelerates coronary atherosclerosis. *Radiother Oncol*. (2012) 105:358–64. doi: 10.1016/j.radonc.2012.08.002
11. Seemann I, Gabriels K, Visser NL, Hoving S, te Poele JA, Pol JF, et al. Irradiation-induced modest changes in murine cardiac function despite progressive structural damage to the myocardium and microvasculature. *Radiother Oncol*. (2012) 103:143–50. doi: 10.1016/j.radonc.2011.10.011
12. Walker CM, Saldaña DA, Gladish GW, Dicks DL, Kicska G, Mitsumori LM, et al. Cardiac complications of oncologic therapy. *Radiographics*. (2013) 33:1801–15. doi: 10.1148/rg.336125005
13. Yarnold J, Brotons MC. Pathogenetic mechanisms in radiation fibrosis. *Radiother Oncol*. (2010) 97:149–61. doi: 10.1016/j.radonc.2010.09.002
14. Madan R, Benson R, Sharma DN, Julka PK, Rath GK. Radiation-induced heart disease: Pathogenesis, management and review literature. *J Egypt Natl Canc Inst*. (2015) 27:187–93. doi: 10.1016/j.jnci.2015.07.005
15. Schultz-Hector S. Radiation-induced heart disease: review of experimental data on dose response and pathogenesis. *Int J Radiat Biol*. (1992) 61:149–60. doi: 10.1080/09553009214550761
16. Kiscsatári L, Sárközy M, Kovári B, Varga Z, Gömöri K, Morvay N, et al. High-dose radiation-induced heart damage in a rat model. *In vivo*. (2016) 30:623–31.
17. Ha M, Kim VN. Regulation of microRNA biogenesis. *Nat Rev Mol Cell Biol*. (2014) 15:509–24. doi: 10.1038/nrm3838
18. Viereck J, Thum T. Circulating noncoding RNAs as biomarkers of cardiovascular disease and injury. *Circ Res*. (2017) 120:381–99. doi: 10.1161/CIRCRESAHA.116.308434
19. Viereck J, Bang C, Foinquinos A, Thum T. Regulatory RNAs and paracrine networks in the heart. *Cardiovasc Res*. (2014) 102:290–301. doi: 10.1093/cvr/cvu039
20. Kumarswamy R, Thum T. Non-coding RNAs in cardiac remodeling and heart failure. *Circ Res*. (2013) 113:676–89. doi: 10.1161/CIRCRESAHA.113.300226
21. Bátkai S, Thum T. MicroRNAs in hypertension: mechanisms and therapeutic targets. *Curr Hypertens Rep*. (2012) 14:79–87. doi: 10.1007/s11906-011-0235-6
22. Ucar A, Gupta SK, Fiedler J, Erikci E, Kardasinski M, Batkai S, et al. The miRNA-212/132 family regulates both cardiac hypertrophy and cardiomyocyte autophagy. *Nat Commun*. (2012) 3:1078. doi: 10.1038/ncomms2090
23. Thum T, Galuppo P, Wolf C, Fiedler J, Kneitz S, van Laake LW, et al. MicroRNAs in the human heart: a clue to fetal gene reprogramming in heart failure. *Circulation*. (2007) 116: 258–267. doi: 10.1161/CIRCULATIONAHA.107.687947
24. Jentzsch C, Leierseder S, Loyer X, Flohrschütz I, Sassi Y, Hartmann D, et al. A phenotypic screen to identify hypertrophy-modulating microRNAs in primary cardiomyocytes. *J Mol Cell Cardiol*. (2012) 52:13–20. doi: 10.1016/j.yjmcc.2011.07.010
25. Mutlak M, Kehat I. Extracellular signal-regulated kinases 1/2 as regulators of cardiac hypertrophy. *Front Pharmacol*. (2015) 6:149. doi: 10.3389/fphar.2015.00149
26. Tobin SW, Hashemi S, Dadson K, Turdi S, Ebrahimian K, Zhao J, et al. Heart failure and MEF2 transcriptome dynamics in response to β-Blockers. *Sci Rep*. (2017) 7:4476. doi: 10.1038/s41598-017-04762-x
27. Li T, Jiang S, Yang Z, Ma Z, Yi W, Wang D, et al. Targeting the energy guardian AMPK: another avenue for treating cardiomyopathy? *Cell Mol Life Sci*. (2017) 74:1413–29. doi: 10.1007/s00018-016-2407-7
28. Ago T, Liu T, Zhai P, Chen W, Li H, Molkentin JD, et al. A redox-dependent pathway for regulating class II HDACs and cardiac hypertrophy. *Cell*. (2008) 133:978–93. doi: 10.1016/j.cell.2008.04.041

29. Sundaresan NR, Pillai VB, Gupta MP. Emerging roles of SIRT1 deacetylase in regulating cardiomyocyte survival and hypertrophy. *J Mol Cell Cardiol*. (2011) 51:614–8. doi: 10.1016/j.yjmcc.2011.01.008
30. Rohini A, Agrawal N, Koyani CN, Singh R. Molecular targets and regulators of cardiac hypertrophy. *Pharmacol Res*. (2010) 61:269–80. doi: 10.1016/j.phrs.2009.11.012
31. Javadov S, Jang S, Agostini B. Crosstalk between mitogen-activated protein kinases and mitochondria in cardiac diseases: therapeutic perspectives. *Pharmacol Ther*. (2014) 144:202–25. doi: 10.1016/j.pharmthera.2014.05.013
32. Kocsis GF, Sárközy M, Bencsik P, Pipicz M, Varga ZV, Pálóczi J, et al. Preconditioning protects the heart in a prolonged uremic condition. *Am J Physiol Heart Circ Physiol*. (2012) 303:H1229–1236. doi: 10.1152/ajpheart.00379.2012
33. Schreckenberg R, Weber P, Cabrera-Fuentes HA, Steinert I, Preissner KT, Bencsik P, et al. Mechanism and consequences of the shift in cardiac arginine metabolism following ischaemia and reperfusion in rats. *Thromb Haemost*. (2015) 113:482–93. doi: 10.1160/TH14-05-0477
34. Csont T, Sárközy M, Szucs G, Szucs C, Bárkányi J, Bencsik P, et al. Effect of a multivitamin preparation supplemented with phytosterol on serum lipids and infarct size in rats fed with normal and high cholesterol diet. *Lipids Health Dis*. (2013) 12:138. doi: 10.1186/1476-511X-12-138
35. Sárközy M, Szucs G, Pipicz M, Zvara Á, Éder K, Fekete V, et al. The effect of a preparation of minerals, vitamins and trace elements on the cardiac gene expression pattern in male diabetic rats. *Cardiovasc Diabetol*. (2015) 14:85. doi: 10.1186/s12933-015-0248-6
36. Sárközy M, Szucs G, Fekete V, Pipicz M, Éder K, Gáspár R, et al. Transcriptomic alterations in the heart of non-obese type 2 diabetic Goto-Kakizaki rats. *Cardiovasc Diabetol*. (2016) 15:110. doi: 10.1186/s12933-016-0424-3
37. Mátyás C, Németh BT, Oláh A, Hidi L, Birtalan E, Kellermayer D, et al. The soluble guanylate cyclase activator cinaciguat prevents cardiac dysfunction in a rat model of type-1 diabetes mellitus. *Cardiovasc Diabetol*. (2015) 14:145. doi: 10.1186/s12933-015-0309-x
38. Sárközy M, Gáspár R, Zvara Á, Siska A, Kovári B, Szucs G, et al. Chronic kidney disease induces left ventricular overexpression of the pro-hypertrophic microRNA-212. *Sci Rep*. (2019) 9:1302. doi: 10.1038/s41598-018-37690-5
39. Sárközy M, Zvara A, Gyémánt N, Fekete V, Kocsis GF, Pipis J, et al. Metabolic syndrome influences cardiac gene expression pattern at the transcript level in male ZDF rats. *Cardiovasc Diabetol*. (2013) 12:16. doi: 10.1186/1475-2840-12-16
40. Kupai K, Szucs G, Cseh S, Hajdu I, Csonka C, Csont T, et al. Matrix metalloproteinase activity assays: importance of zymography. *J Pharmacol Toxicol Methods*. (2010) 61:205–9. doi: 10.1016/j.vascn.2010.02.011
41. Bester DJ, Kupai K, Csont T, Szucs G, Csonka C, Esterhuyse AJ, et al. Dietary red palm oil supplementation reduces myocardial infarct size in an isolated perfused rat heart model. *Lipids Health Dis*. (2010) 9:64. doi: 10.1186/1476-511X-9-64
42. Gáspár R, Pipicz M, Hawchar F, Kovács D, Djirackor L, Görbe A, et al. The cytoprotective effect of biglycan core protein involves Toll-like receptor 4 signaling in cardiomyocytes. *J Mol Cell Cardiol*. (2016) 99:138–50. doi: 10.1016/j.yjmcc.2016.08.006
43. Pipicz M, Kocsis GF, Sárváry-Arantes L, Bencsik P, Varga ZV, Ferdinandy P, et al. Low-dose endotoxin induces late preconditioning, increases peroxynitrite formation, and activates STAT3 in the rat heart. *Molecules*. (2017) 22:E433. doi: 10.3390/molecules22030433
44. Pauschinger M, Knopf D, Petschauer S, Doerner A, Poller W, Schwimmbeck PL, et al. Dilated cardiomyopathy is associated with significant changes in collagen type I/III ratio. *Circulation*. (1999) 99:2750–6. doi: 10.1161/01.CIR.99.21.2750
45. Bishop JE, Greenbaum R, Gibson DG, Yacoub M, Laurent GJ. Enhanced deposition of predominantly type I collagen in myocardial disease. *J Mol Cell Cardiol*. (1990) 22:1157–65. doi: 10.1016/0022-2828(90)90079-H
46. Marijianowski MM, Teeling P, Mann J, Becker A. Dilated cardiomyopathy is associated with an increase in the type I/type III collagen ratio: a quantitative assessment. *J Am Col Cardiol*. (1995) 25:1263–72. doi: 10.1016/0735-1097(94)00557-7
47. Ni YG, Berenji K, Wang N, Oh M, Sachan N, Dey A, et al. Foxo transcription factors blunt cardiac hypertrophy by inhibiting calcineurin signaling. *Circulation*. (2006) 114:1159–68. doi: 10.1161/CIRCULATIONAHA.106.637124
48. Skurk C, Izumiya Y, Maatz H, Razeghi P, Shiojima I, Sandri M, et al. The FOXO3a transcription factor regulates cardiac myocyte size downstream of AKT signaling. *J Biol Chem*. (2005) 280:20814–23. doi: 10.1074/jbc.M500528200
49. Boerma M, Wang J, Kulkarni A, Roberto KA, Qiu X, Kennedy RH, et al. Influence of endothelin 1 receptor inhibition on functional, structural and molecular changes in the rat heart after irradiation. *Radiat Res*. (2008) 170:275–83. doi: 10.1667/RR1093.1
50. Chistiakov DA, Myasoedova VA, Revin VV, Orekhov AN, Bobryshev YV. The phenomenon of atherosclerosis reversal and regression: Lessons from animal models. *Exp Mol Pathol*. (2017) 102:138–45. doi: 10.1016/j.yexmp.2017.01.013
51. Ahamed J, Laurence J. Role of platelet-derived transforming growth factor-β1 and reactive oxygen species in radiation-induced organ fibrosis. *Antioxid Redox Signal*. (2017) 27:977–88. doi: 10.1089/ars.2017.7064
52. Bonow RO, Mann D, Zipes D, Libby P. *Braunwald's Heart Disease: A Textbook of Cardiovascular Medicine, Single Volume*. 9th ed. (2012). Available online at: https://www.elsevier.com/books/braunwalds-heart-disease-a-textbook-of-cardiovascular-medicine-single-volume/bonow/978-1-4377-0398-6
53. Sharma UC, Sonkawade SD, Spernyak JA, Sexton S, Nguyen J, Dahal S, et al. A small peptide Ac-SDKP inhibits radiation-induced cardiomyopathy. *Circ Heart Fail*. (2018) 11:e004867. doi: 10.1161/CIRCHEARTFAILURE.117.004867
54. Sárközy M, Kahán Z, Csont T. A myriad of roles of miR-25 in health and disease. *Oncotarget*. (2018) 9:21580–612. doi: 10.18632/oncotarget.24662
55. Kura B, Yin C, Frimmel K, Krizak J, Okruhlicova L, Kukreja RC, et al. Changes of microRNA-1, -15b and -21 levels in irradiated rat hearts after treatment with potentially radioprotective drugs. *Physiol Res*. (2016) 65(Suppl. 1):S129–37. Available online at: http://www.biomed.cas.cz/physiolres/pdf/65%20Suppl%201/65_S129.pdf
56. Viczenczova C, Kura B, Egan Benova T, Yin C, Kukreja RC, Slezak J, et al. Irradiation-induced cardiac connexin-43 and miR-21 responses are hampered by treatment with atorvastatin and aspirin. *Int J Mol Sci*. (2018) 19:E1128. doi: 10.3390/ijms19041128
57. Papanicolaou KN, Izumiya Y, Walsh K. Forkhead transcription factors and cardiovascular biology. *Circ Res*. (2008) 102:16–31. doi: 10.1161/CIRCRESAHA.107.164186

Conflict of Interest Statement: TT has filed and licensed patents about non-coding RNAs. TT is founder, SB is co-founder and both hold shares of Cardior Pharmaceuticals GmbH.

The remaining authors declare that the research was conducted in the absence of any commercial or financial relationships that could be construed as a potential conflict of interest.